



HAMK
UNIVERSITY OF APPLIED SCIENCES

Proceedings of the METNET Seminar 2014 in Moscow



METNET Annual Seminar in Moscow, Russia, on 21 – 22 October 2014

Kuldeep Viridi and Lauri Tenhunen (Editors)



Proceedings of the METNET Seminar 2014 in Moscow

Kuldeep Viridi and Lauri Tenhunen (Editors)

Editors:
Kuldeep Viridi, Aarhus University
Lauri Tenhunen, HAMK University of Applied Sciences

Proceedings of the METNET Seminar 2014 in Moscow

PRINTED

ISBN 978-951-784-693-6
ISSN 1795-4231
HAMKin julkaisu 15/2014

ELECTRONIC

ISBN ISBN 978-951-784-694-3 (PDF)
ISSN 1795-424X
HAMKin e-julkaisu 35/2014

© HAMK UAS and writers

PUBLISHER

HAMK University of Applied Sciences
PO Box 230
FI-13101 Hämeenlinna, FINLAND
tel. +358 3 6461
julkaisut@hamk.fi
www.hamk.fi/julkaisut

Hämeenlinna, December 2014

Index

PREFACE	5
Dimo Zhelev, University of Architecture, Civil Engineering and Geodesy, Sofia, Bulgaria	
NUMERICAL SIMULATION OF CYCLIC LOAD ON END PLATE CONNECTION	6
Sharmistha Chowdhury, Bauhaus University, Weimar, Germany	
PARAMETER ESTIMATION OF DIFFERENT FATIGUE CRACK GROWTH MODELS	15
Kudishin Y. I., TSNIIPSK named after Melnikov N.P. Grishin A.S., Public Corporation "Atomenergoproekt"	
CURRENT TRENDS IN THE ANALYSIS OF METAL STRUCTURES	26
Grudev Ivan Dmitriyevich, Moscow State University of Civil Engineering (MGSU), Russia	
LOCAL BENDING STABILITY OF TUBES WITH RECTANGULAR CROSS SECTION	39
Ingmar Stade and Carsten Könke, Bauhaus-Universität Weimar, Weimar, Germany,	
GENERATION OF NUMERICAL SIMULATION MODELS IN STRUCTURAL DYNAMICS FROM COMPUTED TOMOGRAPHY IMAGE DATA	50
Peter Olney, Ingmar Stade and Maher Deeb, Bauhaus-Universität Weimar	
DYNAMIC PROPERTIES IDENTIFIED FROM MEASUREMENTS ON IDENTICAL POLE STRUCTURES	58
Raimo Ruoppa and Rauno Toppila, Lapland University of Applied Sciences, Finland Vili Kesti, SSAB, Finland Anna-Maija Arola, University of Oulu, Finland	
BENDABILITY TESTS FOR ULTRA-HIGH-STRENGTH STEELS WITH OPTICAL STRAIN ANALYSIS AND PREDICTION OF BENDING FORCE	68
Leonid Storozhenko, Grigoriy Gasii and Sergey Gapchenko Poltava National Technical University named after Yuri Kondratyuk, Ukraine	
STEEL-REINFORCED CONCRETE STRUCTURAL GUY-ROPE CLADDING	79
L.I. Storozhenko, V.V. Muravlyov and F.S. Shkolyar Poltava National Technical University named after Yuri Kondratyuk, Ukraine	
TESTING CONCRETE BEAMS WITH REINFORCEMENT BAR WEBS	86
Nikolay I. Vatin, Saint-Petersburg State Polytechnical University Jarmo Havula, HAMK University of Applied Sciences Lassi Martikainen, HAMK University of Applied Sciences Alexey S. Sinelnikov, Saint-Petersburg State Polytechnical University Lidia L. Shurovkina, Saint-Petersburg State Polytechnical University	
RETICULAR-STRETCHED THERMO-PROFILE: BUCKLING OF THE PERFORATED WEB	93
Markku Heinisuo and Teemu Tiainen, Tampere University of Technology	
TUBULAR TRUSS JOINTS – HINGED OR RIGID?	104

Devyatov V.V. and Vershinin V.V., Moscow State University of Civil Engineering (MGSU), Russia	
STEEL CONSUMPTION EFFICIENCY IMPROVEMENT IN HOLLOW UNITS MANUFACTURING	107
S.F. Pichugin, Poltava National Technical University named after Yuri Kondratyuk, Ukraine	
RELIABILITY ANALYSIS OF STEEL STRUCTURES.....	115
Vasilkin A.A., Moscow State University of Civil Engineering (MGSU), Russia	
SYSTEM ENGINEERING OF OPTIMAL DESIGN OF BUILDING CONSTRUCTIONS ELEMENTS	123
Tenhunen, Lauri, HAMK University of Applied Sciences, Finland Ranta-Eskola, Arto, SSAB, Finland	
ON THE CHOICE OF EVALUATION ASPECTS IN UNDERSTANDING UNIVERSITY-BUSINESS COOPERATION (UBC) RESULTS	131
Bogdan MOCAN, Stelian BRAD and Mircea FULEA, Technical University of Cluj-Napoca, Romania	
DESIGN FRAMEWORK OF A ROBOT SYSTEM FOR CLEANING EXTERNAL GLASS WALLS OF MODERN BUILDINGS.....	142
Fridkin V.M., Moscow State University of Railway Engineering (MIET), Moscow, Russia Kouzmenko I.M., «Belarusian-Russian University», Mogilev, Belarus Sysa N.S.; «Protos Companies Group», Mogilev, Belarus Kuzmenka D.O., «Belarusian-Russian University» Bogdanov S.V., «Belarusian-Russian University»	
DESIGN, ENGINEERING AND MANUFACTURING OF BEARING ELEMENTS OF THE LOW STEEL WEIGHT	153
Parlashceвич Valentina, Moscow State University of Civil Engineering (MGSU), Russia, Moscow	
SCIENTIFIC RESEARCH ECONOMICAL, SOCIAL-PSYCHOLOGICAL AND TECHNICAL FACTORS OF QUALITY IMPROVEMENT OF BUILDING WELD-FABRICATED CONSTRUCTIONS	165
Evgeny Lebed and Artyom Grigoryan, Moscow State University of Civil Engineering (MGSU), Russia	
DETERMINATION OF INITIAL FORCES IN TWO-LAYER LARGE SPAN METAL DOMES DUE TO ASSEMBLING ERRORS	173
P.G. Yeremeyev, Kucherenko Central Research Institute for Building Structures	
MODERN STADIA. TECHNICAL AND ECONOMIC PROBLEMS OF DESIGN AND OPERATION	179
Anatoly Alekseytsev and Natalia Kurchenko, Bryansk State Academy of Engineering and Technology Department of building production, Bryansk, Russia	
EVOLUTIONARY OPTIMIZATION OF WELDED FRAME CONSTRUCTION IN INDUSTRIAL BUILDINGS.....	188
Khanukhov K.M., Consortium "Isotermic"	
SAFETY MEASURES FOR STORING OF LIQUEFIED GASES IN LARGE WELDED LOW PRESSURE TANKS.....	196

PREFACE

METNET network has been active since 2006. Now over 40 universities, research institutes and enterprises regularly participate in the Annual Seminar, the latest in the series taking place in Moscow. Members actively exchange knowledge, results of research and explore possibilities of cooperation in research and dissemination. Such cooperation opens new options for universities and research organizations to customer- and needs-based product development. It makes it possible to foster innovative processes in partner organizations.

As in previous years the annual METNET Seminar held in Moscow concentrated on presenting new research results in scientific areas relevant to metal structures. The presented papers covered a much wider range of themes covering both experimental and numerical research than in any previous year.

The first session in the Seminar focused on computational mechanics. Papers presented included one on modelling of cyclic loads on end plate connections. The related theme of crack-growth propagation was covered in another paper. Local instability of sections formed the topic of another paper describing computational results.

Experimental results were presented in a number of papers covering, novel techniques such as use of computed tomography image data, extensive site measurements on electric supply poles and use of optical strain analysis for the determination of bendability of steel. A few papers covered the beneficial effects of steel concrete composite construction. Benefits from using steel beams with perforated webs were demonstrated in another paper.

Papers on manufacture of hollow sections, consideration of joint rigidity in trusses, and reliability analysis and a systems approach to optimum design of steel structures all formed a special session on technical issues relating to steel construction.

Traditionally METNET seminars deal with not only technical aspects of metal construction, but also issues of concern to industry on management, planning and sustainability of projects. This year was no exception. One paper covered the topic of university and business co-operation and another on economic and social aspects of quality enhancement of welded structures.

Special topics covered in the seminar included design of modern sports stadia and large welded pressure tanks,

A comprehensive paper was presented on current trends in the analysis of metal structures.

Kuldeep Viridi

Lauri Tenhunen

NUMERICAL SIMULATION OF CYCLIC LOAD ON END PLATE CONNECTION

Dimo Zhelev
(dimosiderov@abv.bg)

University of Architecture, Civil Engineering and Geodesy, Sofia, Bulgaria
Faculty of Structural Engineering
Department of Steel, Timber and Plastic Structures

ABSTRACT

The end plate connections are widely used for beam to column joints in steel frame structure. A numerical simulation of a beam to column joint, loaded with cyclic load, is performed with general purpose software ANSYS APDL. For verification of the numerical simulation of cyclic load on an end plate connection, the numerical results are compared with experimental results from an article of (Gang, et al., 2007).

INTRODUCTION

The end plate connections are a good variant of beam to column connection. Their improvement from welded moment connection is that when designed properly there will not occur high stress due to the welds, so brittle failure is not typical. A lot of experimental and analytical research has been conducted on the behavior and design method of steel seismic moment connections, for example the SAC steel research project.

The behavior of the end plate connection depends on many variables: end plate and column flange thickness, bolt diameter and grade, bolts spacing, shear panel thickness, presence of column and end plate stiffener. Despite of a lot of experimental and analytical work for investigating the extended end plate connection behavior for seismic application, not all aspects are investigated.

In this study a numerical simulations with ANSYS APDL are made to confirm that a joint model made with plane finite elements used for plates and linear elements for bolts, with bilinear kinematic material model of the steel components, leads to satisfactory result, compare with the test results.

NUMERICAL SIMULATION

Geometry

The steel is Q345 and the bolts are M20 and M24. Column stiffeners are applied. The column flange thickness is 12mm, but in the part connected

with the beam plus 100mm on each side is 20mm. Bolt pretension force is according to Figure 1.

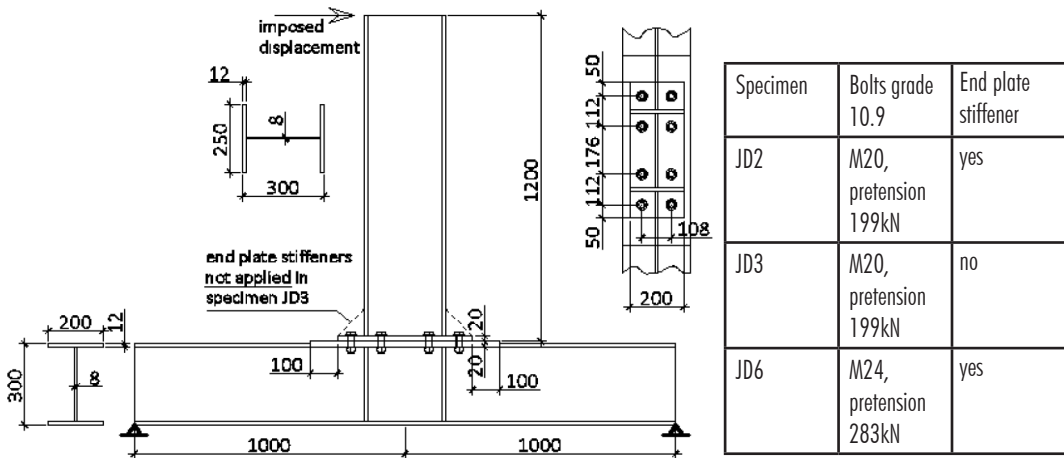


Figure 1. "Specimen geometry".

Finite elements

General purpose software ANSYS APDL is applied for this research. The end plate connection model can be made with solid elements for the bolt and the steel plates (Krishnamurthy, 1978), (Gang, et al., 2008). Shell elements for the plates, solid elements for the bolt nut and head, six link elements for the bolt shank are the elements used in (Sherbourne, et al., 1994). In the current research the plates will be presented as shell elements (SHELL181), the bolts are simulated with link element, working on tension only (LINK180) for the threaded part and BEAM188 for the unthreaded part. The bolt's start and end nodes are connected with the shell element nodes by constraint element MPC184. Initial pretension on the bolt is applied. For the contact between the end plate and the column face are used elements TARGE170 and CONTA174. The benefit of choosing these elements is to make the numerical simulation faster for computation.

Material models

For monotonic load the material model applied could be with isotropic or kinematic hardening. For cyclic load a model of the steel elements should be chosen with kinematic hardening (ANSYS documentation). The stress - strain relationship for the bolts grade 10.9 is applied bilinear kinematic, with values shown on Table 1.

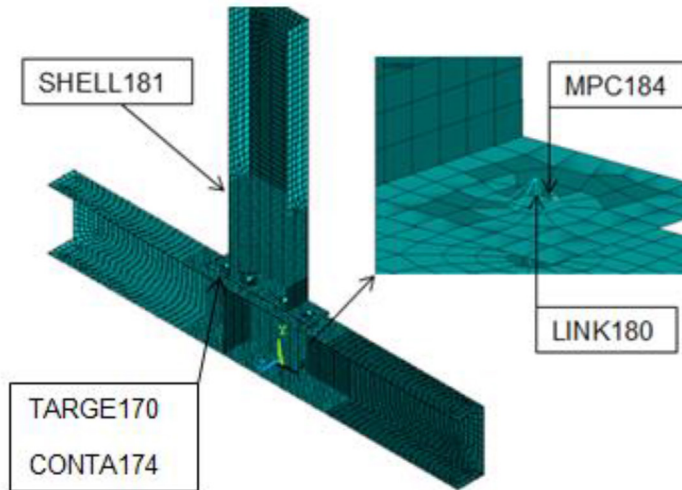


Figure 2. Finite element types (Beam 188).

Table 1. Material properties of bolt grade 10.9 – Bilinear kinematic.

Yield stress	Elastic modulus	Tangent modulus
$\frac{kN}{cm^2}$	$\frac{kN}{cm^2}$	$\frac{kN}{cm^2}$
99.5	20500	205

Table 2. Material properties of steel Q345 – Bilinear kinematic.

Yield stress	Elastic modulus	Tangent modulus
$\frac{kN}{cm^2}$	$\frac{kN}{cm^2}$	$\frac{kN}{cm^2}$
37.2	18867	188

The steel plates are made from Q345 steel. Specimens of steel Q345 are tested on monotonic and cyclic load in the research of (Yongjiu, et al., 2011). The properties are shown in Table 2. The tangent modulus of the steel is assumed according to the results of this publication, also it appears that the value of the tangent modulus is similar to the recommended value for hardening in bilinear model in the Euro code (EN 1993-1-5).

Friction coefficient of 0.44 is applied between the end plate and the column flange.

Loading and boundary conditions

The pretension force in the bolts is applied as first load step, second step is used to “lock” the new length of the bolts. The model is load with imposed displacement on the top – as shown in Figure 1. The cyclic load protocol is the one applied by the study of (Gang, et al., 2007). First a monotonic load is applied and the yielding rotation and yielding moment are discovered. Three steps are applied to reach the yielding rotation. After yielding, each displacement incremental step is 10 mm, with two cycles applied.

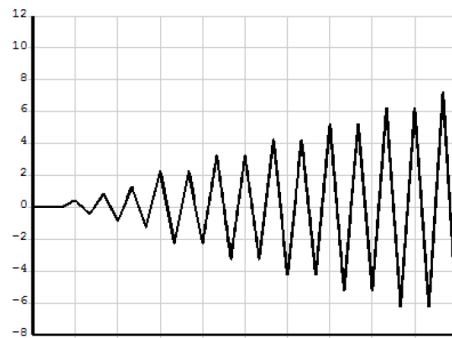


Figure 3. Cyclic load.

RESULTS

Moment in joint versus rotation

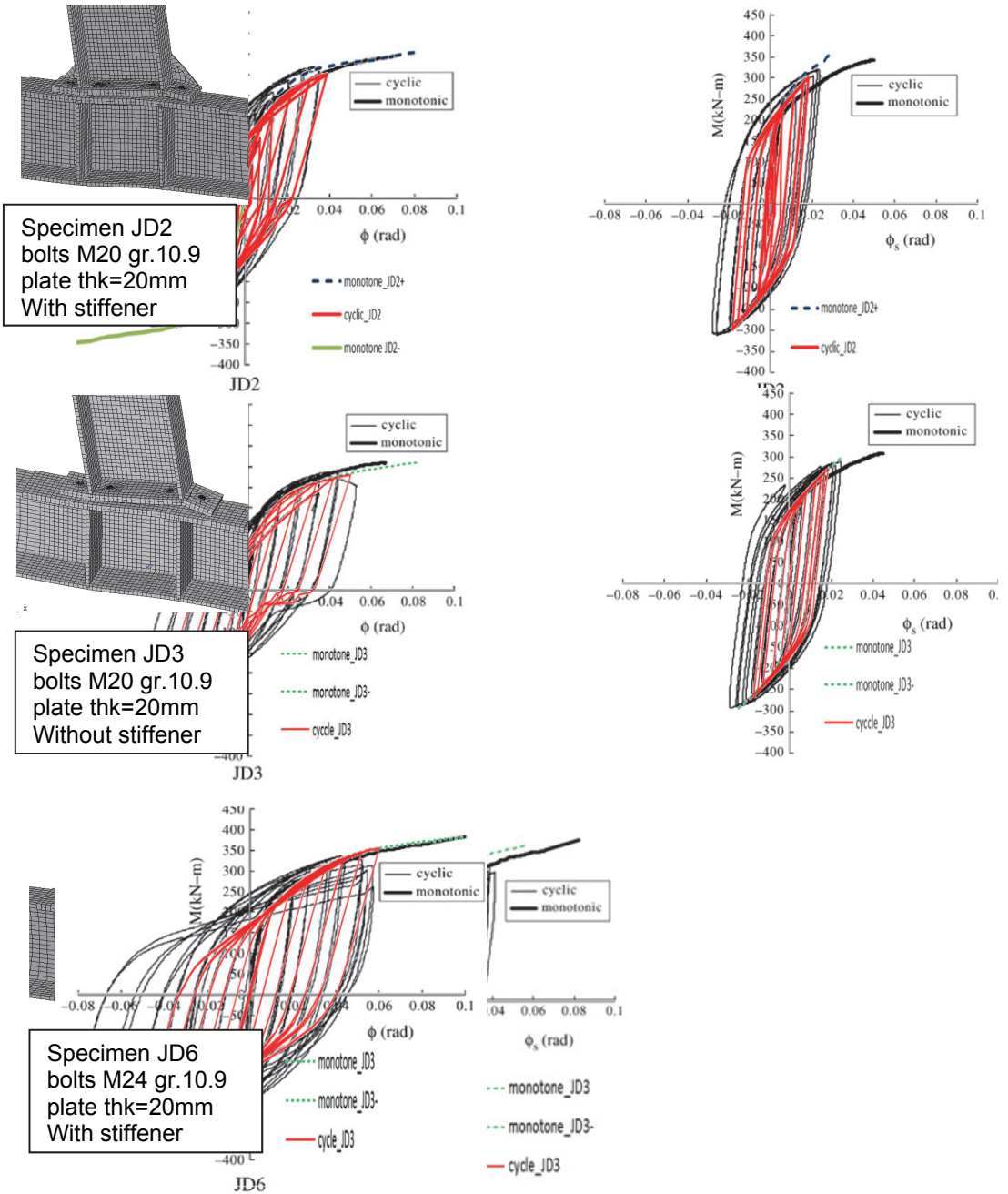


Figure 4. Compare of numerical with test results.

Tension in bolt

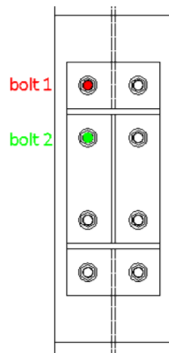
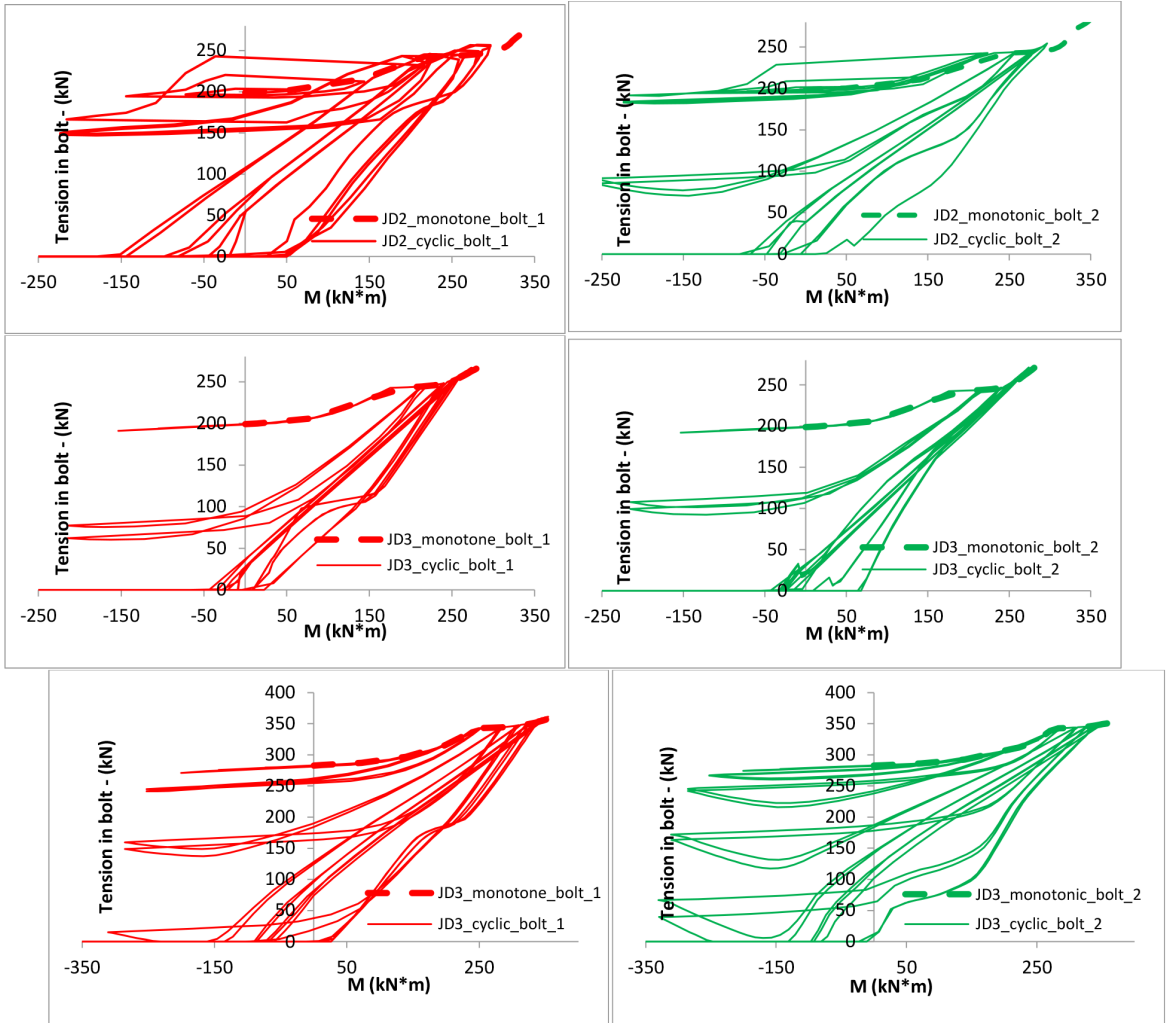
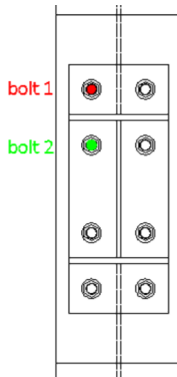


Figure 5. Tension forces in bolts.



In Figure 5 is presented the bolt tension with the moment in the beam. The results confirm that in a pretension bolt, when the bolt is elongating, the pretension has no effect after bolt yielding, because the bolt remain with increased length - the plastic elongation is added, and the bolt does not contact with the plates. So to reduce the stiffness degradation of the connection, during seismic action, the bolts should work in elastic stage. Also this will ensure that the bolts will not be damaged.

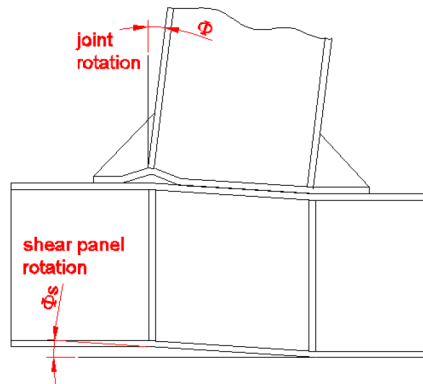


Figure 6. Joint rotation.

The behaviour of the investigated endplate joint depends mainly of the shear panel and of the equivalent T-stub. Higher resistance of the end plate connection will increase the participation of the shear panel in the energy dissipation of the connection through nonlinear work.

Table 3. Ultimate moment resistance from cyclic load.

Specimen	Mu [kN*m]	
	test	numerical
JD2	320,1	296
JD3	288,4	274
JD6	336,2	353

The comparison of the results from cyclic load in the experiment (Gang, et al., 2007) and from the numerical simulation shown in Figure 4 and in Table 3 indicates that despite the simplification of the finite element model, the ultimate moment resistance achieved is with value close to the experimental one. Also the $M - \phi$ curve from monotonic load in the numerical simulation is obtained with very good agreement with the results from the test. The hysteresis loops in the numerical simulation are showing small differences in the unloading part of the loop and in the ultimate moment resistance under cyclic load. The reason for this difference mainly is the bilinear material model applied in the study, so for better agreement with test results another kinematic hardening model should be applied, like multilinear or Chaboche.

CONCLUSION

The comparison between the test results of (Gang, et al., 2007) and the numerical results in this study indicates a good agreement.

To ensure that the connection can provide enough rotation capacity, the end plate should fail before the bolts does, or another option is the shear panel failure.

From Figure 4, it is evident that the pinching in hysteresis loops when an end plate stiffener is applied (specimens JD2, JD6) is smaller than in the case where a stiffener is not provided (specimen JD3). So the energy absorbed is higher when a stiffener is provided, and also the connection resistance is higher.

From Figure 4 in this study and also mentioned in the study (Gang, et al., 2007) it is evident that the $M - \phi$ curve under monotonic load is envelope of the hysteresis loops under the cyclic load.

REFERENCES

Ansys documentation.

Gang, Shi, et al. 2008. Numerical simulation of steel pretensioned bolted end-plate connections of different types and details. *Engineering Structures*. 30, 2008, pp. 2677–2686.

Gang, Shi, Shi, Yongjiu and Wang, Yuanqing. 2007. Behaviour of end-plate moment connections under earthquake loading. *Engineering Structures*. Elsevier, 2007, 29, pp. 703–716.

Krishnamurthy, N. 1978. A Fresh Look at Bolted End-Plate Behavior and Design. 1978. EMBED Equation.DSMT4

Sherbourne, Archibald N. and Bahaari, Mohammed R. 1994. 3D Simulation Of End-Plate Bolted Connections. *Journal of Structural Engineering*. 1994, pp. 3122–3136.

Yongjiu, Shi, Meng, Wang and Yuanqing, Wang. 2011. Experimental and constitutive model study of structural steel under cyclic loading. *Journal of Constructional Steel Research*. Elsevier, 2011, 67, pp. 1185–1197.

PARAMETER ESTIMATION OF DIFFERENT FATIGUE CRACK GROWTH MODELS

Sharmistha Chowdhury

Research Training Group 1462, Scientific researcher, Civil Engineering
Bauhaus University, Berkaerstrasse 9, 99425, Weimar, Germany
sharmistha.chowdhury@uni-weimar.de

ABSTRACT

Damage propagation in a structure under fatigue loading is one of the most unpredictable failure mechanism subjected to cyclic or random loading over its operational period. Monitoring the fatigue prone components of a structure is very crucial due to the presence of several sources of uncertainties which in turn induce uncertainties in the estimation of remaining fatigue life (RFL) or in the crack propagation description. Numerous fatigue crack growth models (CGM) exist to fulfill these purposes but very limited of them are applied, specifically for civil engineering structures. Estimation of the parameters concerning each crack growth model is a prerequisite prior to use of the model. To solidify the purposes of these applications, the author selected two well applicable fatigue crack growth models. A set of experimental fatigue test data is used to support this framework. The test data has been obtained from the NASGRO data manual where the test example is a low-carbon 1005-1012 hot rolled compact tension steel specimen subjected to a sinusoidal load with constant amplitude. The parameters of the fatigue crack growth models were latter estimated with least square, modified least square and maximum likelihood method. As a result, the suitability of each model can be assessed based on their data-fitting approach. The scheme developed from this outcome can be obtained and updated to apply for a more complex geometry with different boundary conditions.

INTRODUCTION

Fatigue is a localized progressive process in which structural damage accumulates continuously due to the repetitive application of external loading leading to complete fracture of the structure (Lampman 1996). Structures under random and/or cyclic operational loading are susceptible to fatigue failure while the loading may be well below the structural resistance capacity. Estimating the remaining fatigue life of the structure is a challenging task for responsible engineers. Therefore, performance of these kinds of structures has to be assessed during the entire service life which in turn requires long-term monitoring and non-destructive evaluation (NDE). However, constant and long-term monitoring, especially for large structures, is very expensive and can be troublesome with respect to data storage and data assessment (Kwon 2011). Since the actual loading conditions are usually not monitored

through the life of a structure, it is necessary to predict remaining fatigue life (RFL) without monitoring.

The greatest challenge to predict the remaining fatigue life (RFL) is to select the right fatigue CGM from the existing numerous mathematical models (Paris 1963, Walker 1970, Collipriest 1972, Forman 1972, Nasgro 2006). The suitability of a certain model largely depends on the parameters associated with it and the majority of fatigue life may fully depend on the estimated parameters. A number of factors, such as, the initial crack length, the loading history of environmental and mechanical stress, the material properties, the geometry of the structural member, and the unexpected loading change can influence the monitored data. These have been considered in several mathematical models (Willenborg 1971, Wheeler 1972, Skorupa 1996, Nasgro 2006). In this paper two simple fatigue CGMs, the Paris-Erdogan (Paris 1963) and the Walker model (Walker 1970) have been considered. To estimate the parameters regarding each model, least square estimation (LSE), modified least square estimation (MLSE) by (Klysz 2012) and maximum likelihood estimation (MLE) method have been applied.

METHODOLOGY

A fatigue crack growth curve (i.e., CGM) is a graphical representation of the stress intensity factor range, ΔK , and crack growth rate, $\frac{da}{dN}$ where a = crack length and N = number of loading cycle. The curve is subdivided into three regions namely: Region I- describing initiation or early development of the crack, Region II- describing linear and stable propagation of the crack and Region III- describing the unstable fatigue crack growth which leads to ultimate failure of the structure, see Figure 1 (Fisher 1984).

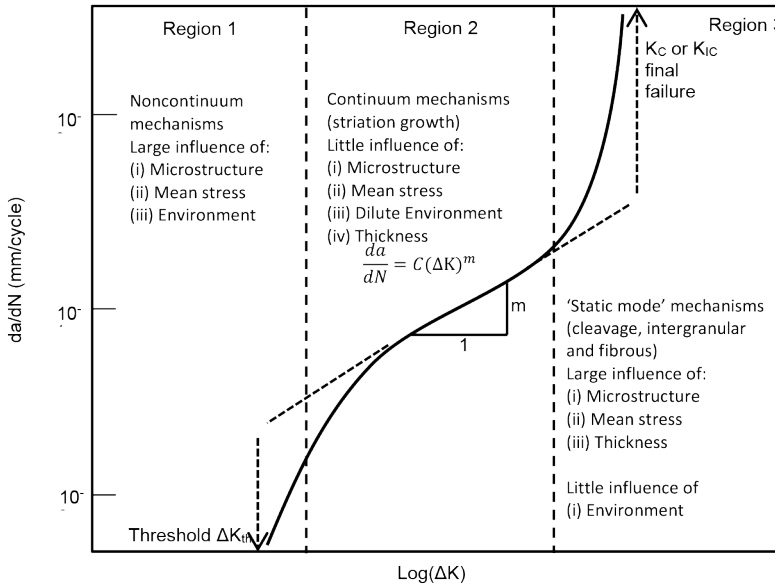


Figure 1. Fatigue crack growth regions versus stress intensity factor, ΔK .

The chosen Paris and Walker models are appropriate for region II but the Walker model is more advanced than the Paris model by means of taking the loading or stress ratio, R into account. Though the Paris model is the most conservative model among all fatigue CGMs, it is still the most applicable model due to its simplicity. Parameters of the both models have been estimated considering three methodologies: Least square estimation (LSE), Modified least square estimation (MLSE) by (Klysz 2012) and Maximum likelihood estimation (MLE).

Fatigue crack growth models (CGM)

Paris-Erdogan: The well-known Paris' law, described by Paris and Erdogan (1963), is the simplest method for predicting fatigue crack propagation and can be represented by the following relationship (Paris 1963):

$$\frac{da}{dN_p} = C_p (\Delta K)^{m_p} \tag{1}$$

Where, a = crack length, N_p = number of loading cycles, ΔK = stress intensity factor, C_p fatigue coefficient and m_p is the slope on the log-log plot of $\frac{da}{dN}$ versus ΔK . The Paris law is simple to use and requires the determination of the parameters C_p and m_p .

Walker Model: The drawback of the Paris law, which does not include the stress ratio, R , has been overcome by Walker. The proposed model from Walker is represented as (Walker 1970):

$$\frac{da}{dN_w} = C_w \left[\frac{\Delta K}{(1-R)^{1-\gamma_w}} \right]^{m_w} \quad (2)$$

The significance of this model is that it introduces a third parameter, γ_w , beside C_w and m_w . It is noted that, for $\gamma_w=1$, the Walker model converts to the Paris model. In other words it can be said that, the stress ratio has no effect on the crack growth model. Since both models are only capable of describing data in region II, they can overestimate the crack propagation rate in region I or underestimate in region III.

Parameter estimation

Parameter estimation is a prerequisite for assessing model quality. Based on studies from researchers in the early 60's, mainly focused on Paris' law, it can be demonstrated that the parameters C and m are material constants but largely influenced by the geometry and size of the structural member (Barenblatt 1980, Barenblatt 1996), the stress or loading ratio, R (Radhakrishnan 1979) and the initial crack length (spagnoli 2005).

The applied methodologies for estimating the parameters can influence the outcome. To observe the effect of different methods, three methodologies have been considered: least square estimation (LSE), modified least square estimation (MLSE) by (Klysz 2012) and maximum likelihood estimation (MLE).

For the LSE approximation of test data to adjust the parameters of a model function to best fit a data set, the method finds the optimum when the sum

$$S = \sum_{i=1}^n (\bar{y}_i - y_i)^2 \quad (3)$$

is minimum, wherein S is the squared residuals between values of the test data y_i , and those of the approximated function, \bar{y}_i .

However, LSE for the parameter estimation could be inappropriate, especially for the models capable of describing regions other than region II. As both regions I and III behave nonlinearly, values of the sum S decreases or increases according to the magnitudes of the approximated values.

In order to eliminate the stated problems, Equation (3), considered as Modified LSE method in this paper and was proposed by (Klysz 2012) as follows:

$$S^* = \sum_{i=1}^n \left(\frac{\bar{y}_i - y_i}{y_i} \right)^2 = \sum_{i=1}^n \left(\frac{\bar{y}_i}{y_i} - 1 \right)^2 \quad (4)$$

To follow the formulation of Equation (3) and (4), the linear regression for the Paris and the Walker model can be written from Equation (1) and (2) respectively as:

$$\log \left(\frac{da}{dN_p} \right) = \log(C_p) + m_p \log(\Delta K) \quad (5)$$

$$\log \left(\frac{da}{dN_w} \right) = \log(C_w) + m_w \log \left[\frac{\Delta K}{(1-R)^{1-\gamma_w}} \right] \quad (6)$$

For the maximum likelihood function, the regression model estimates the randomness of the model arising from the error term, e . The most common practice is to consider the error term e_i is normally and independently distributed as

$$e_i \sim N(\mu, \Sigma) \sim N(0, \Sigma)$$

wherein mean, $\mu = 0$, the covariance = Σ and $i =$ number of samples. The probability density function (pdf) of e_i , then is

$$f(e_i) = \frac{1}{\sqrt{2\pi\Sigma}} \exp \left(-\frac{1}{2\Sigma} e_i^2 \right), \quad i = 1, \dots, n \quad (7)$$

Since the error term, e , is not seen directly; we need to transform u by mapping with y_i . Now the error of the Paris and the Walker models are respectively:

$$e_{i,Paris} = \log \left(\frac{da}{dN_p} \right)_i - \log(C_p) - m_p \log(\Delta K)_i \quad (8)$$

$$e_{i,Walker} = \log \left(\frac{da}{dN_w} \right)_i - \log(C_w) - m_w \log \left[\frac{\Delta K}{(1-R)^{1-\gamma_w}} \right]_i \quad (9)$$

The transformation of random error, e , into random variable y_i , require the *Jacobian of transformation*, and is given by:

$$J(e_i \rightarrow y_i) = \left| \frac{\partial e_i}{\partial y_i} \right| = 1 \quad (10)$$

Following this, for Paris model, pdf of y_i or more specifically pdf of $\log\left(\frac{da}{dN_p}\right)$ is

$$\begin{aligned} f \left[\log \left(\frac{da}{dN_p} \right)_i \right] &= \frac{1}{\sqrt{2\pi}\Sigma_p} |J| \exp \left(-\frac{1}{2\Sigma_p} e_{i,Paris}^2 \right) \\ &= \frac{1}{\sqrt{2\pi}\Sigma_p} \exp \left(-\frac{1}{2\Sigma_p} e_{i,Paris}^2 \right); \text{ as } J = 1 \end{aligned} \quad (11)$$

For n observations, as $\log\left(\frac{da}{dN_p}\right)_1, \log\left(\frac{da}{dN_p}\right)_2, \dots, \log\left(\frac{da}{dN_p}\right)_n$ are independent, the joint pdf can be constructed as:

$$\begin{aligned} f \left[\log \left(\frac{da}{dN_p} \right)_1, \log \left(\frac{da}{dN_p} \right)_2, \dots, \log \left(\frac{da}{dN_p} \right)_n \right] \\ &= \left[\frac{1}{\sqrt{2\pi}\Sigma_p} \exp \left(-\frac{1}{2\Sigma_p} e_{1,Paris}^2 \right) \right] \dots \left[\frac{1}{\sqrt{2\pi}\Sigma_p} \exp \left(-\frac{1}{2\Sigma_p} e_{n,Paris}^2 \right) \right] \\ &= (2\pi)^{-\frac{n}{2}} (\Sigma_p)^{-\frac{n}{2}} \exp \left\{ -\frac{1}{2\Sigma_p} \sum_{i=1}^n (e_{i,Paris})^2 \right\} \end{aligned} \quad (12)$$

Since the joint pdf of observable random variable is the likelihood function, L , it can be written as

$$\begin{aligned} L \left(C_p, m_p, \Sigma_p \mid \log \left(\frac{da}{dN_p} \right)_1, \log \left(\frac{da}{dN_p} \right)_2, \dots, \log \left(\frac{da}{dN_p} \right)_n \right) = \\ \text{constant} (\Sigma_p)^{-\frac{n}{2}} \exp \left\{ -\frac{1}{2\Sigma_p} \sum (e_{i,Paris})^2 \right\} \end{aligned} \quad (13)$$

The maximum likelihood estimator of the parameters C_p, m_p, Σ_p is obtained by maximizing the likelihood function with respect to these parameters. The same procedure can be applied also to Walker model to estimate the C_w, m_w, Σ_w .

Once the parameters are estimated, the number of cycles, N , to propagate the crack from any initial crack stage, a_o , to a certain final crack stage, a_f can be obtained by rearranging and integrating Equation (1) and Equation (2), which provides the relation respectively as follows:

$$N_p = \frac{1}{C_p \sigma^{m_p}} \int_{a_o}^{a_f} \frac{1}{(\sqrt{a} F_1)^{m_p}} da \tag{14}$$

$$N_w = \frac{1}{C_w} \left(\frac{1 - R}{\sigma} \right)^{m_w} \int_{a_o}^{a_f} \frac{1}{(\sqrt{a} F_1)^{m_w}} da \tag{15}$$

Where, σ = stress, $F_1= f(a)$ = compliance function for a certain geometry and boundary condition.

APPLICATION EXAMPLE

To illustrate the approach, experimental data have been obtained from the NASGRO data manual (Youseffi 1978, Nasgro 2006) where the test example is a low-carbon 1005-1012 hot rolled compact tension test specimen subjected to a sinusoidal load with constant amplitude, see Figure 2.

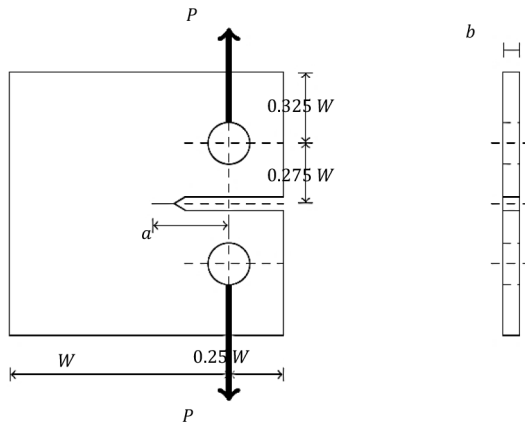


Figure 2. Typical compact tension test specimen for fracture test.

The general formula that describes the stress intensity factor is as follows (Fisher 1984):

$$\Delta K = \sigma\sqrt{a} \cdot F_1\left(\frac{a}{W}\right) \tag{16}$$

where, σ = stress caused by the applied load P ahead of the crack tip, a = crack length, W = width of the plate. The compliance function to compute the crack length in the CT specimen has the form (Youseffi 1978):

$$F_1\left(\frac{a}{W}\right) = 29.6\left(\frac{a}{W}\right) - 185.5\left(\frac{a}{W}\right) + 655.7\left(\frac{a}{W}\right)^2 - 1017\left(\frac{a}{W}\right)^3 + 638.9\left(\frac{a}{W}\right)^4 \tag{17}$$

Incorporating Equation.7 into Equation.1 and Equation.2 one can get the number of loading cycle for a given crack length according to the respective model.

Results

Table 1 summarizes the parameter estimated from both Paris and Walker models according to LSE, modified LSE and MLE methods. Parameters m and C are considered as respectively normally and log-normally distributed. In the current study, the parameter γ_w was chosen equal to 0.

Table 1. Estimated parameters with LSE, modified LSE and MLE

Parameters	Paris			Walker		
	LSE	LSE (mod)	MLE	LSE	LSE (mod)	MLE
C	2.13E-16	1.86E-16	2.206E-16	1.40E-16	1.22E-16	1.45E-16
m	3.968	3.987	3.96	3.968	3.987	3.96

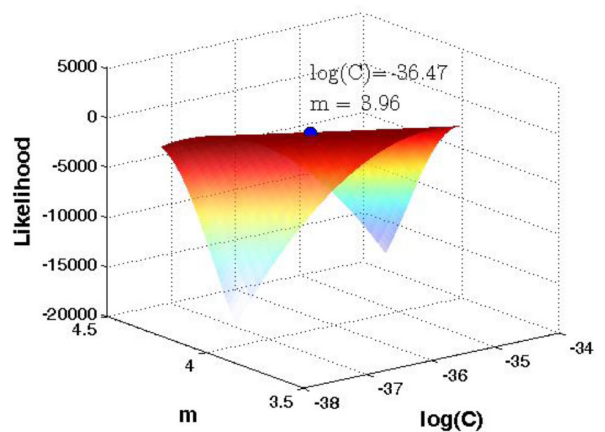
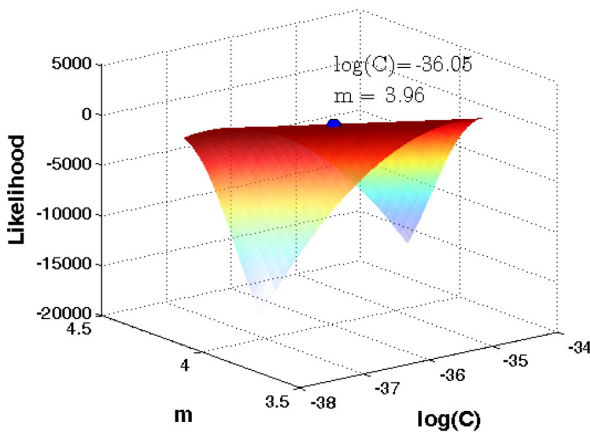


Figure 3. Likelihood values estimated by MLE: Paris (left) and Walker (right).

The parameters obtained by the all methodologies for a single model are very close to each other. In general, m is similar for all models but the value of C is smaller in the Walker model than for the Paris model due to the effect of the stress ratio, R . Figure 3 shows the likelihood of the parameters for both models and the best $\log(C)$ and m combination giving the highest likelihood is marked.

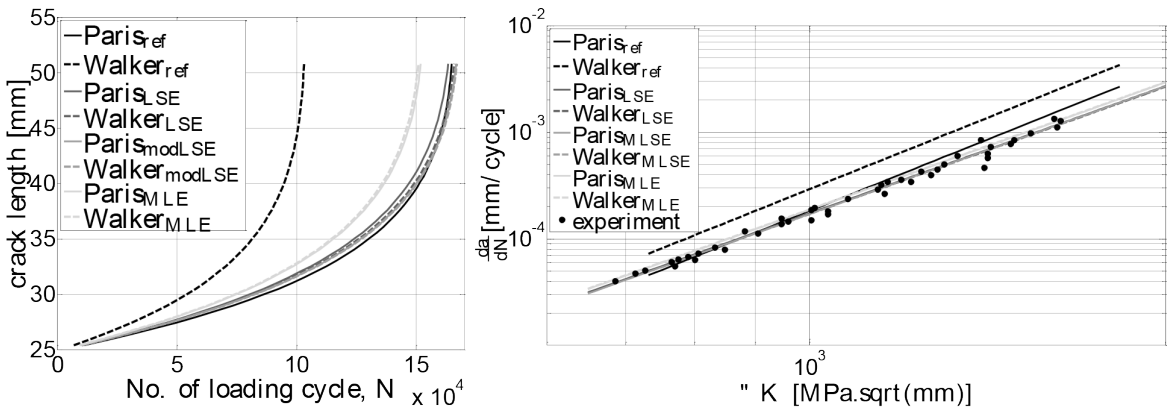


Figure 4. Fatigue crack growth rate curves with estimated C and m value.

Fatigue crack growth rate curves have been plotted by using the estimated parameters and also by using the parameters obtained from the NASGRO data manual (Youseffi 1978, Nasgro 2006); in Figure 4.

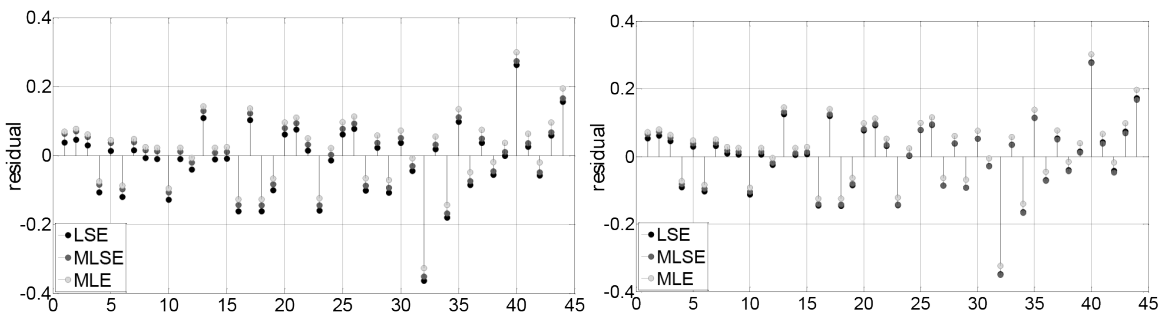


Figure 5. Residual estimation: Paris (left) and Walker (right).

Figure 5 shows the residual obtained in each model obtained from the parameters estimated by all three methods.

CONCLUSION AND OUTLOOK

The parameters of two fatigue crack growth models have been estimated with three different methods. The methods considered uncertainty associated with the estimated parameters as well as with other influencing parameters, such as, stress ratio. At the current stage of this work one cannot jump into the conclusion that the one model is better than the other one. But this leads to the fundamental question that how to select the best model among a set of competitive models. The answer would be a model should be selected not only based on its ability to fit current data but also to predict future data. So, a realistic data set has to be considered to assess the reliability of the presented approach. Besides that, fatigue CGMs capable of describing region I and region III are also necessary to take into account for the better assessment of parameter estimation methods.

ACKNOWLEDGEMENT

Financial support for this work was provided by the German Research Foundation (DFG) via Research Training Group “Assessment of Coupled Experimental and Numerical Partial Models in Structural Engineering (GRK 1462)”, which is gratefully acknowledged.

REFERENCES

Barenblatt, G. a. (1980). Incomplete self-similarity of fatigue in the linear range of crack growth. *Fatigue & Fracture of Engineering Materials & Structures*, 3(3), 193 – 202.

Barenblatt, G. I. (1996). *Scaling, self-similarity, and intermediate asymptotics: dimensional analysis and intermediate asymptotics* (Vol. 14). Cambridge University Press.

Collipriest Jr, J. (1972). An experimentalist’s view of the surface flaw problem. *The Surface Crack- Physical Problems and Computational Solutions*, 43 – 61.

Compact Tension Specimen. (n.d.). Retrieved from Wikipedia: http://en.wikipedia.org/wiki/Compact_tension_specimen

Fisher, J. W. (1984). *Fatigue and fracture in steel bridges. Case studies*. John Wiley and Sons.

Forman, R. (1972). Study of fatigue crack initiation from flaws using fracture mechanics theory. *Engineering fracture mechanics*, 4(2), 333 – 345.

Klysz, S. a. (2012). *Good Practice for Fatigue Crack Growth Curves Description*. InTech.

Lampman, S. R. (1996). *ASM Handbook: Volume 19, Fatigue and Fracture*. ASM International.

NASGRO. (2006). (NASA-JSC and Southwest Research Centre) Retrieved from Fracture Mechanics and Fatigue Crack Growth Analysis Software: <http://www.swri.org/4org/d18/mateng/matint/nasgro/>

Paris, P. a. (1963). A critical analysis of crack propagation laws. *Journal of Fluids Engineering*, 85(4), 528 – 533.

Radhakrishnan, V. (1979). Parameter representation of fatigue crack growth. *Engineering Fracture Mechanics*, 11(2), 359 – 372.

Skorupa, M. (1996). *Empirical trends and prediction models for fatigue crack growth under variable amplitude loading*. ECN.

Spagnoli, A. (2005). Self-similarity and fractals in the Paris range of fatigue crack growth. *Mechanics of materials*, 37(5), 519 – 529.

Walker, K. (1970). The effect of stress ratio during crack propagation and fatigue for 2024-T3 and 7075-T6 aluminum. *Effects of environment and complex load history on fatigue life*, ASTM STP, 462, 1 – 14.

Wheeler, O. E. (1972). Spectrum loading and crack growth. *Journal of Fluids Engineering*, 94(1), 181 – 186.

Willenborg, J. a. (1971). *A crack growth retardation model using an effective stress concept*. DTIC Document.

Youseffi, K. a. (1978). *Fatigue crack initiation and propagation in steels exposed to inert and corrosive environments. Final report*, May 1, 1977--December 31, 1977. doi:DOI: 10.2172/5005512

CURRENT TRENDS IN THE ANALYSIS OF METAL STRUCTURES

Kudishin Y. I.

**Professor, PhD, Chief Specialist, JSC "TSNIIPSK named after Melnikov N.P.",
ykudishin03@gmail.com**

Grishin A.S.

**Candidate of Science, Chief Scientist in Dynamics and Seismic Stability Department,
Public Corporation "Atomenergoproekt",
gandrey24@gmail.com**

INTRODUCTION

Nowadays in domestic and foreign regulatory literature limit states verification of metal structures are carried out only for individual structural elements (CP 16.13330.2011 2011, EN 1993-1-1 2005, EN 1993-1-3 2006). For example, for a beam under axial force and bending, limiting state verification is checked by the formula:

$$\frac{N}{A \cdot \varphi} \leq R \quad (1)$$

where N is the design force in the beam with appropriate partial factors;

A is the geometric parameter of a cross section - the cross-sectional area in the case of compression/tension; the section modulus in the case of bending;

φ is the buckling coefficient, representing the ratio of the critical buckling stress σ_{cr} to the design resistance R ;

R is the design resistance calculated on the value of yield strength.

Formula (1) can also be rewritten as:

$$N \leq N_c \quad (2)$$

where $N_c = R \cdot A \cdot \varphi$ is the ultimate bearing capacity of a beam.

It should be noted that the ultimate bearing capacity is defined for a particular structural element reaching its yield stress or critical buckling stress. However, this is not actually true, as the structure remains functional after the transition of the material in a plastic state, as well as into the post-

buckling phase of functionality. The most evident example can be observed in the functionality of the so-called light steel thin-walled structures (LSTS).

Currently, by means of modern engineering software, there is the possibility (Federal Statute # 184-FS 2003, Federal Statute # 384-FS 2009) of explicitly determining the value of the ultimate bearing capacity of a structure corresponding to the right side of the formula (2). And this is done not only for an individual structural element, but also for multiple structural complexes composed of beams, shells, solids, etc. with different physical and mechanical properties.

However, the existing framework for structural analysis (CP 16.13330.2011 2011, EN 1993-1-1 2005, EN 1991-1-3 2006) is almost entirely based on simplified calculation methods and does not contain regulations that allow an engineer to use all the features of modern engineering software.

The purpose of the article is to demonstrate the current trends in the analysis of metal structures.

The goals of the work are the following: illustration of a new approach to the analysis of metal structures by ultimate bearing capacity; taking into account features of LSTS analysis; and the direction of current framework development due to the wide range of applications of computer technologies.

MATERIALS AND METHODS

Material Model

In performing calculations of metal structures a bilinear material model with isotropic hardening was used. This material model describes well the majority of structural metals. Figure 1 shows a bilinear material model for steel C245 that is used in this paper.

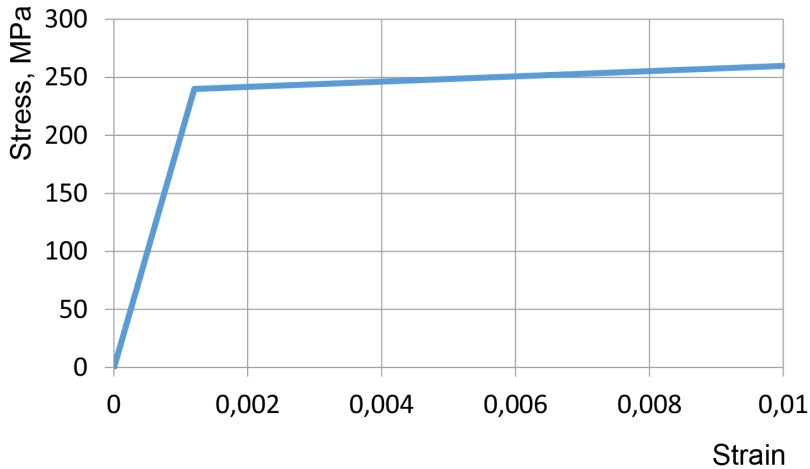


Figure 1. Bilinear material model of steel C245 with isotropic hardening (yield stress $R_y = 240$ MPa, tangent modulus $E_t = 2 \cdot 10^9$ MPa).

Analysis Method

To solve the problems of deformable solid mechanics the multi-physical software ANSYS and NASTRAN were used. These programs are based on the finite-element method and enable us to perform a geometrically and physically nonlinear analysis of building structures.

Computational Procedure for Calculation of The Ultimate Bearing Capacity

Solving the problem of the static equilibrium of a structure in a geometrically and physically nonlinear formulation determines the ultimate bearing capacity of a structure or a separate structural element. Modern computer software uses the Newton-Raphson approach to solve nonlinear problems - the external load is subdivided into a series of load increments that are applied over several load steps.

Let us assume that there is a finite number (i) of any types of loads and impacts (P_i) such as self-weight of a structure, service load, wind and snow loads, etc. which can be represented by components of a load vector $P = P(P_1; P_2; P_3; \dots; P_i)$. Then, taking into account the hypothesis of simple loading, the solution of the nonlinear task gives the following dependence of the maximum nodal displacement of the structure on the load vector, shown in Figure 2.

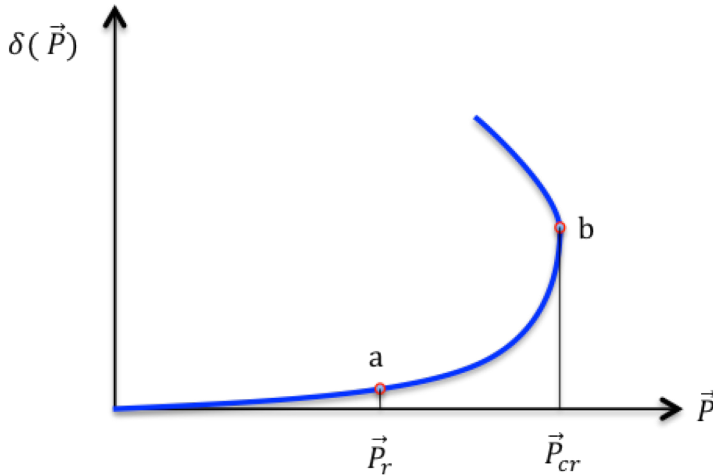


Figure 2. Dependence of the maximum nodal displacement of the structure on the load vector.

Theoretically, there is a point b on the curve, where the derivative $\frac{d\delta}{dP} \rightarrow \infty$. This point corresponds to the ultimate bearing capacity of the whole structure, since further increase of displacement is only possible when decreasing the load vector. At point b, the criterion of Lyapunov's stability meets - when for a small load increment ΔP there is an instantaneous change in the function $\Delta\delta$ (Malkin 1966, Demidovich 1967).

The ratio of the ultimate bearing capacity of a structure P_{cr} to the design load P_r is the overall factor of safety (γ) of the structure:

$$\gamma = \frac{P_{cr}}{P_r} \geq [\gamma] \tag{3}$$

This ratio indicates a margin of safety of a structure in relation to design loads and must be standardized, and its minimum value is to be specified in a project statement or in special regulations.

Along with the graph on Figure 2, non-linear analysis provides information on the stress-strain state of all structural elements. The criteria for the implementation of ultimate limit states of bearing capacity are the following expressions:

- for beam elements:

$$\gamma_n \cdot \frac{\sigma_{max}}{R_y \cdot \gamma_c} \leq 1 \quad \text{and} \quad \gamma_n \cdot \frac{\tau_{max}}{R_s \cdot \gamma_c} \leq 1 \tag{4}$$

where σ_{\max} and τ_{\max} are the maximum normal and shear stresses in structural elements at the unfavourable combination of design loads;

R_y and R_s are the material design resistances to normal and shear forces, respectively;

γ_n is a reliability factor for the importance of the structure or a partial factor covering uncertainty in the resistance model plus geometrical deviations if these are not modelled explicitly;

γ_c is a service factor or a conversion factor taking into account volume and scale effects, effects of moisture and temperature, and any other relevant parameters.

- for plane, shell and solid elements the maximum value of von Mises stresses $(\sigma_{\text{eqv}})_{\max}$ shall not exceed the design resistance with appropriate safety factors:

$$(\sigma_{\text{eqv}})_{\max} = \sqrt{\sigma_x^2 + \sigma_y^2 - \sigma_x \cdot \sigma_y + 3\tau_{xy}^2} \leq \frac{R_y}{\gamma_n} \cdot \gamma_c \quad (5)$$

Sometimes in local zones of stress concentration, plastic deformation may occur which is acceptable under static loads. However, the maximum strain value in these areas should not exceed 3%:

$$(\varepsilon_{\text{eqv}})_{\max} = \sqrt{\varepsilon_x^2 + \varepsilon_y^2 - \varepsilon_x \cdot \varepsilon_y + 3\varepsilon_{xy}^2} \leq 3\% \quad (6)$$

DESCRIPTION OF TESTS

Two series of computational tests were performed. The first series of calculations (Tests 1 - 3) is set up with the purpose of illustrating the determination of the ultimate bearing capacity of almost any kind of beams using Lyapunov's criterion. The second series (Test 4) is to determine correction factors according to formula (7).

The ultimate bearing capacities were determined by the examples of structures with the following parameters:

Test 1. Eccentrically compressed U-beam of length 4.1 m, wall thickness - 2 mm, height - 400 mm and a flange width - 125 mm. Longitudinal compressive forces are applied to the butt ends of the beam.

Test 2. A thin-walled I-beam (LSTS class) of length 6 m, cross-sectional height is 500 mm, wall thickness - 2 mm, cross-section of the flange of the beam - 180x5 mm. The beam is subjected to transverse uniformly distributed load applied to the top flange.

Test 3. A thick-walled I-beam, with the same parameters given in Test 2, but with increased thicknesses: wall - 9 mm, flange of the beam - 14 mm.

The ratio of the width of the plate (b) to its thickness (t) is the plate slenderness, $\lambda_w = b/t$.

The results of calculations for Tests 1-3 were obtained for individual structural members using shell finite elements. However, three-dimensional modelling of complicated structures with shell elements leads to cumbersome design models. The alternative to it is to use beam-type finite elements.

In this regard, there is an issue of the adequacy of analysis obtained with beam and shell finite-element design models, bearing in mind that, all other factors being equal, the latter give more correct results.

Test 4. On the basis of individual structural members by varying different parameters such as the geometric shape of a cross section (channel, C-section, I-beam), the flexibility of plates ($\lambda_w = b/t = 50 \dots 300$), the type of loading (eccentric compression, lateral bending), their ultimate bearing capacities were determined by modelling structural members with beam and shell finite elements.

As a result of the corresponding calculations the coefficient k representing the ratio of the ultimate bearing capacities of structures, obtained using shell ($P_{cr \text{ shell}}$) and beam ($P_{cr \text{ beam}}$) finite element schemes was calculated:

$$k = \frac{\vec{P}_{cr \text{ shell}}}{\vec{P}_{cr \text{ beam}}} \quad (7)$$

RESULTS

Tests 1 and 2

Figure 3 shows examples of the post-buckling stages of the considered structures made of LSTS (shell finite elements are used). Test 1 was carried out for a U-beam at the slenderness of the beam web $\lambda_w = b/t = 400/2 = 200$ (Figure 3a). In Test 2 an I-beam with the slenderness of the beam web $\lambda_w = b/t = 500/2 = 250$ was analysed (see Figure 3b).

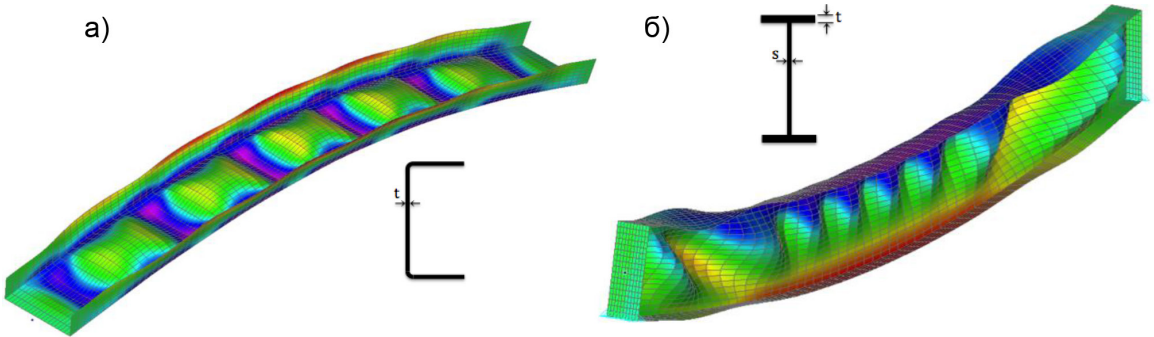


Figure 3. Deformed shapes of the eccentrically compressed U-beam (a) and the I-beam made of LSTS under bending (b). Highlighted contour plots of the normal stresses

Graphs of the maximum nodal displacements over the corresponding load vectors for the eccentrically compressed U-beam (Test 1) and the I-beam under bending (Test 2) are shown in Figure 4. In Figure 4a the horizontal axis represents the compressive force applied in the design model as a proportion to 100 kN. The vertical axis in Figure 4a shows displacements (in cm) at the point located at the mid-span of the web of the U-beam. In Figure 4b the abscissa is the transverse load in a proportion to 306 N/cm applied to the top flange of the beam. The vertical axis in Figure 4b represents displacements (in cm) at the top edge of the beam web at the mid-span.

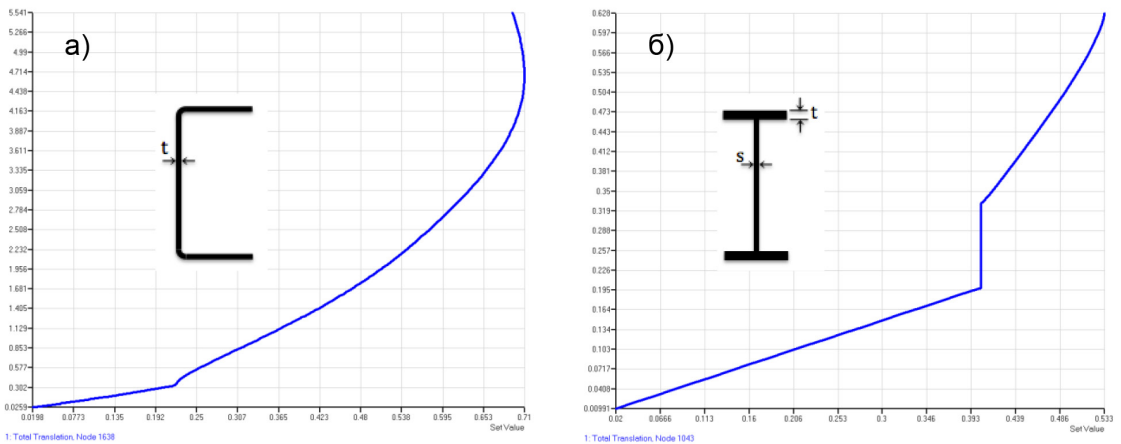


Figure 4. Dependencies of the maximum nodal displacements (cm) on the corresponding load vectors (in proportions) for the eccentrically compressed channel beam (a) and the I-beam under transverse bending (b)

When the slenderness of a beam web $\lambda_w > 100$, local buckling appears without structural failure. The local buckling is marked with sudden changes in the

graphs in Figure 4. In both cases, the stresses in the elements do not exceed the yield stress, i.e. the building structures continue to function elastically in the post-buckling stage up to the complete exhaustion of the bearing capacity.

As is shown in Figure 4a, the structural failure occurs at load $P_{cr} = 0,71 \cdot 100 = 71 \text{ kN}$. Substantial growth of displacements begins around load $\vec{P}_r = 0,6 \cdot 100 = 60 \text{ kN}$. Thus the overall factor of safety is $\gamma = \frac{P_{cr}}{\vec{P}_r} = \frac{71}{60} = 1,18$.

The graph in Figure 4b shows that the structural failure occurs at uniform load $\vec{q}_{cr} = 0,533 \cdot 306 = 163,1 \text{ N/cm}$. The design load can be taken as equal to $\vec{q}_r = 0,5 \cdot 306 = 153 \text{ N/cm}$. Then the overall factor of safety is $\gamma = \frac{\vec{q}_{cr}}{\vec{q}_r} = \frac{163,1}{153} = 1,07$.

It should be noticed that in both graphs in Figure 4, there are jumps of displacements, which correspond to the loss of local stability of the elements. Then, the post-buckling stages of the beams begin, leading up to complete structural failure. Let us note that in the case of the U-beam the post-buckling zone of functionality is more than twice longer subcritical zone, which is a significant reserve in the design that is not taken into account in the design standards. For the I-beam the reserve of the post-buckling functionality is approximately 25%.

From Figure 4a it is clearly visible the reverse branch, which is due to the geometric nonlinearity in the functionality of the compressed structure. Points on the reserve branch correspond to the static equilibrium of the beam at a decrease of the external load. The balance is provided by the increase of its deflection. However, this phenomenon is not always possible. For example, on the transverse bending of the beam shown in Figure 4b the graph of displacement versus load cannot have a reverse branch as increasing the deflection while decreasing load is physically impossible. The absolute values of displacements with local buckling in the structural members of LSTS are not significant, as shown in enlarged form in the figures above. In any case, they are comparable with the values of the imperfections of real structures.

Test 3

A force-displacement diagram for the thick-walled beam is plotted in Figure 5. Such dependence is typical for structural members with the slenderness of its compound plates $\lambda_w < 100$. Exhaustion of the bearing capacity of these bars is accompanied by so-called plastic hinges. Structural failure of resembling beams occurs with the appearance of plastic hinges.

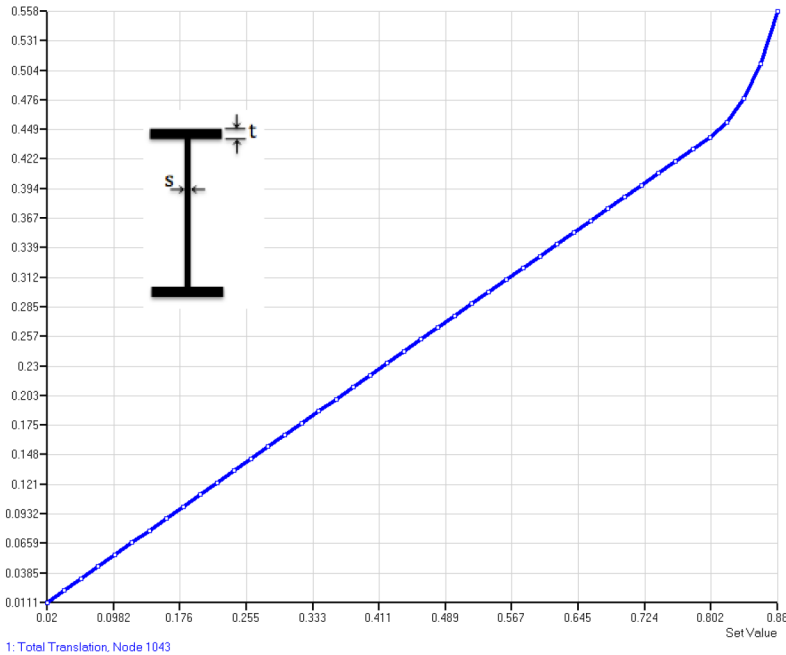


Figure 5. A force-displacement diagram for the thick-walled I-beam.

The applied load for the calculation is 1080 N/cm. The ultimate bearing capacity is $\vec{q}_{cr} = 0,88 \cdot 1080 = 950,4$ N/cm. So the design load is $\vec{q}_r = 0,8 \cdot 1080 = 864$ N/cm. Thus the overall safety factor is

$$\gamma = \frac{\vec{q}_{cr}}{\vec{q}_r} = \frac{950,4}{864} = 1,1.$$

Test 4

In this test, the graphs of a change of the coefficient k in accordance with formula (7) are obtained for several types of cross sections and types of loading by varying the greatest beam web composing a cross-sectional shape $\lambda_w = b/t$, for different slenderness ratios of the beam $\lambda = l_0/i$, where l_0 is the effective length of a beam, i is the minimal beam section radius of inertia. Figures 6 and 7 illustrate the dependence of k on the beam web λ_w for eccentrically compressed U- and C-shaped beams at various slenderness ratios λ (26, 29.8, ... 104.2), respectively.

Figures 8 and 9 show the similar dependences for C-shaped and I-shaped bending beams, respectively. Bending occurs in the plane of the beam web under uniformly distributed load. For convenience of presentation and generalization of the results of calculations in Figures 6 - 9 dimensionless parameters are used - slenderness of the beam web λ_w and slenderness ratio of the beam λ .

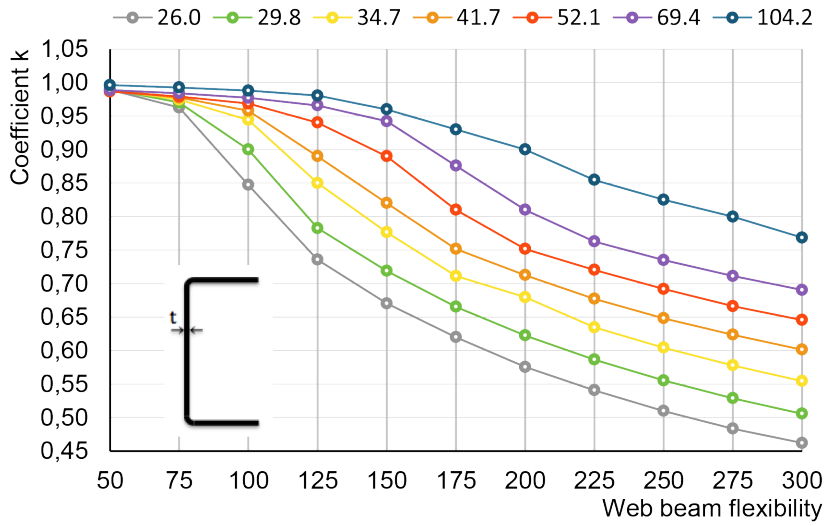


Figure 6. Eccentrically compressed U-beam. Dependence of k on the beam web at various slenderness ratios.

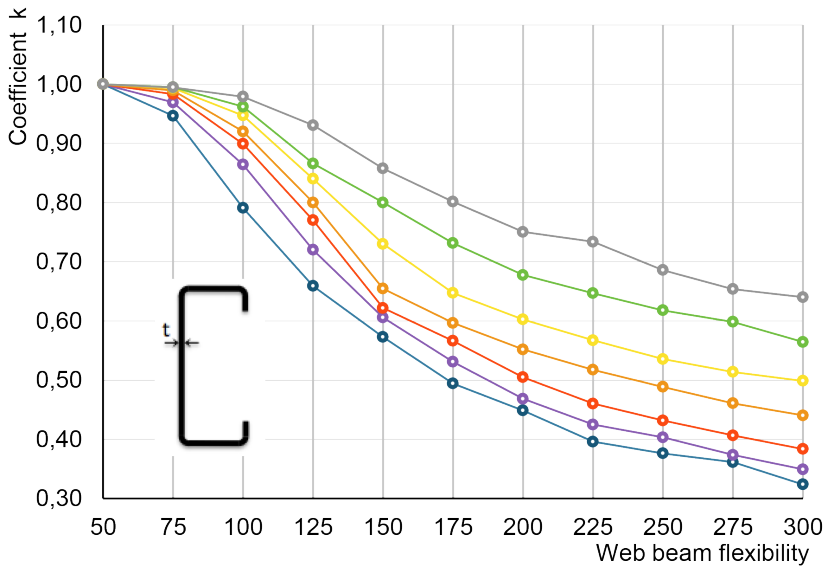


Figure 7. Eccentrically compressed C-shaped beam. Dependence of k on the beam web at various slenderness ratios

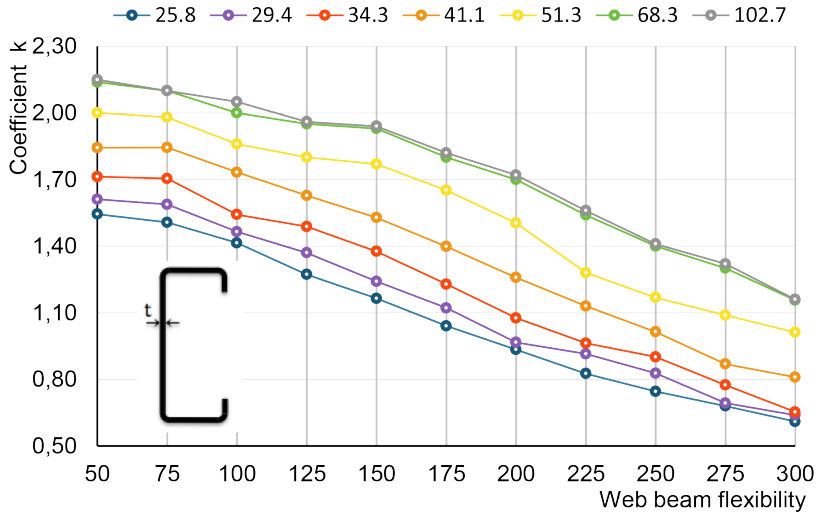


Figure 8. C-shaped beam under uniformly distributed load. Dependence of k on the beam web at various slenderness ratios.

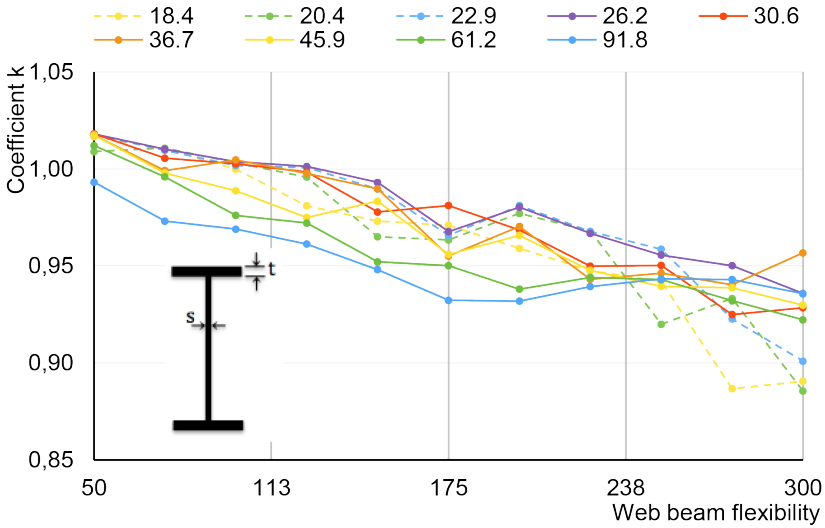


Figure 9. I-shaped beam under uniformly distributed load. Dependence of k on the beam web at various slenderness ratios.

DISCUSSION AND CONCLUSIONS

This paper presents a new approach to the analysis of metal structures on the ultimate bearing capacity taking into account broad capabilities of computational software. This approach will further move away from manual element-by-element verifications of limit states including strength, stability and stiffness of building structures. The proposed method allows us to consider the entire design as a whole system.

From the design experience of the application of this technique, the value of $[\gamma]$ in formula (3) may vary from 1.1 to 1.6 depending on deformation behaviour. It is desirable that the value of the design load corresponds to the beginning of a sharp, avalanche-like growth of displacements during iterative process of computing. In most instances, the quantity $[\gamma]$ is much higher than the mentioned values.

For beams with relatively small slenderness of beam webs (about 50 ... 100) composing a cross-sectional shape their force-displacement curves exhibit a smooth behaviour up to structural failure. Plastic hinges accompany the structural failure of similar beams.

Studies have shown that for thick-walled structural elements coefficient k is substantially equal to unity. For thin-walled elements (LSTS) coefficient k can take values less than or greater than unity. Then the calculation results obtained with beam elements must be corrected by multiplying them by coefficient k .

The graphs shown in Figures 6 - 9 should be regarded as illustrative material. In general, the value of the correction factor k should be specifically determined for each type of structure subjected to particular loading, fastening, and other relevant features, as these factors can significantly affect the results of the calculations, especially for the structures made of LSTS.

REFERENCES

Code of Practice CP 16.13330.2011 Steel Structures (Harmonized edition of SNiP II-23-81* Steel Structures).

Demidovich B.P. Course on mathematical theory of stability. Chapter II — M.: Science, 1967.

EN 1993-1-1: 2005 Design of steel structures - Part 1-1: General rules and rules for buildings.

EN 1993-1-3: 2006 Supplementary rules for cold formed members and sheeting.

Federal Statute # 184-FS of the 27th of December 2003. About Technical Regulations.

Federal Statute # 384-FS of the 30th of December 2009. Technical regulations on the safety of buildings and facilities.

Malkin I.G. Stability theory of motion. — M.: Science, 1966.

LOCAL BENDING STABILITY OF TUBES WITH RECTANGULAR CROSS SECTION

Grudev Ivan Dmitriyevich

Doctor of Engineering Science, Professor
Moscow State University of Civil Engineering (MGSU), Russia

ABSTRACT

Cross -bending stress state of thin-shell tube with rectangular cross section is described with terms of elastic theory without using the flat cross-section hypothesis. But hereby we realize, that shear stresses play the basic role as in tube walls so in compressed and tensile flanges of tube. Distribution of lateral stresses and the flat cross-section hypothesis ensue only from requirements of tube bending in the plane of mirror symmetry and the ratio of thin walls and flanges of tube. From equations of elastic theory it follows, that lateral axis stresses in the flanges of tube are constant by width, but in the walls they are changed linearly along height. Those particular results provide the basis for the flat cross-section hypothesis. The shear flows in tube flanges and walls near the corners of cross-section are coordinated. Stress state of longitudinal fibers is determined by shear stresses caused by the load and the elastic foundation. The action of elastic foundation results from secondary cross-bending of the tube walls and flanges. The median fibers of compressed flange in the most stressed cross-section have secondary buckling and form a short fold under load of transverse forces imposed because of the plastic property of material. It is the secondary buckling which determines the load-carrying capacity of a beam in general. A post-critical deformation occurs during the decreasing load. The method of calculating of the secondary buckling process and the post-critical deformation of a beam, which determines it's load-carrying capacity, is presented in this paper.

INTRODUCTION

The cross-bending of a tube with rectangular cross-section is considered. It is known, that the cross-section of a tube is characterized by four dimensions L , b , h , t . They are shown on a Figure 1, the dimensions satisfy next inequalities:

$$L \gg b, h \gg t \quad (1)$$

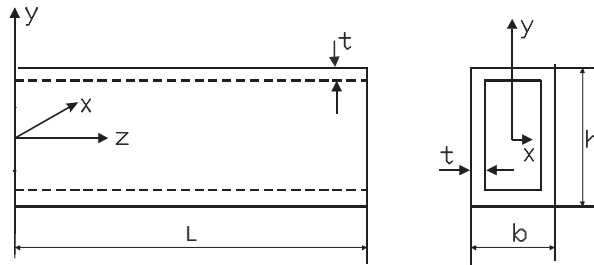


Figure 1. Geometrical dimensions of a tube.

The special terminology is used here: side walls of a tube are called left and right walls, the wall of a tube when $y = h/2$, is called the top flange, and the wall when $y = -h/2$ is called bottom flange.

At first, calculation model, which is shown in Figure 2, it is assumed as classical model: the load Q in the middle when $z = L/2$ acts along a line and is imposed only to the walls, the forces on the supports are imposed to the edges $z = 0$ and $z = L$ and are determined by shear stresses, τ_{zy} .

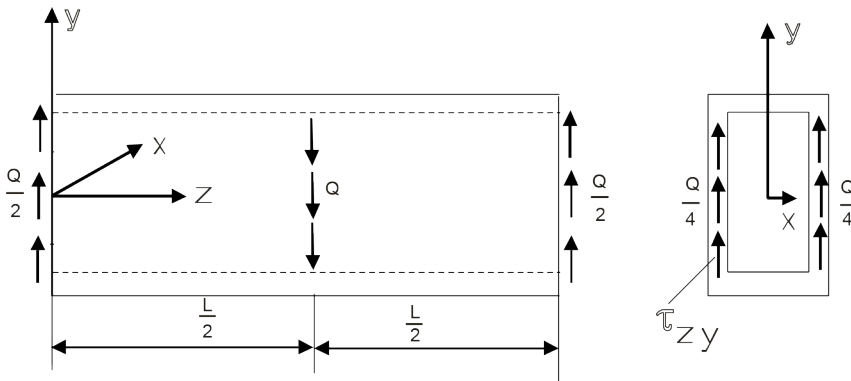


Figure 2. The model of the application of forces when $z = 0, z = L/2, z = L$.

Background

The stress condition is determined by equations of stability of the theory of elasticity in a simple form:

$$\frac{\partial \sigma_x}{\partial x} + \frac{\partial \tau_{xy}}{\partial y} + \frac{\partial \tau_{xz}}{\partial z} = 0; \frac{\partial \tau_{yx}}{\partial x} + \frac{\partial \sigma_y}{\partial y} + \frac{\partial \tau_{yz}}{\partial z} = 0; \frac{\partial \tau_{zx}}{\partial x} + \frac{\partial \tau_{zy}}{\partial y} + \frac{\partial \sigma_z}{\partial z} = 0. \tag{2}$$

There are no any loads acting in the direction of x-axis in this problem, there are no also external normal loads at the y-axis. So at the first approximation we can write the evident relationships.

$$\sigma_x = 0; \sigma_y = 0; \tau_{xy} = 0. \quad (3)$$

Considering these relationships, the system of equations (2) is resulted to the next equations:

$$\frac{\partial \tau_{xz}}{\partial z} = 0; \frac{\partial \tau_{yz}}{\partial z} = 0; \frac{\partial \tau_{zx}}{\partial x} + \frac{\partial \tau_{zy}}{\partial y} + \frac{\partial \sigma_z}{\partial z} = 0. \quad (4)$$

From the first two equations follows

$$\tau_{zx} = \tau_{zx}(x, y), \tau_{zy} = \tau_{zy}(x, y). \quad (5)$$

In the last equation (4) it is appropriate to pass on to the next non-dimensional variables:

$$x = \frac{2x}{b}; y = \frac{2y}{h}; \tilde{z} = \frac{2z}{L}. \quad (6)$$

The equation will be:

$$\frac{1}{b} \frac{\partial \tau_{zx}}{\partial x} + \frac{1}{h} \frac{\partial \tau_{zy}}{\partial y} + \frac{1}{L} \frac{\partial \sigma_z}{\partial \tilde{z}} = 0 \quad (7)$$

Now we can analyse the stress state of the top (compressed) flange of the left half of the beam, and the stress state of the bottom (stretched) flange and the right half of the beam can be written according to symmetry.

The stresses τ_{zy} on the upper and lower faces of the both flanges are strictly equal to null, that's why at the first approximate, if we take in account the inequation(1), we can consider that in all cross-sections of flanges:

$$\tau_{zx} = \tau_{zx}(x), \tau_{zy} = 0, \sigma_z = \sigma_z(x, z). \quad (8)$$

Equation (7) can lead to the next:

$$\frac{\partial \tau_{zx}}{\partial x} + \frac{b}{L} \frac{\partial \sigma_z}{\partial z} = 0. \quad (9)$$

This equation is strictly satisfied, if the both members of the sum are separately equal to the constant. In this case every member of sum is simply integrated and as a result we get:

$$\tau_{zx} = \tau_{zx1}x + \tau_{zx0}; \sigma_z = \sigma_{z1}\tilde{z} + \sigma_{z0}, \text{ where } \tau_{zx1}; \tau_{zx0}; \sigma_{z1}; \sigma_{z0} \text{ are constants} \quad (10)$$

For the top flange $\sigma_{z1} < 0$.

When $z=0$ the inequation is $\sigma_z=0$, so $\sigma_{z0}=0$. Considering the symmetry we should understand, that $\tau_{zx}(x) = -\tau_{zx}(-x)$, that's why we should regard $\tau_{zx0}=0$. As a result we have:

$$\tau_{zx} = \tau_{zx1}x, \sigma_z = \sigma_{z1}\tilde{z}. \quad (11)$$

From the equation (9) follows the connection between the two last constants, one of which will be determined hereinafter:

$$\tau_{zx1} = -\frac{b}{L}\sigma_{z1} \quad (12)$$

Now we should analyse stresses in the walls, taking into account that due to symmetry both walls are in identical stress state. Shear stresses τ_{zx} on external and internal faces of every wall are strictly equal to null. Thus, at the first approximate we obtain:

$$\tau_{zx} \equiv 0; \tau_{zy} = \tau_{zy}(y); \sigma_z = \sigma_z(y, \tilde{z}) \quad (13)$$

Equation (7) will takes the next form:

$$\frac{d\tau_{zy}}{dy} + \frac{h}{L} \frac{\partial \sigma_z}{\partial \tilde{z}} = 0 \quad (14)$$

For the solution of this equation with the solution for the flanges it is logical to accept

$$\sigma_z = \sigma_{z1}y\tilde{z} + \sigma_{zw} \quad (15)$$

and σ_{z1} - introduced hereinbefore constant.

From the boundary condition $\sigma_z = 0$ when $\tilde{z} = 0$ follows:

$$\sigma_{zw} = 0 \quad (16)$$

Finally, we have for the wall:

$$\sigma_z = \sigma_{z1}y\tilde{z} \quad (17)$$

The equation (14) takes the form:

$$\frac{d\tau_{zy}}{dy} + \frac{h}{L}\sigma_{z1}y = 0 \tag{18}$$

This equation is easily integrated and gives:

$$\tau_{zy} = -\frac{h}{2L}\sigma_{z1}\tilde{y}^2 + \tau_{zy0} \tag{19}$$

Considering that normal axis stress changes linearly in both variables: \tilde{y} and \tilde{z} , so we can use the formula:

$\sigma_z = \frac{M}{W}$ and among other factors $\sigma_{z\max} = \frac{M_{\max}}{W}$, where W -moment resistance of the whole cross-section and it can be written as:

$$W = (b - 2t)t(h - t)^2/h + th^2/3 \quad \text{or} \quad W = Ch^2t, \quad \text{where} \tag{20}$$

$$C = \left(\frac{b}{h} - \frac{2t}{h}\right)\left(1 - \frac{t}{h}\right)^2 + \frac{1}{3},$$

Besides, the constant's degree of order is unity.

Considering the equations $\sigma_{z\max} = \sigma_{z1}; M_{\max} = QL/4$ and relations (12), we get from the fluid-flow analogy that streams of shear stresses in the corners of cross-section should be continuous:

$$\tau_{znpu\tilde{x}=1} = -\tau_{zynpu\tilde{y}=1} \tag{21}$$

whence it follows that $\tau_{zy0} = -\tau_{zx1} + \frac{h}{2L}\sigma_{z1}$ which gives:

$$\tau_{zy0} = -\frac{Q}{4W}\left(b + \frac{h}{2}\right) \tag{22}$$

Substituting the values of found constants in the equation (19) we get:

$$\tau_{zy} = -\frac{Q}{4W}\left[b + \frac{h}{2}(1 - \tilde{y}^2)\right] \tag{23}$$

Maximal value of shear stresses in absolute magnitude when $\tilde{y} = 0$ is equal

$$\tau_{zy\max} = \frac{Q}{4W}\left(b + \frac{h}{2}\right)$$

and the values of shear stresses in the right upper corner are equal:

$$\tau_{zx} = \tau_{zy} = -\frac{Qb}{4W}$$

Graphs of shear and normal stresses are shown on a Figure 3.

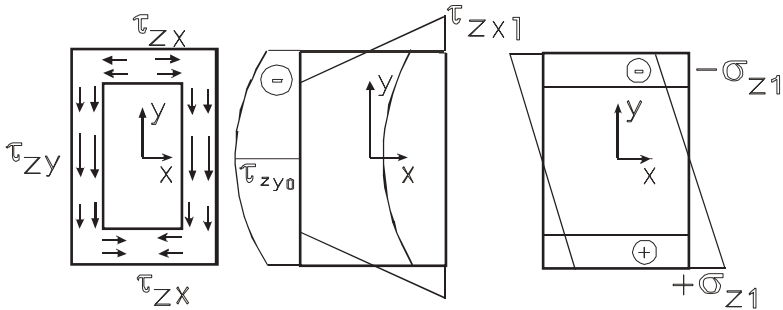


Figure 3. Shear and normal stress diagram.

METHOD

Presently we should analyse a strip notched out from the top (compressed) flange along the whole length of the tube, the width of which is δ_x , which satisfy equations $t < \delta_x < b$.

At first it is convenient to take this strip in the middle of the top flange, as it is shown in Figure 4.

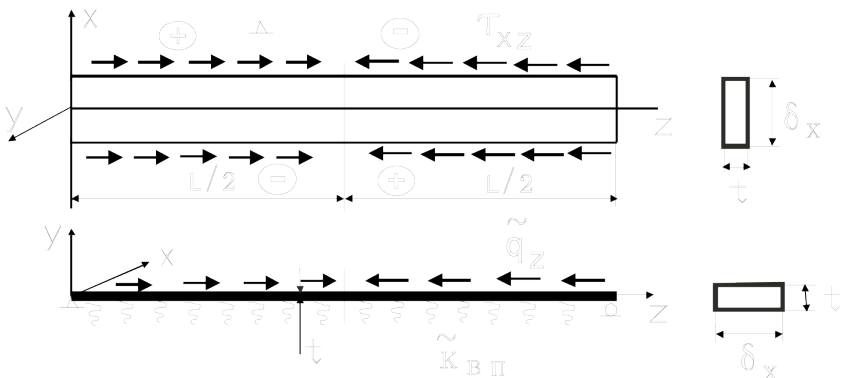


Figure 4. The central strip notched out from the top (compressed) flange with the width of δ_x .

The axis load q_z is determined by shear stresses τ_{zx} , acting in side faces of the notched out strip :

$$q_z = 2\tau_{zx}t \tag{24}$$

In terms of the results above, the values of shear stresses affect the strip and are:

$$\tau_{zx} = \frac{\delta_x}{b} \tau_{zx1} \tag{25}$$

from which we get formula for the load:

$$q_z = \pm \frac{Q\delta_x t}{2W} \tag{26}$$

Because of symmetry the loads have different signs at each half of the bar (Figure 4). For solving the problem of stability of the notched out strip it is necessary to introduce dimensionless variables for the moments, forces and loads [1]:

$$\bar{M} = \frac{ML}{EJ}; \bar{N} = \frac{NL^2}{EJ}; \bar{q} = \frac{qL^3}{EJ}, \quad \text{where} \quad J = \frac{\delta_x t^3}{12}.$$

We have from the previous formulas for dimensionless longitudinal loading:

$$\bar{q}_z = \pm \frac{6Q}{Ch^2 E} \left(\frac{L}{t}\right)^3 \tag{27}$$

It must be emphasized, that formulation for dimensionless load does not depend on width δ_x of the notched out strip. Besides. it does not depend on the location of the notch through the width of flange, as it is determined only by the derivative $\frac{\partial \tau_{zx}}{\partial x}$, which is constant through the width of the flange.

For the clarity of the graphs obtained, an example is now given of a thin-shell tube with the dimensions: $b=100\text{mm}$, $h=120\text{ mm}$, $t=2\text{mm}$ and the length $L=1\text{m}$. Design strength is taken as $R_y=24\text{kN/cm}^2$. Radius of gyration of the notched out strip is

$$i = \sqrt{\frac{J_{on}}{\delta_x t}} = \frac{t}{\sqrt{12}} = \frac{1}{\sqrt{3}} \text{ MM}.$$

Slenderness of the notched out strip $\lambda_{on} = L/i = 1732$, which is a large value in calculations of bar stability, the bearing capacity of the flexural bar in normative documents is determined by formula:

$$\sigma_{\max} = \frac{M_{\max}}{W} \leq R_y \gamma_c, \tag{28}$$

In other words, it is considered that the loads comparable to design strength are admitted in the most loaded element of cross-section. Considering this it is essential to make a conclusion, that an axial compressed bar (in our case a notched out strip) needs stabilization with the help of other elements of cross-section because of its heavy stress and ease flexibility. Stated another way, a notched out strip should have elastic foundation. Stiffness of foundation must be determined as accurately as it is possible. At the first approximation we need to calculate dependence of deflection in the middle of of compressed flange on normal load using calculation model, which is shown in Figure 5.

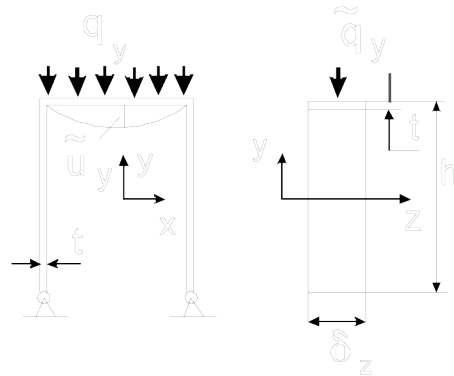


Figure 5 - A calculation model for the foundation stiffness of the notched out strip.

Thus, we have a problem of determination of dimensionless stiffness stabilization k_{on} of notched out strip from the other elements of tube's cross-section. Dependence of vertical distributed load, acting along the axis of notched out strip q_{yven} on deflection of notched out strip in the middle of the top flange of tube is determined.

The solution of this problem is made according to method from the book [1] using program Visual Basic for arc. A cross stripe with a width δ_z is notched out from a tube with the rectangular cross-section and is loaded with a uniformly distributed load q_{ymn} .

RESULTS

As a result the vertical deflection u_{mn} is calculated in the middle of beam. The strip is considered to have hinged ends (Figure.5). Check calculations have shown that the result depends weakly on character of ends' supports. The initial data is geometric sizes of strip and calculated according to them geometric characteristics:

$$b=100\text{mm}; h=120\text{mm}; t=2\text{mm}; \quad (29)$$

$$L_{mn} = b + 2h; i = t / \sqrt{12}; \lambda_{mn} = L_{mn} / i; J_{mn} = \frac{\delta_z t^3}{12}.$$

As follows from the calculation, linear dependence with small deflections is determined between dimensionless values of load and deflection, which is shown in Figure 6.

$$\tilde{q}_{ymn} = \tilde{k}_{mn} \tilde{u}_{ymn}, \text{ где } \tilde{q}_{ymn} = \frac{q_{ymn} L_{mn}^3}{E J_{mn}}; \tilde{k}_{mn} = \frac{k_{mn} L_{mn}^4}{E J_{mn}}; \tilde{u}_{mn} = \frac{u_{mn}}{L_{mn}}. \quad (30)$$

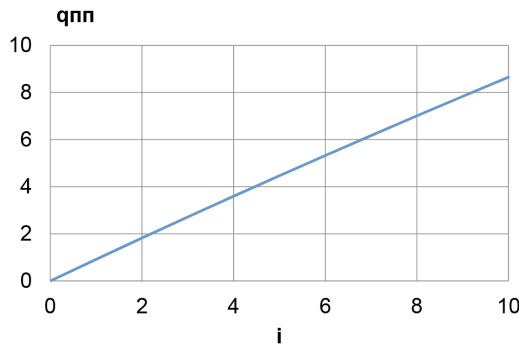


Figure 6. Dependence $\tilde{q}_{ymn}(\tilde{u}_{mn})$ by steps of deformation

A step of deformation is equal to $\Delta \tilde{u}_{mn} = 0.00001$, when stiffness is determined as $\tilde{k}_{mn} = \frac{\tilde{q}_{ymn}}{\tilde{u}_{ymn}} = 18350$.

Thus, for convenience we can have the equation of lateral dimensions of notched out strips: $q_{y_{en}} \delta_z = q_{ymn} \delta_x$ where from follows $q_{y_{en}} = q_{ymn}$. If we will consider, that dimensional deflections and moments of inertia are equal

$$u_{mn} = u_{en}; J_{mn} = J_{en} = \frac{\delta l^3}{12}$$

of dimensional stiffnesses: $k_{mn} = k_{en}$, and dimensionless quantities of stiffnesses are connected between each other:

$$\tilde{k}_{en} = \tilde{k}_{mn} \left(\frac{L}{b + 2h} \right)^4 = 1,373 * 106 \quad (31)$$

Now, the calculation of dimensional critical value of the load Q is left in order to determine the load-bearing capacity of tube with the rectangular cross-section during it's bending. A computer program is used to solve it. The program is devised for solving a similar problem concerning bending of an I-section beam. The problem is solved in physical and geometrical non-linear position by this program. The process of deformation of the notched out strip under

the load \tilde{q}_{yem} is calculated by taking into account stiffness of foundation \tilde{k}_{em} , change of deflections of a bending strip and plastic characteristics of steel with the help "unified diagram of construction steel".[2].

A curve of resistance is calculated, in other words a dependence of the load q_z on contraction of the notched out strip is determined. The contraction is created by displacing of the right end $\tilde{u}_z(1)$, (Figure 4). A curve of resistance is shown in Figure 7.

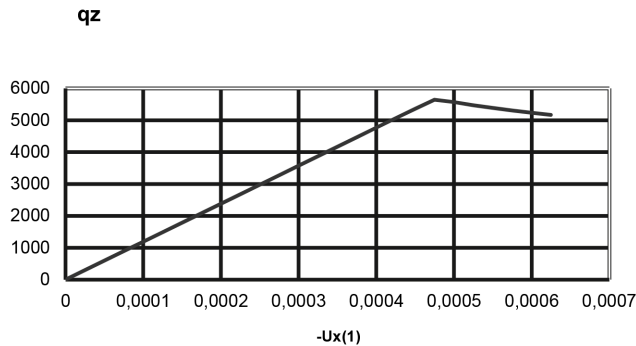


Figure 7. A curve of resistance of the notched out strip.

A point of limit of elasticity and appearance of plastic deformation in bottom fiber of notched out strip corresponds to critical state when the maximum load $\tilde{q}_{zcr} = 5644$, after this all the deformations take place in post-critical condition when the load is decreasing. That is why the displacing of the right end of the notched out strip is used as an argument. The load is not used as an argument. The critical value of transverse load Q_{cr} is written by formula (27) and is equal

$$Q_{cr} = \frac{Ch^2E}{6} \left(\frac{t}{L} \right)^3 \tilde{q}_{zcr} = 17,85 \text{ KH.}$$

A kind of secondary buckling of the notched out strip is very interesting, the strip is shown for critical value in Figure 8 when $\tilde{u}_x(1) = 0,00045$ and for two post-critical values $\tilde{u}_x(1) = 0,000475$ and $\tilde{u}_x(1) = 0,0005$.

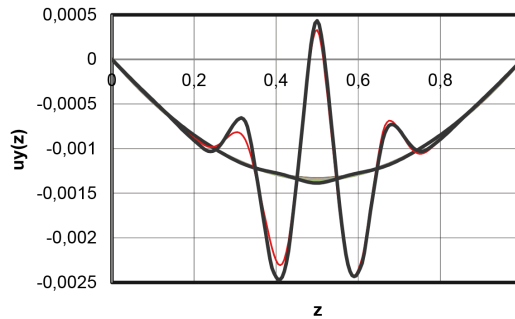


Figure.8. Deflections $\tilde{u}_y(\tilde{z})$ for critical and two post-critical conditions.

Post-critical deflections in the middle point of the length have bigger value in absolute magnitude then initial deflection.

CONCLUSIONS

A traditional test of strength with the same basic data with the use of relation and formulas (20) and (28) gives:

$$Q = \frac{4WR_y\gamma_c}{L} = 29.07$$

when coefficient of the conditions of work $\gamma_c = 0.95$

So, traditional calculation leads to oversize result and, ultimately, to stress emergency situation.

REFERENCES

1. Grudev I.D. Load bearing capacity of compression elements of braced structures: monograph, FSEI HPE, Moscow: MGSU, 2012.-386 p.
2. Odessky P.D, Belsky G.E. About single approach to use of diagrams of work of construction steel. Industrial engineering, 1980, № 7, p. 4 – 6.

GENERATION OF NUMERICAL SIMULATION MODELS IN STRUCTURAL DYNAMICS FROM COMPUTED TOMOGRAPHY IMAGE DATA

Ingmar Stade

**Bauhaus-Universität Weimar, Research Training Group 1462, Weimar, Germany,
ingmar.stade@uni-weimar.de**

Carsten Könke

**Bauhaus-Universität Weimar, Institute of Structural Mechanics, Weimar, Germany,
carsten.koenke@uni-weimar.de**

ABSTRACT

The paper presents a strategy for and the outcome of the generation of numerical simulation models in structural dynamic simulations based on image data, which is obtained from X-ray computed tomography scan. The derivation of FE-models utilizing real manufactured components reduces the influence of geometrical uncertainties in dynamic simulations, which are main sources of uncertainties besides material properties and damping. In comparison to optical measurements, this non-destructive testing method creates a data set of the entire volume including all internal and hidden features. For the FE-model generation the exterior and interior surfaces are extracted from the volume data set. A surface model is created which also can distinguish between different materials in the structure and which is the basis for the automatic mesh generation process. The quality of the image-based FE-models is validated with an example from mechanical engineering by comparing simulation results to those obtained by experimental dynamic tests.

INTRODUCTION

In numerical simulations different sources of uncertainties can affect the obtained solution. Besides discretization errors also variations of the material parameters like Young's modulus, density and Poisson's ratio, uncertainties in the geometry or damping parameters have an impact on the results. To reduce deviations between geometry of real manufactured components and numerical models for structural dynamic applications the generation and the use of FE models based on 3D image data is shown.

For capturing the geometrical dimensions of a structure or a component different measurement methods are available. They can be divided into destructive and non-destructive procedures. While tactile or optical non-destructive procedures can provide information about the geometry of

exterior boundary surfaces the technique of X-ray computed tomography (CT) can also obtain data of internal surfaces for complex structures.

COMPUTED TOMOGRAPHY

X-ray computed tomography relies on measuring the weakening of X-ray beams by penetrating through a structure. The attenuation of the intensity of the X-ray beams is caused by the interaction of photons with the atoms of a material. Different interaction mechanism between a photon and an atom like photoelectric effect, Compton effect or pair production depending on the energy of the radiation can be distinguished. Therefore, the weakening of the radiation is dependent on the energy of the photons, on the atomic number of the involved elements, on the density and the thickness of the investigated object. Equation (1) relates the attenuated intensity I of a beam ray to the initial intensity I_0 for monochromatic radiation

$$I = I_0 e^{-\int_0^d \mu(x) ds} \quad (1)$$

with the attenuation coefficient $\mu(\mathbf{x})$.

To obtain a three dimensional distribution of the attenuation coefficient of an inhomogeneous object, a high number of weakening integrals or projections have to be acquired from all different directions, at minimum covering an angle range of 180° . The investigated sample volume is then computed by use of mathematical reconstruction algorithms like filtered backprojection, Fourier method or iterative reconstruction. The result is a three dimensional image (regular grid) which consists of volume pixels (voxels) with a gray value representing the attenuation coefficient.

For polychromatic radiation the intensity is obtained by integration over all energies Equation (2) (Kalender 2006). In that context the energy dependence of the linear attenuation coefficient is problematic, especially it is responsible for the existence of beam hardening artefacts.

$$I = \int_0^{\max E} I_0(E) e^{-\int_0^d \mu(x,E) ds} dE \quad (2)$$

In general the setup of a CT device consists of an X-ray source and a detector. The radiated beam can have a fan or cone geometry in combination with a line or a flat panel detector. The investigated sample is placed between X-ray source and detector. In comparison to medical devices where the CT scanner and detector rotate around the investigated object, in industrial applications the sample is positioned on a rotating table and rotates during the measurement.

DERIVATION OF NUMERICAL MODELS

The generation of FE models is based on surfaces, which are extracted from the 3D image data set (Stade 2014). To consider different existing materials, for each material pairing a boundary surface is extracted. The Marching Cubes isosurface contouring algorithm (Lorenson 1987) implemented in the free open source C++ library Visualization Toolkit (VTK) (Schroeder 2004) is used to obtain these surfaces. The threshold value needed for each material combination is determined based on the detection of connected edge voxels by approximation of spatial derivatives of the grey values in the voxel data set. For this, the canny edge detection algorithm (Canny 1986) available in the free open source C++ library Insight Segmentation and Registration Toolkit (Ibanez 2003) is applied. After extraction, the polygonal surfaces are smoothed and the number of triangles are reduced using algorithms implemented in the software GOM Inspect 7.5 SR1 (GOM 2012). Further, disturbing artefacts were repaired by deleting and filling of small parts of the surfaces.

The different surfaces are further treated with the help of mesh processing algorithms implemented in the software packages GOM Inspect 7.5 SR1 and ANSYS ICEM CFD. In a first step each surface is cut at the line where the different materials meet each other. The part of each surface that did not belong to the applied threshold for the specific material combination is removed. After that, the resulting surfaces are combined to a single surface model through application of hole filling and surface extension algorithms.

For the generation of a finite element volume model using the prepared surfaces, the meshing software package ANSYS ICEM CFD is used. A robust octree-based meshing algorithm which is able to deal with small errors like small gaps, overlaps or distorted elements in the polygonal surface representation is adopted. During the mesh generating process the meshes are adaptively refined based on the curvature properties of the input surfaces. Subsequently the element and node number are reduced with the help of automatic coarsening algorithms by keeping the mesh size constant for elements building the surface. After improving the mesh quality based on the aspect ratio of the element volumes in relation to the circumscribed radius the linear 4-node tetrahedral elements are converted to 10-node elements

APPLICATION EXAMPLE IN STRUCTURAL DYNAMICS

Introduction

As an application example a casted 6 cylinder aluminium engine block is used. The die-casted engine block is composed of the crankcase (upper part) and of the bedplate (lower part) (Figure 7). The parts consists of aluminium as the main material with cylinder linings made out of cast iron and bearing inserts made out of sintered steel. The engine block has a length of 660 mm, a height of 220 mm and a width of around 420 mm.

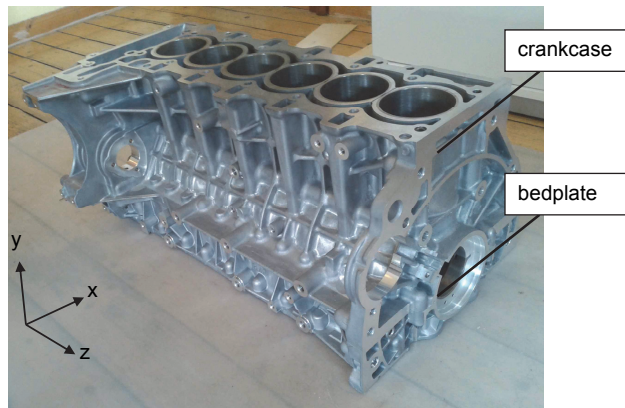


Figure 7: Investigated 6-cylinder engine block

3D image acquisition

Due to the dimensions of the investigated 6-cylinder casted aluminium engine block, a high energy X-ray computed tomography device was used. The setup consisted of a linear accelerator with a X-ray energy up to 11 MeV in combination with a line detector. Due to reduced scattered radiation in comparison to the use of a flat panel detector, high quality 3D images with only low noise influences (random variation of the voxel values) and a high contrast were produced. Only small, stripe-shaped artefacts through the attendance of 2 different materials with high density differences are obtained. The disadvantage of this setup is the relatively high scanning time of 25 hours. The obtained image consists of 1395 and 1080 voxels in x- and y-directions and 1393 layers in z-direction (longitudinal axis). The voxel spacing in x- and y-direction is 0.29 mm. In z-direction 0.48 mm spacing was reached. Two slices in longitudinal direction out of the whole 3D image data set are shown in Figure 8.

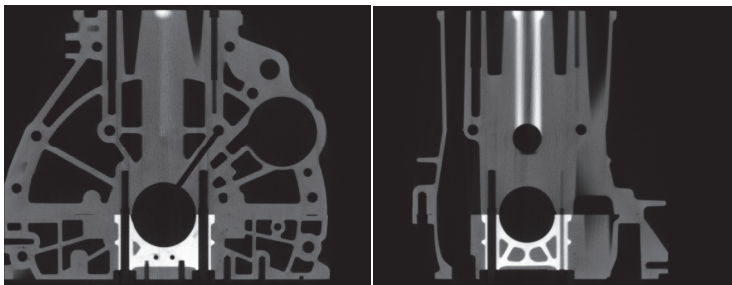


Figure 8: 2 slices of the volume data set (z-direction)

FE-model

The generation of the FE model is based on surfaces, which were extracted from the 3D image data set. To consider the different existing materials, for each material pairing (air-aluminium, aluminium-steel, steel-air) a boundary surface was computed. The result taking into account the different existing materials for the engine block and the cylinders can be seen in Figure 9.

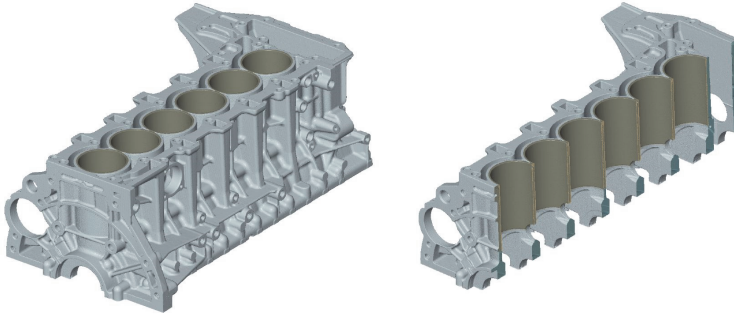


Figure 9: Extracted and processed surface, regions in grey describe the aluminium part of the engine block, regions in brown describe steel liners in the cylinders

Different meshes with varying minimal element sizes from 1.5 to 4.5 mm were generated (Figure 10). The resulting meshes contained between 1.1 (4.5 mm minimal element size) and 9 million (1.5 mm minimal element size) nodes. The material parameters Young's modulus, density and Poisson's ratio were determined from material specimen of similar components. For the Young's modulus and Poisson's ratio ultrasonic testing with a relative measurement uncertainty below 3 % was used. The density was determined using Archimedes principle with an uncertainty below 1%

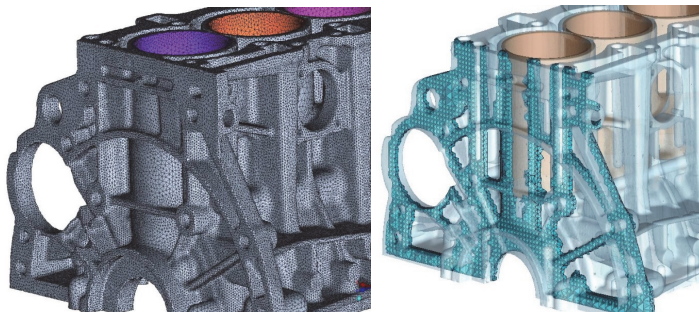


Figure 10: FE volume mesh min. element size 2.5 mm (left, exterior view) and 4.5 mm (right, section view)

Experimental investigation

The mode shapes and natural frequencies were determined up to 2500 Hz with a Polytec PSV-400 scanning laser vibrometer in combination with shaker excitation (Stade 2014). The natural frequencies were verified with additional measurements performed with a tri-axial accelerometer and hammer excitation. The structure was supported on elastic cables on 3 positions which can be seen in Figure 11.

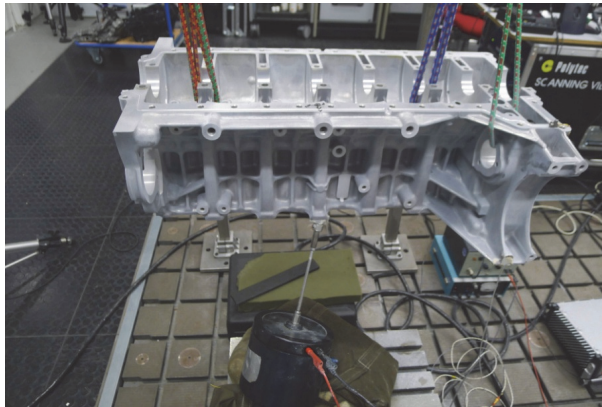


Figure 11: Experimental setup

Results

The results from the image based FE-simulation and from the experimental modal analysis are compared. 18 mode shape pairs are investigated. Since the modes are only lightly coupled due to the low damping properties of the structure the mode shapes were determined based on the real part of the frequency response function (velocity responses). The comparison between the obtained natural frequencies from the image based FE-simulation and experiments are shown in table Table 4. A finite element mesh with a minimal element size of 4.5 mm has been applied for the simulation. Only small deviations of maximum 0.9 % and of an average of 0.3 % between measured and computed natural frequencies can be observed. For the correlation of the numerical and experimental mode shapes the Modal Assurance Criterion (MAC) is used.

It is defined as

$$\text{MAC}(\{\psi_X\}, \{\psi_A\}) = \frac{|\{\psi_X\}^T \{\psi_A\}|^2}{(\{\psi_A\}^T \{\psi_A\})(\{\psi_X\}^T \{\psi_X\})} \quad (3)$$

where $\{\psi_A\}$ represents the numerical eigenvector containing the measured degrees of freedom. $\{\psi_X\}$ is the eigenvector of the experimental derived mode.

Figure 12 shows the comparison between the numerical and experimental obtained mode shapes. Values mostly higher than 0.9 on the main diagonal were evaluated which indicate a high correlation (Ewins 2000). The good quality in the obtained results is also represented by small off-diagonal terms.

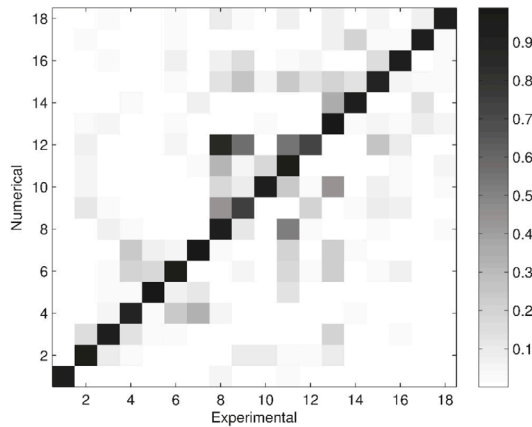


Figure 12: Comparison numerical and experimental mode shapes (MAC Matrix)

Table 4: Comparison natural frequencies from experimental test and image-based FE-model

Mode	Exp. Freq. [Hz]	Sim. Freq. [Hz]	Difference [%]	MAC
1	378	376	-0.5	0.92
2	810	809	-0.1	0.96
3	1028	1027	-0.1	0.91
4	1094	1093	-0.1	0.89
5	1268	1262	-0.5	0.98
6	1308	1300	-0.6	0.96
7	1350	1341	-0.7	0.99
8	1646	1640	-0.2	0.92
9	1676	1669	-0.4	0.75
10	1760	1760	0	0.94
11	1928	1927	-0.1	0.97
12	2044	2047	+0.2	0.72
13	2102	2097	-0.2	0.98
14	2208	2202	-0.3	0.93
15	2276	2266	-0.4	0.89
16	2326	2324	-0.1	0.94
17	2378	2355	-0.9	0.95
18	2454	2443	-0.5	0.96

CONCLUSION

The presented work describes the possibilities of the derivation of FE-models from 3D image data. Further, it shows the quality of the image based simulation by comparing experimental and simulated natural frequencies and mode shapes for a mechanical engineering application example. The used model strategy is able to produce high quality FE-meshes from image data even for large, complicated structures. The very good correlation of the results of experimental tests and numerical simulations shows the capabilities of numerical models based on the real geometry for structural dynamic applications.

ACKNOWLEDGEMENTS

Financial support for this work was provided by the German Research Foundation (DFG) via Research Training Group 1462, which is gratefully acknowledged.

REFERENCES

- (Canny 1986) Canny J. A Computational Approach to Edge Detection. IEEE Transactions on Pattern Analysis and Machine Intelligence, Vol. 8, No. 6, 1986, pp. 679 – 698.
- (Ewins 2000) Ewins D.J. Modal Testing: Theory, Practice and Application. Research Studies Press, 2000
- (GOM 2012) Inspektion, V7.5 SR1 Handbuch (Grundwissen und Aufbauwissen). GOM – Gesellschaft für optische Messtechnik mbH, 2012
- (Ibanez 2003) Ibanez L., Schroeder W. The ITK Software Guide. Kitware Incorporated, 2003
- (Kalender 2006) Kalender W.A. Computertomographie: Grundlagen, Geräte-technologie, Bildqualität, Anwendungen. Publicis Corporation Publ., 2006
- (Lorenzen 1987) Lorenzen W.E., Cline H.E. Marching cubes: A highresolution 3D surface construction algorithm. ACM Computer Graphics. Vol. 21, No. 4, 1987, pp. 163 – 169
- (Schroeder 2004) Schroeder W., Martin K., Lorenzen B. The Visualization Toolkit: An Object-oriented Approach to 3D Graphics. Kitware Incorporated, 2004
- (Stade 2014) Stade I., Guist C., Könke C., Richter T. Assessment of image-based FE Models in structural dynamics. Proceedings of ISMA 2014

DYNAMIC PROPERTIES IDENTIFIED FROM MEASUREMENTS ON IDENTICAL POLE STRUCTURES

Peter Olney, Ingmar Stade, Maher Deeb

Research Training Group 1462

Bauhaus-Universität Weimar

Berkaer Straße 9, 99425 Weimar, Germany

ABSTRACT

Variability in structures necessitates the consideration of properties as stochastic variables. Often, however, civil engineering structures are unique; they differ in size, use, and boundary conditions, which can limit investigations of variability to material properties. In the context of experimentation, variability also exists in identified parameters due to uncertainties in measurements, sensors, and identification procedures. Poles, such as those often used for electricity cables or lighting poles, provide the opportunity to investigate the stochastic variability of many nearly identical structures that are not complex in form or size. This paper will detail the experimental investigations undertaken to determine the variability of these simple structures. Dynamic vibration measurements were collected on 15 poles along a newly constructed high-speed railway track. Ambient, impulse, and shaker excitations were applied while measuring the response with accelerometers. The variability of the identified parameters for the set of poles is shown related to the individual experimentation methods. Then uncertainties associated with the individual poles are shown through a comparison of the identified parameters. Questions related to the quality of the measurement system, the sensor positions, the excitation, and the collected data are outside the scope of the current discussion and can reasonably be omitted since the same experimental setup was used on each pole investigated. These presented investigations illustrate the types and amount of variability that may exist in structures and the uncertainties related to experiments.

INTRODUCTION

Variability in structures necessitates the consideration of properties as stochastic variables. Often, however, civil engineering structures are unique; they differ in size, use, and boundary conditions, which can limit investigations of variability to material properties. In the context of experimentation, variability also exists in identified parameters due to uncertainties in measurements, sensors, and identification procedures. Poles, such as those often used for electricity cables or lamp posts, provide the opportunity to investigate the stochastic variability of many nearly identical structures that are not complex in form or size. Materials used to build poles include wood, steel, and reinforced concrete; the ones considered in this

study are prestressed concrete poles. While certain phenomena observed on wood, steel and concrete structures are different, the principles of applying experimental modal analysis remain the same. All types of structures can be described by the same differential equations independent of the material, which often simply relate to the coefficients in these equations. For a system described by the standard equation of motion, these coefficients are reduced to basic dynamic structural properties (natural frequencies, damping and mass). Concrete structures tend to be stiffer than their steel counterparts, with higher mass and damping. This influences the frequency and damping values obtained from dynamic experimentation, but does not have a large influence on the conclusions drawn from repeated experiments on structures designed and built to be identical. It is generally known that variability in concrete structures tends to be higher than in steel ones, namely occurring from differences in manufacturing processes for both geometry and material. However, the focus of this work is not so much on the magnitudes of the variances themselves, but on the differences that can be seen in repeated experiments of real, theoretically identical, structures.

EXPERIMENTAL INVESTIGATIONS

A series of poles that will be used for electricity distribution along a new railway line were chosen for this investigation. Since sets of the poles were designed and manufactured to be identical, they proved to be the perfect candidates for repeated experimentation. Their location along a railway construction site also provided convenient access to a large number of them in close proximity. As in the case of typical experimentation on civil engineering structures, dynamic measurements were collected using accelerometers. While the structural system is rather simple (cantilever column), the fact that there are a large number of identical poles allows for types of investigations that are usually not possible for most civil engineering structures. Each pole considered in this study was of the same type (same material, reinforcement, and intended use) and was 10m tall including the foundation. The measurement system is shown in Figure 1, including an example setup on one pole as well as the sensor positions for the two setups used.

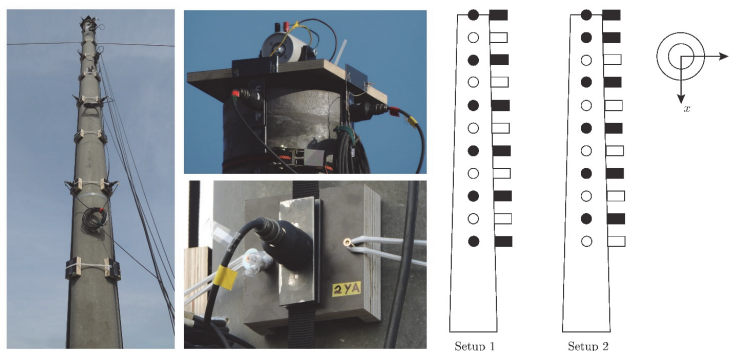


Figure 1. Measurement system. Pole with attached sensors (left), shaker (middle top), sensor attachment (middle bottom), sensor positions (right).

An apparatus was constructed to quickly attach the sensors on each pole and to ensure that the measurement locations remained the same relative to the top of the structure. The shaker and two fabric ribbons were attached to a wooden top plate. The ribbons were placed on each side of the wooden plate to create two lines of sensors perpendicular to each other. Small wooden blocks were placed along the ribbons at a distance of 0.75m that conformed to the curved shape of the pole and had small steel plates fixed to them. The accelerometers were fastened to a separate set of steel plates of the same size with high strength magnets on the opposite side. Elastic bands were wrapped around the pole and fixed to the wooden blocks to keep them securely fastened to the structure. The sensor magnet assembly could then be quickly fixed to and removed from the pole at each measurement location. Two setups of the accelerometers were used: one reference and five roving sensors per setup and measurement direction. This totalled in 11 components in each direction with a fairly dense vertical grid over the top 7.5m of the pole. Four different excitations were used: sweep sine shaker, ambient, hammer near the base, and Gaussian white noise from the shaker. The first three excitations returned the best response data to observe the lowest modes. The shaker with noise excitation proved nearly unusable for identification purposes probably due to low shaker acceleration amplitudes and the resulting small response. Additionally for technical reasons due to limitations of the shaker, the frequency range was from 10 to 100 Hz for the sweep sine excitation. The ambient and hammer excitations may vary slightly from pole to pole, however, the input amplitude from the shaker was kept constant. Of course the environmental conditions, such as wind and temperature, could not be controlled since the measurements were taken outside on site. A total of 26 poles were investigated over the course of four days; 15 of these poles are assessed in this study.

TEST RESULTS

The acceleration time histories from each excitation and pole were combined between the two setups and used to identify the dynamic properties of each individual pole. Stochastic subspace identification (SSI) was used to obtain these results, which are summarized in Table 1 by their occurrence and statistical properties. Eight modes were consistently identified on the poles, although the number of times that each was identified varied by pole and excitation. For this reason, the number of identifications (the last column in the table) is not constant for each mode. There was also a tendency for the lower case of closely spaced modes to have more identifications than the upper. This relates to the limitations of applying SSI and assigning identified frequencies and mode shapes to a particular mode.

Table 1. Results summary: statistical properties. (μ - mean, σ - standard deviation, CoV - coefficient of variation)

mode	Frequency [Hz]			Damping [%]			#
	μ	σ	CoV [%]	μ	σ	CoV [%]	
1	3.48	0.07	2.0	0.6	0.3	45.0	43
2	3.91	0.08	2.1	5.2	2.4	45.8	31
3	17.48	0.52	3.0	2.0	0.8	40.2	52
4	17.60	0.30	1.7	0.8	0.2	32.5	31
5	45.63	0.95	2.1	2.1	1.1	50.3	43
6	45.20	0.99	2.2	2.2	0.7	32.6	22
7	87.47	1.27	1.5	3.7	0.5	12.3	11
8	87.96	1.04	1.2	3.7	0.7	18.5	12

It should be noted, however, that in each instance, more than one mode of a pair was identified from a set of measurements. There were never more than two modes for each pair. For example, if a set of measurements resulted in the identification of two third modes, no fourth mode was assigned. Figures 2 and 3 show histograms of the frequencies identified and the corresponding damping ratios for the first and third modes, respectively. Also found in the figures are plots of the mode shape components over the height of the pole and in the x-y cross-section plane. The typical mode shapes of first and second bending for a cantilever column are clearly visible from the plots of the x-component over the height.

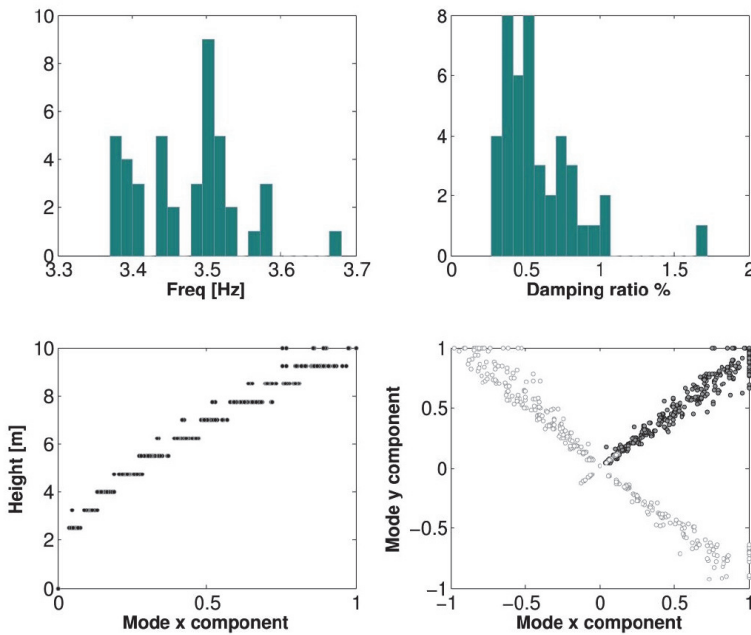


Figure 2. Statistical results: 1st mode

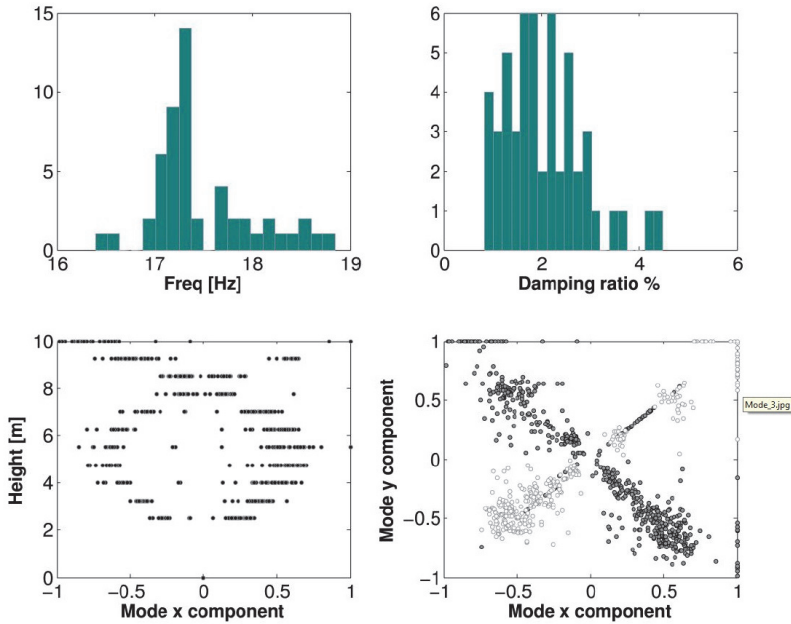


Figure 3. Statistical results: 3rd mode

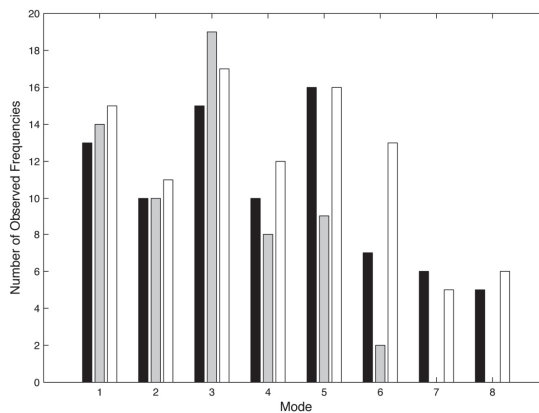


Figure 4. Observed frequencies by mode and excitation: black - sweep sine shaker (in X), grey - ambient, white - hammer near base (in Y)

Figure 4 shows an overview of the number of identified frequencies separated by excitation and mode. The shaker and hammer excitations produced data with reasonably similar frequency content, while the ambient excitation suffered in the higher modes. The first two modes were identified with the sweep sine excitation even though the sweep started with 10Hz, well above the first frequency around 3Hz. The existence of this frequency in the shaker excitation can probably be traced to the fact that it is visible in the ambient excitation data.

Table 2 gives an overview of the ranges of the frequencies observed for the first eight modes as a comparison by considering individual poles in contrast to the previous table that showed the range by means of standard deviation over all excitations and pole.

Table 2. Observed range [%] of frequency values as percentage of mean, for all excitations on individual poles and separated by excitation comparing all combinations of two poles.

mode	Single Pole		Pole to Pole (mean)			Pole to Pole (max)		
	mean	max	shaker	ambient	hammer	shaker	ambient	hammer
1	0.5	2.7	2.6	2.1	2.4	8.3	5.6	6.3
2	1.1	4.6	2.8	1.8	2.5	6.9	5.7	8.1
3	2.9	9.0	3.4	4.1	4.8	9.1	13.1	12.3
4	0.3	0.7	1.4	2.3	2.2	3.8	6.4	7.0
5	0.8	2.7	1.5	1.4	2.4	4.4	4.4	9.1
6	0.3	1.4	0.7	7.6	2.0	1.5	7.6	8.5
7	0.1	1.0	1.4	-	2.0	3.4	-	4.8
8	0.2	2.0	1.8	-	1.1	3.6	-	2.5

The single pole column shows the mean and maximum ranges of frequencies for all excitations on each individual pole. The pole to pole columns take the frequencies identified on individual poles for each excitation and shows the mean and maximum ranges when considering every combination of two poles. This table emphasizes the possible variance in the identified frequencies caused by different excitations and shows what variance exists between two poles related to the separate excitations. Three conclusions from the table highlight aspects from this study that can only be seen since the experimentation was performed on a series of identical poles.

1. Over all modes, the small variation of frequencies identified on a single pole shows a weak dependence of the range on the excitation.
2. In general, the pole to pole mean and maximums are greater when compared to their respective single pole ranges, which is an indication of actual differences between the poles.
3. Larger uncertainty in the third mode shows difficulties in applying the identification method (SSI) with two closely spaced modes.

FURTHER DATA ANALYSIS

MAC evaluation

For the comparison of numerical and experimental mode shapes, the Modal Assurance Criterion (MAC) also known as Modal Shape Correlation Coefficient (MSCC) is used. It can be written as

$$\text{MAC}(\psi_X, \psi_A) = \frac{|\{\psi_X\}^T \{\psi_A\}|^2}{(\{\psi_A\}^T \{\psi_A\})(\{\psi_X\}^T \{\psi_X\})} \quad (1)$$

where ψ_A represents a numerical eigenvector containing the measured degrees of freedom. ψ_X is the mode shape of an experimental derived mode. If two modes are perfectly correlated, a value of one will be obtained where low correlation results in values near zero. In real applications a value of 0.9 shows a good correlation where values of less than 0.1 indicate uncorrelated modes (Ewins 2000). The comparison of the numerical and experimentally obtained mode shapes is shown in Table 3 for one pole, where the high values on the main diagonal show a very good correlation.

Table 3. MAC matrix computed between experimental (f_{exp}) and numerical (frequencies, f_{num}) mode shapes. ($\epsilon_{\text{rel}} = (f_{\text{exp}} - f_{\text{num}}) / f_{\text{exp}}$)

mode	1	2	3	4	5	6	f_{num} [Hz]	ϵ_{rel} [%]
1	0.996	0.001	0.003	0.046	0.022	0.004	2.84	18.5
2	0.001	0.995	0.012	0.001	0.000	0.025	2.98	23.8
3	0.000	0.000	0.959	0.014	0.003	0.049	16.74	4.2
4	0.071	0.001	0.034	0.977	0.069	0.002	17.74	-0.8
5	0.028	0.001	0.003	0.064	0.864	0.002	44.88	1.6
6	0.001	0.002	0.026	0.001	0.116	0.938	45.53	-0.7

Sensitivity investigation

In order to obtain some indication of the possible causes of the observed variations in the poles as described in the previous sections, it is reasonable to perform a sensitivity analysis using a numerical model. Numerical model parameter sensitivities give a direct measure of model response variations. Since a full sensitivity analysis is outside the scope of the current study, a simple evaluation based on partial derivatives is computed. While it is known that partial derivatives are the easiest way to approximate parameter sensitivities, this result also becomes apparent from model updating procedures. Considering a model updating procedure based upon maximum likelihood and assuming normally distributed random variables, the posterior covariance matrix of estimated parameters taken from (Ledesma et al. 1996) is:

$$\hat{C}_\theta = \left(\frac{\partial y^T}{\partial \theta} C_y^{-1} \frac{\partial y}{\partial \theta} + C_\theta^{-1} \right)^{-1} \quad (2)$$

where C_y is the covariance matrix of the measured data, C_θ is the initial covariance matrix of the parameters, θ are the parameters and y represent the model that solves the forward problem. Treating the distribution of the parameters as uniform, C_θ drops out and only the sensitivity term in equation (2) remains with the partial derivatives of the model response with respect to the model parameter.

The posterior covariance matrix is a direct measure of the parameter uncertainty, which can be considered as a part of model quality (Olney et al. 2014). Since a model updating procedure is not actually performed, the posterior covariance matrix is not computed. However, the motivation to use partial derivatives to obtain sensitivity information remains. The partial derivatives themselves can be approximated by finite differences; a reduction that is advantageous for numerical computations. Table 4 gives the approximate change in the numerical model parameters to achieve the variance seen in the poles ($2\sigma=4\%$). Assuming the observed variation can be taken as a Gaussian probability distribution, most values are within plus and minus two standard deviations of the mean ($\mu\pm 2\sigma=95\%$). This table contains the required change in various parameters to achieve the approximate change in frequency.

Table 4 - Approximate change required in selected numerical model parameters to achieve observed variance in frequencies ($2\sigma = 4\%$). (*average over higher modes, 1st and 2nd modes much more sensitive)

Parameter	Δ [%]
Young's Modulus	8
outer diameter	4
outer diameter*	6
outer diameter*	8
wall thickness	25
wall thickness*	67
wall thickness*	41
soil stiffness	70-80

The table shows that the most sensitive parameter is the outer diameter of the pole, which is the most exact due to the manufacturing process and the least uncertain due to the fact that it can be measured directly. The least sensitive parameter, the soil stiffness, however, shows that large variations are necessary to achieve the small observed variation in frequency. While the soil stiffness is the most likely to vary since the site is long, the effect may not be noticeable in the observed frequencies. It should be noted that the model used to obtain these results is a very simplified one, including beam elements, simple material models and a rotational spring for the soil. A more advanced sensitivity analysis on a more sophisticated numerical model may produce different results; however, these computations give an impression of the possible outcomes of further investigations.

DISCUSSION

Repeated experiments on nearly identical pole structures demonstrated that variations exist in properties identified on individual poles as well as larger variations comparing individual poles with each other. The brief sensitivity study showed that the pole to pole variations can be explained by reasonable variation in some model parameters. This can be related to actual differences

in material and geometry of poles manufactured to be identical. Of course, large deviations of parameters from accepted values would more likely compensate for modelling errors than describe real system. Other possible reasons for the observed variations of both single and compared poles include:

- numerical modelling errors (poor approximation/discretisation, geometry, material, etc.)
- neglect of other parameters or phenomena in the simulation critical to an accurate dynamic response
- errors in identification of dynamic properties from the experimental data
- flaws in experiments (uncertainties in measurements, environmental influences)

Each of these cases, as well as others not mentioned, highlight that both observed variations and discrepancies between model and experimental responses show that differences exist between reality, measurements and model abstraction. Model abstraction, or the process of creating mathematical and computational models from theory and observed reality, leads to one set of quantities (model responses, properties, etc.) that will inevitably always vary from those that are measured. The important point is that while there are flaws generated by creating models of reality, measured quantities are also not full representations or reconstructions of reality. Measurements can contain errors due to external effects and limitations of measuring devices. Extracting useful information from experimental data is not always a trivial process. Finally, it is impossible to measure everywhere and every phenomena (both known and unknown) on structures.

CONCLUSIONS

Further steps for this work include applying different identification methods on the data, performing a full sensitivity analysis, creating more detailed numerical models, and identifying the dynamic properties of the remaining 11 poles.

Structures assumed to be identical show variations. While small, the variations substantiate the need for more methods to quantify both model and experimental quality (most likely by means of uncertainties), in order to judge the results obtained from both measurement data (believed to be true, yet containing errors) and numerical models (known to be approximations, yet trusted as representing reality). There will also be a difference between what we believe about our structures, what we measure on them, and what we determine about through simulation. The question remains to be answered: what does this mean for our structures and for those who may use them.

ACKNOWLEDGEMENT

The research of the authors is supported by the German Research Foundation (DFG) via Research Training Group “Evaluation of Coupled Numerical and Experimental Partial Models in Structural Engineering (GRK 1462)”, which is gratefully acknowledged.

REFERENCES

D. Ewins, *Modal testing: theory, practice, and application*, Mechanical engineering research studies: Engineering dynamics series, Research Studies Press, 2000.

A. Ledesma, A. Gens, E. E. Alonso, Parameter and variance estimation in geotechnical backanalysis using prior information, *International journal for numerical and analytical methods in geomechanics* 20 (2) pgs. 119–141, 1996.

P. Olney, G. Morgenthal, T. Lahmer, Model based design of experiments and monitoring systems for parameter identification of structures, In *Proceedings of the 37th IABSE Symposium: Engineering for Progress, Nature and People*, Madrid 3–5 September, 2014.

BENDABILITY TESTS FOR ULTRA-HIGH-STRENGTH STEELS WITH OPTICAL STRAIN ANALYSIS AND PREDICTION OF BENDING FORCE

Raimo Ruoppa, Rauno Toppila
Lapland University of Applied Sciences, Finland

Vili Kesti
SSAB, Finland

Anna-Maija Arola
University of Oulu, Finland

ABSTRACT

It is known that the total elongation from a tensile test is a poor indicator of the bendability of ultra-high-strength steel (UHSS) because deformation is highly localised in the bent parts. Therefore it is important to understand how different ultra-high-strength steels withstand local deformation. The aim of this study was to investigate the local strains of three different UHSS, Optim®700 MC Plus, Optim 960®QC and Raex®400, during bending and tensile testing. Bendability was examined with three-point bending tests using a hydraulic press with various tools and bending angles. Prior to the tests, the sample surfaces were marked with a grid of dots using laser marking. After the bending, the deformation on the outer surface was measured using a GOM ARGUS strain analysis system and the results were analysed together with the general bendability results, which were evaluated by visual inspection. Tensile tests were carried out with a GOM ARAMIS deformation analysis system in order to define the local strains and the results were compared to the strains measured in the bending tests. Preliminary evidence of correlation between the maximum local strains before fracture in the tensile and bending tests was found. Cross-sections of some bends were also examined with hardness measurements and the location of the neutral axis and reduction of the thickness in the bend were defined. The measured maximum forces were used to establish a better force prediction model.

INTRODUCTION

Ultra-high-strength steels (UHSS) are usually considered to be steels with a yield strength of more than 550 N/mm² and an ultimate tensile strength of more than 700 N/mm². Optim®700 MC Plus steel is thermo-mechanically hot-rolled with accelerated cooling and the microstructure is developed especially for cold forming processes. Optim®960 QC and Raex®400 steels are manufactured by controlled rolling and subsequent direct quenching. The steels have a fine-grained martensitic or bainitic-martensitic microstructure and good strength and toughness properties. The use of UHS steels has been

increasing and the demand for them have been increasing, because their high strength can be utilised in lightweight structures. At the same time, the challenges in product manufacturing have also increased as more demanding high-strength structures are designed and therefore the workshop usability of UHS steels is becoming more and more important.

A typical method for manufacturing products from UHS steels is forming with a hydraulic bending press. Steel plates are usually formed with three-point bending using different punches and V-dies according to the bending recommendations of the material. If the bending radius is too small or the bending angle too high compared to the formability of the material, it may lead to defects such as surface waviness, cracking and nut shaping. The defects are caused by the deformation conditions in the plate and it is evident that too great an elongation on the surface leads to surface waviness or, in more serious cases, cracking, which makes the use of the product impossible.

In a previous work [Ruoppa et al. 2012], UHS steels were studied using bending tests with various punch radii and diameters of the V-die. The focus was mainly on measuring spring-back and evaluating the bending force. As a result, a model for the prediction of the bending force was also developed. Recently, a new characterisation approach based on optical strain measurement to identify the failure stages, critical strains and bending angles was presented [Kaupper et al. 2013]. In the present work, the aim was to study the relationship between the bending defects and the local strains and compare the bendability of different steel grades. Another target was to improve the model for the bending force prediction based on the new data.

EXPERIMENTS

Three different UHS steels, Optim®700 MC Plus, Optim 960®QC and Raex®400, with sheet thicknesses of 6 mm, were examined. Typical mechanical properties of the test materials are shown in Table 1.

Table 1. Typical mechanical properties of the test materials

Test material	$R_{p0,2}$ min	R_m min	A_5 min	Charpy V min	
	N/mm ²	N/mm ²	%	T (°C)	J
Optim®700 MC Plus	700	750-930	15	-20	40
Optim®960 QC	960	1000	7	-40	34
Raex®400	1000	1250	10	-40	20

For the bending tests, 300x300mm samples were cut from the sheets. For each test piece, an 80x80mm area in the centre of the sample surface was shot-blasted and laser-marked with a dot grid. The diameter of the dot was 0.5 mm and the distance between the measurement points was 1.5 mm. The test pieces were bent with a hydraulic bending machine using various bending angles between ~ 30 and 110 degrees (unbent = 0 degrees) and punch radii. The diameter of the V-die was 60 mm with Optim®700 MC Plus and Raex®

400 and 80 mm with Optim®960 QC. The bending axis was either parallel to the rolling direction (RD) or transverse to the rolling direction (TD). The bending force was measured during the tests with a pressure sensor mounted on a hydraulic cylinder of the machine. After bending, the samples were measured with the GOM ARGUS 3D forming analysis system and visually inspected in order to evaluate the bending result. The GOM ARGUS system is illustrated in Figure 1a and an example of the surface strain map is shown in Figure 1b.

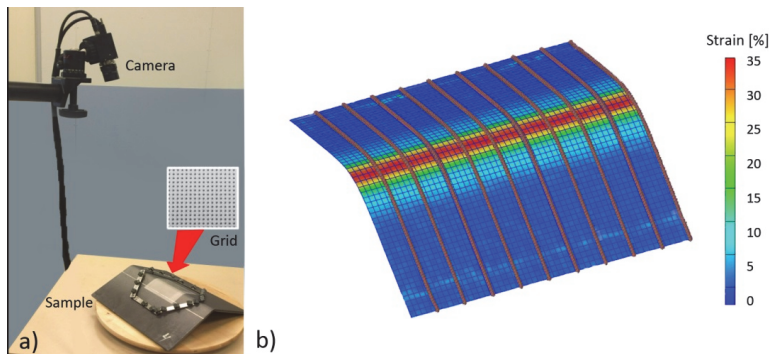


Figure 1. a) Measurement of the strain distribution with GOM ARGUS 3D forming analysis system:
b) example of strain mapping in the bent sample

After mapping, the surface was divided into sections and strain distribution charts were drawn along 10 section lines in a direction transverse to the bending line, as seen in Figure 1b. The peak strain in each section was defined and an average of the peak strains was calculated and used for the comparison of the samples. One section with a peak strain corresponding to the average was chosen to represent the strain distribution of the entire measurement area.

From the bent samples, the surface was inspected visually with the aim of quantifying the presence of defects and to define the bending result. For the expression of the bendability and bending result, a particular bendability index was specified: [Kaijalainen et al. 2012, 2014]

$$BI = 0.1xA + 0.5xB + 1xC + 3xD + 10xE \quad (1)$$

where: A describes the plate separation (from the upper tool)
B describes the nut shape of the bend
C describes the surface waviness
D describes the surface cracks
E describes the cracks through the sample

If the defects A or B are present, the value of its parameter in Equation 1 is 1, while in other cases it is 0. If some of the defects C, D or E are present only the most serious one is taken into account and is given a value of 1. The higher the

value of the bendability index, the worse the bendability is i.e. the bendability is inversely proportional to the value of the bendability index.

Some of the samples were also studied by means of microscopic examination of cross-sections and hardness measurement. The thickness of the plate in different points of the bend was measured and the thickness reduction was calculated. In aim to define the location of the neutral axis, some radial lines of the bend were selected from the cross-section. Along these lines the hardness (HV5) was measured at regular intervals of 0.25 mm.

In addition to the bending tests some tensile tests were also carried out using the GOM-ARAMIS 3D deformation analysis system. The aim was to measure local strains in a tensile test sample and compare them with the strains in the bending samples. In ARAMIS, the stochastic pattern shown in Figure 2a is used for the strain measurement. An example of a strain map is seen in Figure 2b where the strain distribution just before the fracture of the tensile test sample is illustrated.

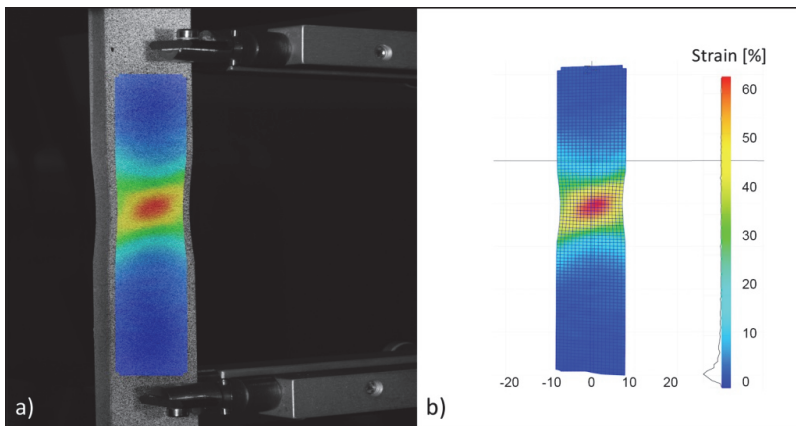


Figure 2. a) Measurement of the strain with the GOM ARAMIS deformation analysis system in the tensile test:
b) Strain distribution map

RESULTS AND DISCUSSION

Some strain distributions measured from the bends are shown in Figure 3. The strain distributions of samples bent to 90 degrees in different directions are shown on the left and the strain distributions of samples which are bent with different bending angles in the rolling direction are shown on the right.

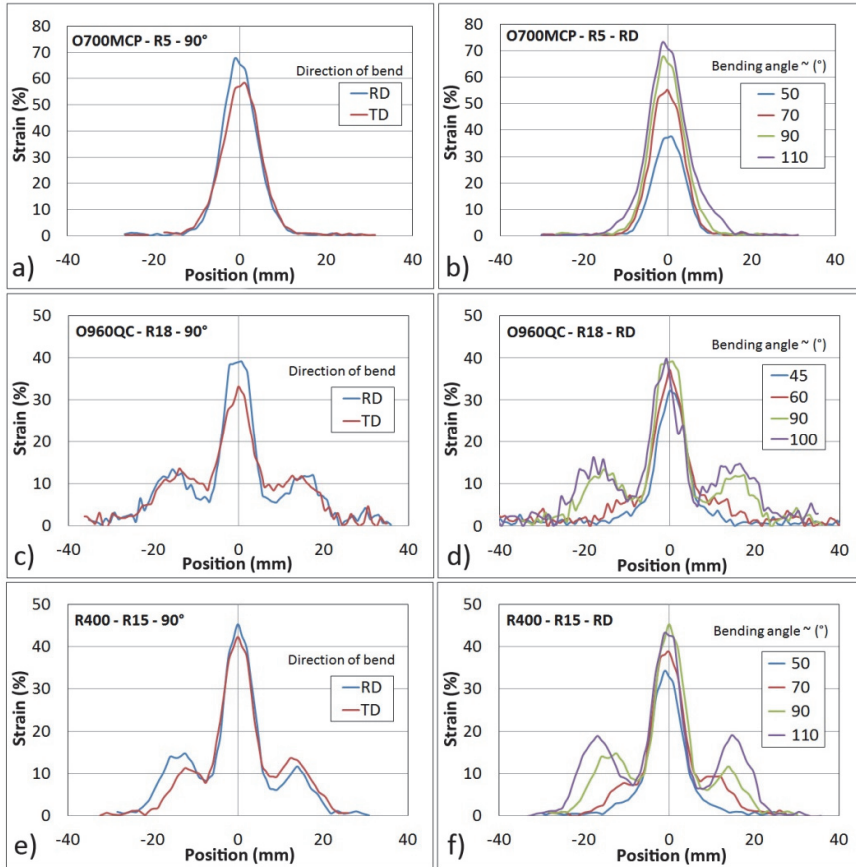


Figure 3. Strain distributions of different steels bent to a 90° angle in different directions (a, c and e) and to different angles in the rolling direction (b, d and f). Position 0 = bending line.

The influence of the bending directions on the peak strain can be seen in Figures 3a, 3c and 3e. The peak strain is slightly higher when the bending line is in the rolling direction (RD). In Figures 3b, 3d and 3f, it can be seen that the peak strain increase with an increase in the bending angle. Further, the materials have different behaviour as Optim®960 QC and Raex®400 have “side peaks” in the strain curve located on both sides of the maximum strain which also grow with an increase in the bending angle. This is obviously a consequence of the nut shape which was found as a defect with the bending of these steel grades.

The test materials had different variations of the bending radii as a result of their different recommendations. However, testing using a bending radius of 11 mm was carried out for all the steels in order to have a proper comparison point. The strain distributions measured from these samples are shown in Figure 4. With Optim®700 MC Plus the peak strain is much lower and the strain distribution is broader than with Raex®400 and Optim®960 QC. The latter have a very sharp peak as the strain is mainly localised near the centre of the bending line. With Optim®700 MC Plus the plastic deformation is spread

over a larger area. The difference may be understood as a consequence of the better forming properties (e.g. work-hardening) of Optim®700 MC Plus.

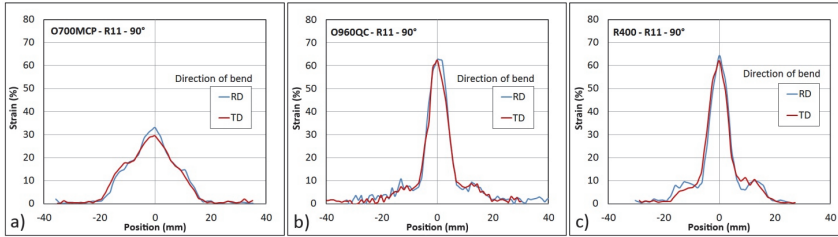


Figure 4. Strain distributions of different steels bent with an 11 mm punch radius to a 90-degree angle

The peak strains measured in each test using different punch radii are illustrated in Figure 5 as a function of the bending angle. The peak strains increase with an increase in the bending angle and a decrease in the bending radius. Because of the assumed better formability, the bending radii used with Optim®700 MC Plus were relatively small compared to the other two steels and this caused higher peak strains in Optim®700 MC Plus. However, when the same bending radius (11 mm) was used for all the steel grades, the peak strain was actually lower with Optim®700 MC Plus, which is also shown in Figure 4. The influence of the direction of the bend on the peak strains is seen in Figure 5. In most cases, when the bending line is parallel to the rolling direction (RD), the peak strain is higher than in the transverse direction (TD). It also seems, in particular with Optim®960 QC, that when the bending radius increases the influence of the bending angle on the peak strain becomes negligible (Figure 3b).

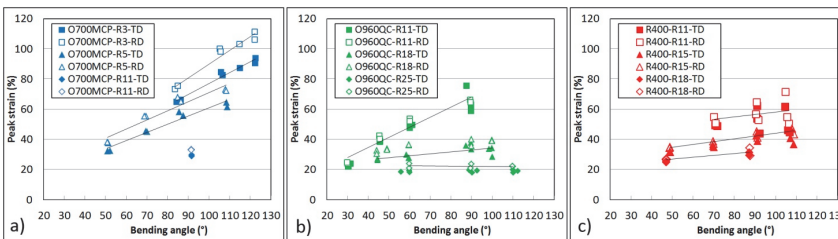


Figure 5. Influence of the bending angle and bending radius on the peak strain of different steels

Bendability was defined by visual inspection and expressed by the bendability index; see Equation 1. The correlations between the measured peak strains and bendability index for each test material bent in a) the rolling direction and b) the transverse direction are shown in Figure 6. The bendability decreases (the bendability index increases) with an increase in the peak strain, as may be expected. The bendability of Optim®960QC and Raex®400 seems to be quite similar. When the strain reaches about 25-30 %, surface waviness appears and the bendability index exceeds a value of 1. A further increase in

the strain induces more serious defects. Correspondingly, with Optim[®]700 MC Plus the peak strain reaches 50-60 % before the bendability begins to decrease. This indicates the much better bendability of the latter. If Figures 6a and 6b are compared, it can be seen that when the bending direction is in the rolling direction, (RD) less strain is required for the same bendability index compared to the transverse bending direction. In the rolling direction the bendability index reaches value of 10, which means that even cracks through the sample exist, whereas in the transverse direction only surface cracks are present. More serious cracking is obviously caused by the higher peak strains in the rolling direction, as shown in Figures 3, 4 and 5.

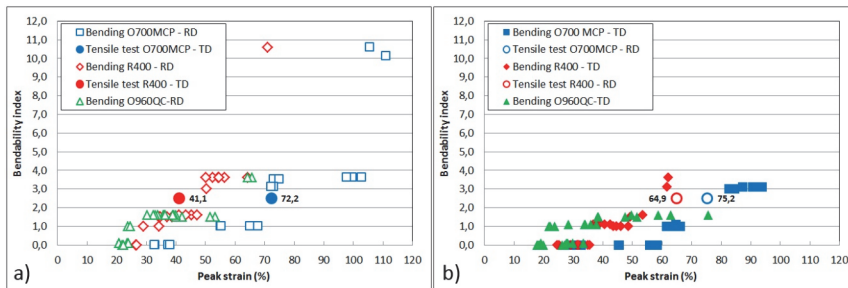


Figure 6. Correlation between peak strain and bendability a) bent in the rolling direction (RD); b) bent in the transverse direction (TD)

In addition, tensile tests were carried out using the GOM ARAMIS optical strain measurement system. The aim was to find a correlation between the strains in the tensile and bending tests. The maximum strains just before fracture (see the example in Figure 2) were measured for Optim[®]700 MC plus and Raex[®]400 and the results were placed in Figure 6 with the results of the bending tests. The tensile tests in the transverse direction are compared with the bending tests in the rolling direction and the other way around because of the correspondence of deformation states. The values of the maximum local strain before fracture in the tensile test (round markers) are placed in the charts in Figure 6 to compare them to the strain level at which the fracture initiates during bending (transition from surface waviness to surface cracking in the bendability index). It can be seen that the maximum strains before cracking measured in the tensile tests and bending tests do indeed show quite a good correlation.

Cross-sections of some bent samples were examined with a microscope and hardness measurements were performed. An example of a cross-section is shown in Figure 7. The minimum hardness of each line is marked with red dots, which represent the neutral axis. From the location of the neutral axis, the k-factors were calculated as described in the previous work [Ruoppa et al. 2012] and the thickness reductions were also measured. The results are shown in Table 2.

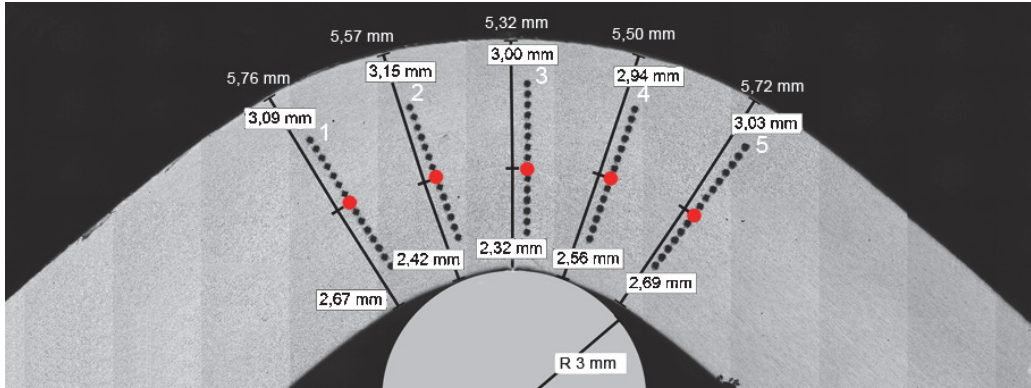


Figure 7. Cross section of Optim®700 MC Plus. Bending radius 3 mm, angle 90 degrees, transverse direction (RD). The red dots indicate the minimum hardness points

Table 2. Thickness reductions and k-factors. T = total thickness, t = distance from the inner surface to the neutral axis. TR(mid) = thickness reduction in the middle, TR(aver3) = Average of the thickness reduction in three positions around the middle

Test material	Direction of bend	R(mm)	Peak strain %	t(mm)	T(mm)	k	TR(mid)	TR(aver3)
Optim®700 MC Plus	RD	3	73.1	2.52	5.50	0.46	12.4%	8.7%
	TD	3	64.7	2.43	5.46	0.45	11.8%	9.4%
	RD	5	67.8	2.49	5.46	0.46	11.1%	9.5%
	TD	5	58.3	2.51	5.64	0.45	8.6%	6.5%
	RD	11	33.1	2.60	5.68	0.46	7.0%	5.9%
	TD	11	29.5	2.78	5.74	0.49	5.5%	4.9%
Raex®400	RD	11	64.2	2.61	5.49	0.48	11.6%	8.9%
	TD	11	62.1	2.51	5.59	0.45	9.0%	7.4%
	RD	15	43.4	2.77	5.64	0.49	8.5%	6.4%
	TD	15	36.8	2.63	5.69	0.46	6.0%	5.7%

It is seen that the k-factors varying between 0.45...0.49, indicating that the neutral axis is moving from the centre-line towards the inner arc of the bend ($k < 0.5$). With Raex 400 there seems to be a slight difference between the k-factor in the transverse direction (TD) and the rolling direction (RD). The thickness reductions increase with a decrease in the bending radius which is caused by the increasing strain. The thickness reduction in the rolling direction (RD) is higher than in the transverse direction (TD). This is obviously due to the higher strains in the rolling direction which is shown in the results above.

In the previous works [Ruoppa et al. 2012, Kesti et al. 2013], a new model for the prediction of the bending force was developed:

$$F = 0.8 \times \frac{b \times R_m \times t^2}{W - (1.73 \times R_p)} \tag{2}$$

where: R_m is the ultimate tensile strength (N/mm²)
 b is the bending length (mm)
 t is the sheet thickness (mm)
 W is the diameter of the V-die (mm)
 R_p is the punch radius (mm)

Equation 2 above also takes into account the punch radius, which some older sheet bending force models lack [Ruoppa et al. 2012]. On the basis of the data acquired previously [Ruoppa et al. 2012, Kesti et al. 2013] and new data including the tests above and some other unpublished tests, a new model was developed:

$$F = \left(0.5 + \frac{4 \times t}{W}\right) \times \frac{b \times R_m \times t^2}{W - (1.5 \times R_p)} \quad (3)$$

The variables in Equation 3 correspond with the variables in Equation 2. The calculated forces using previous the formula and the new formula with measured forces are shown in Figures 8a and 8b, respectively.

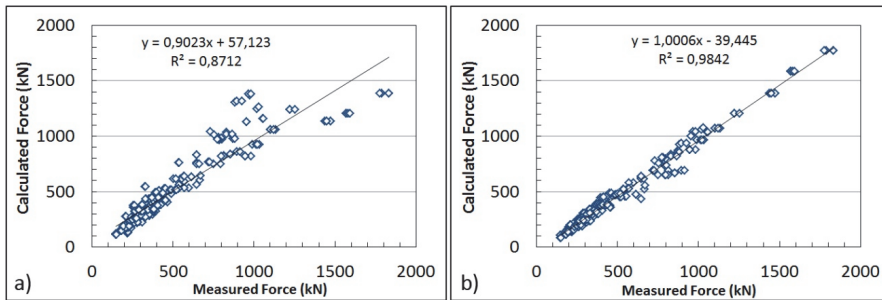


Figure 8. Correlation between measured and calculated force using a) Equation 2 and b) Equation 3

In the data which Figures 8a and 8b are based on, the sheet thicknesses have been varied between 4.5 and 25mm, the ultimate tensile strength 780 and 1950 N/mm², the punch radius 3 and 140 mm and the diameter of the V-die 50 and 360 mm. As can be seen from Figure 8b, by using Equation 3, a very good correlation between the measured and calculated forces is achieved. However, because of the limited force of the equipment, about 1000 kN, the bending length was not greater than 300 mm, which is relatively short compared to the bending lengths commonly used in the sheet metal industry. Therefore, the model may not necessarily be valid within a length range which deviates greatly from this. To get more information, tests in which the bending length is varied on an larger scale are needed. These tests will be possible after the ultimate bending machine described in previous work [Toppila et al. 2011] is available. The tools for the machine are under construction at Lapland University of Applied Sciences and testing will be started in the near future. The maximum bending length will be 1200 mm and the maximum force 30000 kN.

CONCLUSIONS

An increase in the bending angle and a decrease in the bending radius lead to an increase in the strain on the outer surface of the bend during three-point bending. When the critical limit of the peak strain is exceeded on the bend surface, bending defects occur and the bent part cannot be used in industrial applications. Therefore, it is essential to use proper punch radii together with correct bending angles in order to prevent too high peak strains in the bend surface. Within the steels studied here, the peak strain of Optim®700 MC Plus is allowed to be higher before the bendability begins to decrease meaning better bendability than Optim®960QC and Raex®400. In the strain distribution of Optim®960QC and Raex®400 “side peaks” appear with an increase in the bending angle and this obviously indicates the presence of nut shaping.

When the bending line is parallel to the rolling direction, lower bendability is observed in all the materials that were tested. In the rolling direction the peak strains and thickness reductions are higher, which causes more serious bending defects.

The local strains measured in tensile tests just before fracture show evidence of correlation with the strains measured in the bending test in the state where the fracture is initiating (transition from surface waviness to surface cracking in the bendability index). This correlation between the maximum local strains might be used in the bendability estimations between different steels as it is known that the total elongation from a tensile test does not predict the bendability of UHS steels [Oka et al. 1986, Yamazaki et al. 1995].

The new model for bending force prediction is more accurate than those that have been previously published and can be applied to a wider variety of bending radii but may not necessarily be valid within a length range which deviates greatly from that studied here. Further studies with varied lengths are needed to confirm the universal usability of the model.

ACKNOWLEDGEMENTS

The authors would like to acknowledge the financial support of Tekes – the Finnish Funding Agency for Technology and Innovation and Ruukki Metals Oy.

REFERENCES

Kaijalainen, A. et al. Effect of inclusions on the properties of ultra-high-strength low-alloy steel with a martensitic-bainitic microstructure. Proc. 8th Int. Conf. Clean Steel, 2012, Budapest, Hungary.

Kaijalainen, A.J., Suikkanen, P., Karjalainen, L.P., and Jonas, J.J., *Metall. Mater. Trans. A*, 2014, vol. 45, pp. 1273–83.

Kaupper, M., Merklein, M., Bendability of advanced high strength steels—A new evaluation procedure. *CIRP Annals Manufacturing Technology* 62 (2013), pp. 247–250

Kesti, V. et al. Bendability and microstructure of direct quenched Optim 960QC. *Materials Science Forum Vols. 783–786* (2014) pp 818–824, Trans Tech Publications, Switzerland

Oka M. et al. The effect of metallurgical factors on the formability of steel sheets, *Formability and Metallurgical Structure Symposium*, The Metallurgical Society Inc. 1986

Ruoppa, R., Toppila, R., Sipola, J., Kesti, V., Bending properties of some ultrahigh-strength steels. *MetNet 2012 Izmir, TURKEY*, 10–11 October 2012.

Toppila, R., et al. Investigation of behavior of HSS using advanced techniques. *MetNet 2011 Aarhus, DENMARK*, 12–13 October 2011.

Yamazaki K. et al. Recent advances in ultrahigh-strength sheet steels for automotive structural use, *Nippon Steel Technical Report*, vol. 64 (1995) pp. 37–44.

STEEL-REINFORCED CONCRETE STRUCTURAL GUY-ROPE CLADDING

Leonid Storozhenko

Grigoriy Gasii

Sergey Gapchenko

Poltava National Technical Yuri Kondratyuk University

ABSTRACT

Designers face the problem of searching for new materials and forms which will allow them to work more efficiently while meeting all design and architectural requirements. One such materials is steel-reinforced concrete that combines concrete, reinforcement and rolled section.

Flat structures are designed from various systems of cross frames. Frames that intersect at a single node, form different structural constructions. Each structure includes a repeated volume element (crystal): half octahedron or tetrahedron the construction of which is justified by the laws of crystallography.

The purpose of our research is to explore the bearing capacity and deformability of structural-guy rope cladding, to determine experimentally their bearing capacity and deformation characteristics and make calculations concerning strength, moving covering items and nodes. An important point in the design of space frames is a calculation of nodes interconnecting a slab with rods and rods with guy ropes.

The new forms of steel-reinforced concrete structural-guy rope cladding providing joint operation of concrete, reinforcement and guy rope elements are suggested. Performance peculiarities and possible shapes of structural-guy rope cladding model deformation are revealed. The obtained findings can be applied in the construction sphere for cladding large-span buildings (sports complexes, swimming pools, warehouses, airports, exhibition halls).

STATEMENT OF THE PROBLEM

When erecting buildings prefabricated light cladding is important to speed assembly structures, their stiffness at low weight, small number of sizes, ease of transportation. Structural and guy rope cover fully meet the above requirements and therefore should be carefully analyzed and studied.

In the construction practice of structural designs gained distribution [3]. For their design recommendations [2], but structural-guy rope cladding spans

are replaced by flexible guy rope [1] and therefore the nature of the different designs.

On the basis of experimental studies of model structural-guy rope cylindrical shell scheme is studied deformation are analysed.

CONSTRUCTION

Structural-guy rope claddings are complex constructions, which include a slab upper zone, lattice elements and guy ropes. The peculiarity of steel-reinforced concrete structural-guy rope cladding is that the upper compressed steel belt structure replaced ferrocement or reinforced concrete slab, and the elements of the lower chord – for guy ropes or flexible rods that experience only tensile force.

Structural-guy rope cladding is sent to the construction site in an integrated design with lightweight elements (Figure 1), which are made in the factory.

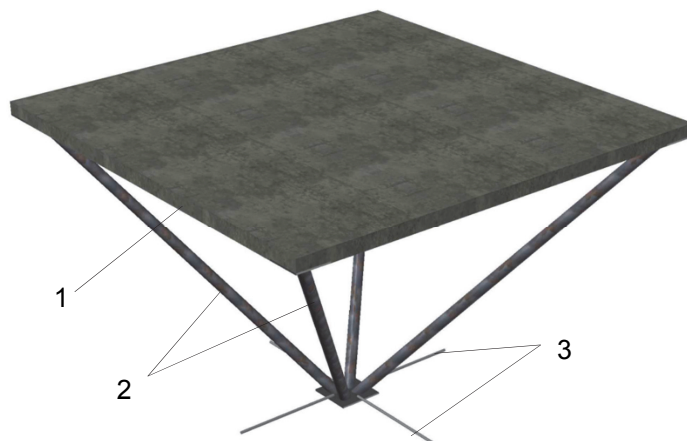


Figure 1 - Separate element of steel-reinforced concrete structural-guy rope cladding
1 – slab; 2 – tubes; 3 – guy ropes

Structural and guy rope claddings have possibilities of different configurations. It is possible to create various designs: flat cover, cylindrical shell, the shell of double curvature, canopy and cantilever canopies.

EXPERIMENT

For the experimental results, which would enable to adequately judge the features of composite structural-guy rope claddings were designed and manufactured cylindrical shell model (Figure 3), which consists of seven arch structures (Figure 2), each of which has been gathered of individual elements – «crystal».

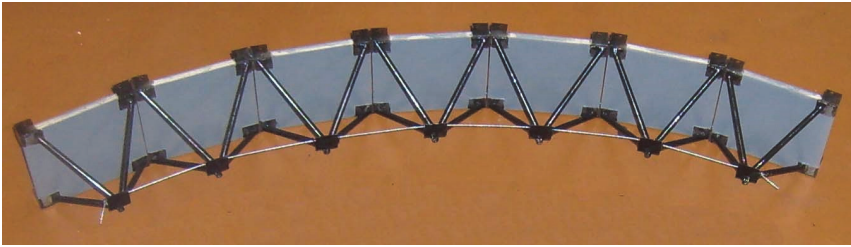


Figure 2. Team arched section covering model

The elements are combined into a coherent design bolts. Curvature cladding controlled tension guy rope are fixed in the extreme nodes. In order to design there was no horizontal support efforts, both sides pivotally mounted.

Measuring deflections performed photogrammetric method using markings that were placed in three sections on the plates of the upper zone and made it possible to track deflections in every part of the cladding. After the experiment, obtained photographs measuring and measured displacement markings relatively fixed rear stand.

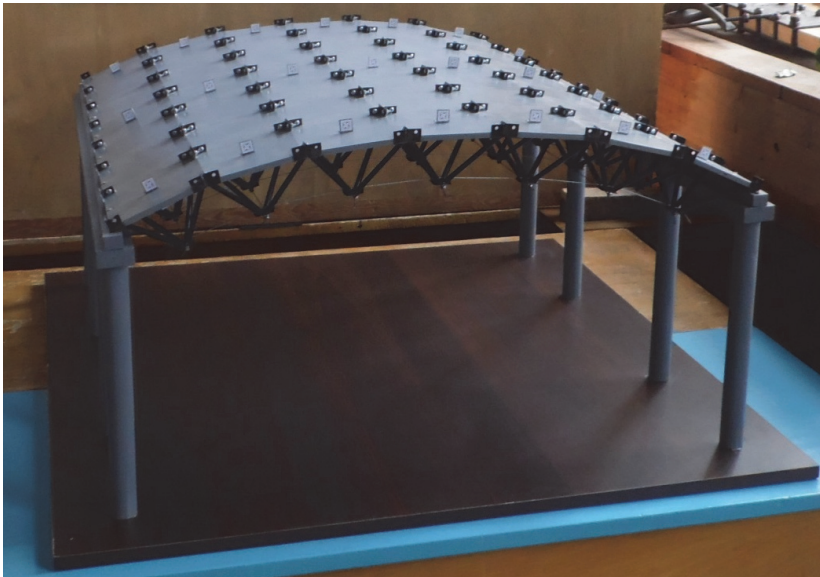


Figure 3. Model structural-guy rope cylindrical shell

The scheme adopted asymmetric loading (Figure 4). Originally hang loads on secondary elements, and then gradually moved to the side, and so to fully load.

$\frac{11}{4}$	$\frac{11}{4}$	$\frac{11}{4}$	$\frac{4}{4}$	$\frac{9}{4}$	$\frac{9}{4}$	$\frac{9}{4}$	$\frac{9}{4}$
$\frac{11}{4}$	$\frac{11}{4}$	$\frac{11}{4}$	$\frac{3}{4}$	$\frac{9}{4}$	$\frac{9}{4}$	$\frac{9}{4}$	$\frac{9}{4}$
$\frac{11}{4}$	$\frac{11}{4}$	$\frac{11}{4}$	$\frac{2}{4}$	$\frac{9}{4}$	$\frac{9}{4}$	$\frac{9}{4}$	$\frac{9}{4}$
$\frac{11}{4}$	$\frac{11}{4}$	$\frac{11}{4}$	$\frac{1}{4}$	$\frac{6}{4}$	$\frac{7}{4}$	$\frac{8}{4}$	$\frac{4}{4}$
$\frac{11}{4}$	$\frac{11}{4}$	$\frac{11}{4}$	$\frac{5}{4}$	$\frac{10}{4}$	$\frac{10}{4}$	$\frac{10}{4}$	$\frac{4}{4}$
$\frac{11}{4}$	$\frac{11}{4}$	$\frac{11}{4}$	$\frac{5}{4}$	$\frac{10}{4}$	$\frac{10}{4}$	$\frac{10}{4}$	$\frac{4}{4}$
$\frac{11}{4}$	$\frac{11}{4}$	$\frac{11}{4}$	$\frac{5}{4}$	$\frac{10}{4}$	$\frac{10}{4}$	$\frac{10}{4}$	$\frac{4}{4}$

Figure 4. Scheme of load models

Simulated coverage consists of 49 identical elements and has a span of 0.745 meters in the form of seven arch sections. The served as embedded parts made of steel plate elements with thickness 0.5mm. In the upper zone for connection elements used bolts with a diameter of 3 mm at the bottom to connect the cable 1mm apply that fix in designated areas.

For the experiment weights in the form of plates, weighing 265 grams, were specially manufactured. The model was loaded at nodes in the lower zone with a gradual increase in the number of plates. Load were carried by steel plates on the lower belt attached to the nodes of the grid connection rods guy rope (Figure 5). During the experiment, strain began to appear only when the load was close to failure (Figure 6).



Figure 5. Loads at the nodes along the lower zone



Figure 6. Deformed model diagram at full load

After unloading the cover returned to its original position with small residual deformations. This indicates that all elements of the model worked in elastic stage and have not been brought to failure.

Based on the data obtained by photogrammetric method, a graph of deflection depending on load growth is constructed (Figure 7). Asymmetrical deflection on the chart is due to circuit loading model. The intensity of growth depressions in the initial stages of loading is small enough this is due to the full inclusion of all elements of design work when loading certain sections.

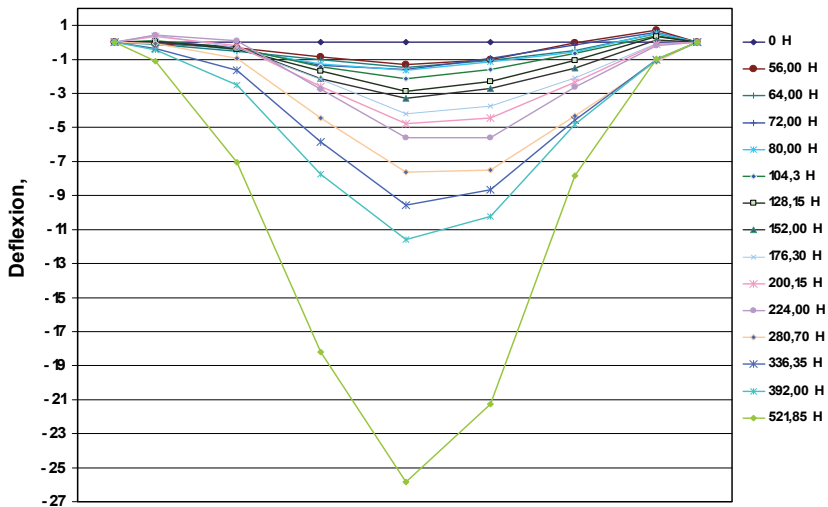


Figure 7 - The dependence of the deflection of the load

CALCULATION

Using a numerical method was simulated and calculated cladding that is fully consistent with the model. Connection nodes are made hinges. Comparison with experiments conducted on the basis of the obtained deformed scheme is shown in Figure 8. In the course of the experiment was noted visually deviations in geometry from the original form, indicating significant spatial rigidity. Significant convergence deformation indicates the validity of the approach to the model of the real structure.

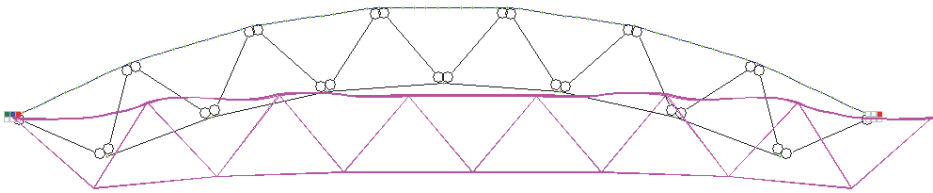


Figure 8. Deformed circuit model for numerical calculation

Lower rod is modelled as finite element, which works on stretching and is fixed in each node connecting to the lattice rods. With such a scheme of fixing guy ropes is the ability to change the cross-section depending on the perceived force (Figure 9). In the upper zone plates arise mainly from compression stress due to displacement of the movable hinge support and disclosure construction (Figure 10).

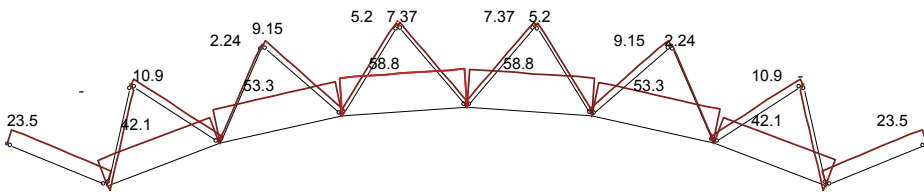


Figure 9. Efforts in the elements of the lattice and guy ropes (Newton)

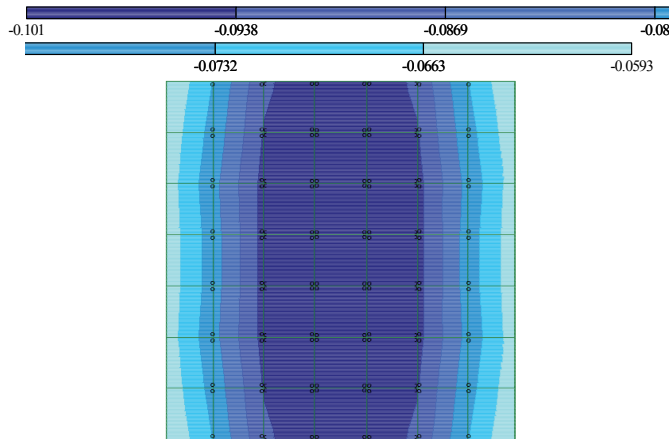


Figure 10. Stresses in slabs (MPa)

The experimental results make it possible to get an idea of the nature of structural-guy rope cylindrical shell. The applied technique using design models can qualitatively assess the nature of deformation of structural-guy rope cladding.

REFERENCES

Patent for Utility Model 59293 Ukraine, IPC E04V 1/04 Structural design of cable-stayed composite arch / L. Storozhenko, G. Gasii, owner PoltNTU. № u201012539; publ. 10.05.2011. Bull. № 9.

Recommendations for the design of structural designs / Center. n. - and Inst constructions them. Kucherenko. - M. Stroyizdat, 1984. – 303 p.

Storozhenko L.I. Research and design of composite structural designs: Monograph / L. Storozhenko, V. Timoshenko, O. Nyzhnyk, G. Gasii, S. Murza. - Poltava: ASMI, 2008. – 262 p.

TESTING CONCRETE BEAMS WITH REINFORCEMENT BAR WEBS

L.I. Storozhenko
Dr. The. Sc., Professor.

V.V. Muravlyov
Ph.D.

E.S. Shkolyar
Postgraduate student

Poltava National Technical Yuri Kondratyuk University

ABSTRACT

The results of experimental researches of reinforced concrete beams with reinforcement work obtained, followed by development of the method of the experiment, obtaining data on bearing capacity, deformation, character of destruction and fracture samples.

INTRODUCTION

Modern building is characterized by using new types of structures. Search for new kinds of combinations of steel and concrete is prospective direction, which saves material and creates a new class of building structures that differ in as in the structural characteristics, and the degree of utilization of the factors collaborative work of both materials. New types of constructions require experimental research related to the study of their bearing capacity, deformation and fracture.

REVIEW THE LATEST SOURCES OF RESEARCH AND PUBLICATIONS

Based on the analysis of recent trends in the reinforced concrete structures rendered reinforcement [1] and Patent situational studies [2] it was reported that concrete constructions reinforced with rendered are widely used throughout the world [3]. Is already proved their rationally using for covering large spans (slabs, beams, girders, trusses, etc.) as a rack which withstand the heavy loads (columns of industrial and civil buildings, supports various purposes, electric poles etc.) in engineering structures. Cross-section of these structures can be extremely varied, some have already experimentally investigated [4].

The analyzed volume of information sources gave positive results in finding articles and research papers on the analysis of experimental studies the authors proposed sections of reinforced concrete beams with reinforcement

rendered. Also not fully elucidated is fracture and impact of external factors on constructions.

PROBLEM STATEMENT

As a result of work it is necessary to develop a methodology the experiment to obtain the necessary experimental data on carrying capacity, deformation and fracture samples, obtaining a clear figure of how strains in cross-section, and in the area of the transverse forces and bending moments, make sure that such reliable construction in operation and exploitation and can be used in industrial and civil construction.

BASIC MATERIAL AND RESULTS

Essence of prototypes series B-1 (Figure 1), is a constructive solution of the cross-section, made with the use a wire armature A240 Ø28 мм (2), which is in conjunction with a linear component reinforced concrete structure (1) is made of concrete class C32/40 size 120x80мм. Compatibility of concrete and steel provided by V- similar anchors were made from wire armature A400 Ø10 мм (3) and steel plates (4) size 100x100x8mm. Samples were tested at achieving concrete project strength, but not earlier than 28 days after steaming. Before testing the metal surface samples purified from the influx of concrete and covered with varnish. Tests were conducted on Amsler's press capacity of 60 tons with manual transmission.

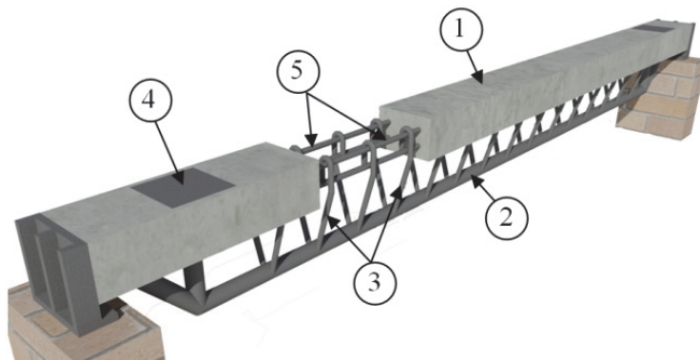


Figure 1. General view of the sample series B-1

1 concrete linear component; 2 wire armature; 3, 4 anchors; 5 reinforcing grid

Deformation of metal components were measured using strain gauge type 20 – 200 V, outer surface of concrete using strain gauge type 50 – 325 V. Data logging for strain gauge was done using a multichannel measurement system for static tests (Figure 2).



Figure 2. Multichannel measuring tensometric system for static tests

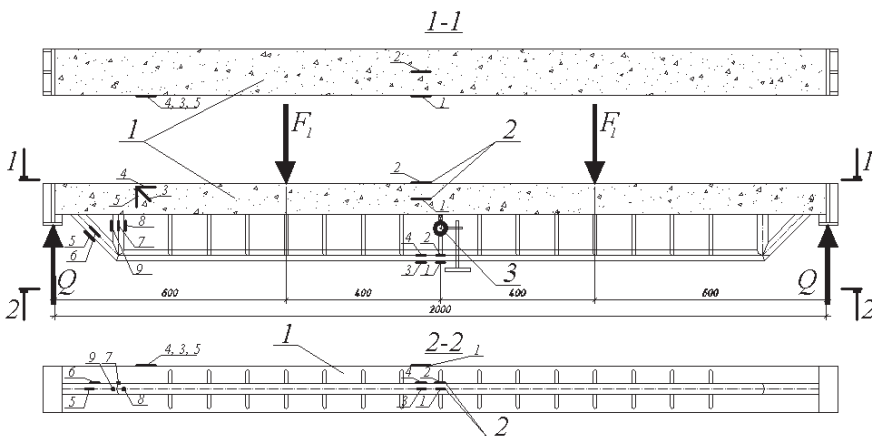


Figure 3. Layout of strain gauges in the testing sample series B-1
1 sample; 2 strain gauge; 3 deflectometer

Layout of instrumentation for the study of the normal cross section is shown in Figure 3. According to the accepted methodology of experimental researches trials conducted on pure bending.

During investigation of normal sections under the influence of normal load was marked the development of cracks in concrete, with increasing load until a critical fracture of concrete shelf happened and there was ductility in the steel component. Also was recorded an increase in the intensity of the deflection at the beginning of the beam in the plastic stage.

As a result, the measurement of displacements in the middle of the span and the occurrence of microcracks in the extreme fibers of the samples by using

indicators such as clock, deflectometer and strain gauge resulted in graphs of strain depending upon the load. In the middle of the span were placed gauges - strain gauge, fittings and pasted on the shelf, deflectometer to determine deflections. The graphs of load deformation are shown in Figures 4 – 8.

From these graph it shows that at the initial stage of loading mainly elastic deformations occur. At higher load levels, which correspond to deformations in which there is ductility and the formation of cracks on the concrete shelf, there is a loss of carrying capacity of the specimen. In general, the beam at all stages of loading worked as a single monolithic structure. Figure 8 shows the distribution of force deformation height of normal cross section of the samples.

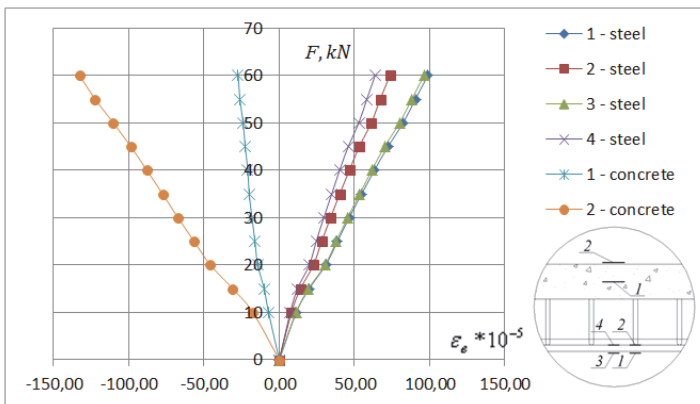


Figure 4. Deformations in the normal section of a series of samples B-1, measured strain gauge arranged by height cross section

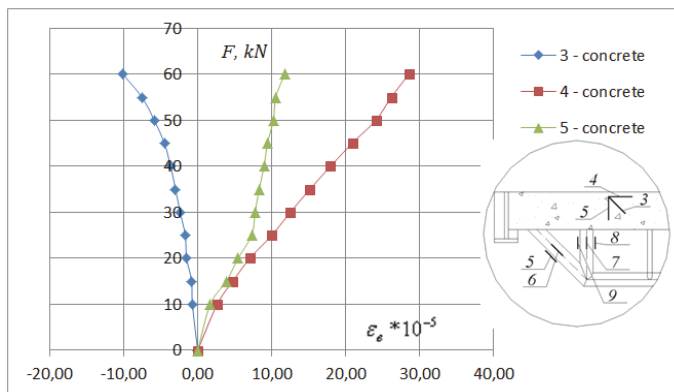


Figure 5. Deformations of the beam, measured strain gauge to concrete (3, 4, 5 are strain gauge numbers, with locations shown in Figure 3)

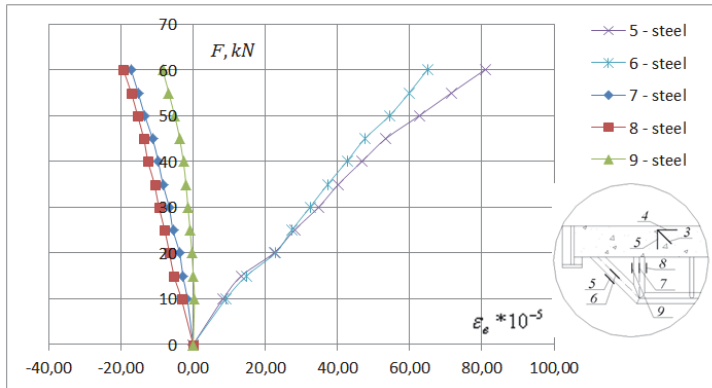


Figure 6. Deformations of the beam, measured strain gauge on metal (5, 6, 7, 8, 9 are strain gauge numbers, with locations shown in Figure 3)

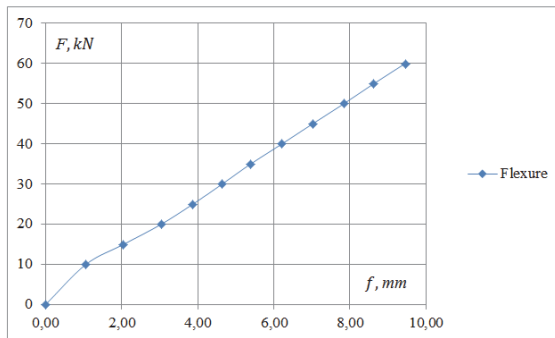


Figure 7. Graph of deflection under load deflectometer

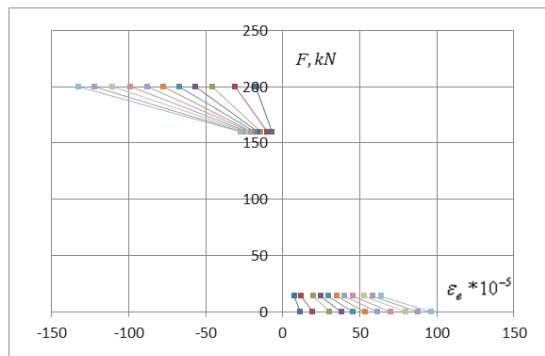


Figure 8. Diagrams of strain distribution in height of normal cross section of samples

When the beam deformation Б - 2 (Figures 5 – 12) observed elastic reinforcement and concrete work to achieve 75 % of the failure loads. Upon reaching loads greater than 75 % of the failure began to emerge a significant crack in concrete shelves due to what happened in the middle of the complete destruction of the samples. Cracks observed at the place of applying the load F1, which was the highest moment and shear force. Destination crack growth was observed on the place of application of force F1 at an angle to support response Q.



Figure 13 - Fracture of the sample

For loads that met the failure moment M_u began to observed significant deformation of the beam, the deflection reached the limit state, then beam lost its load carrying capacity. Brittle fracture specimens was not observed, but rather held plastic, which is typical for steel structures. In general, the studied beam at all stages of loading worked as a single monolithic structure.

CONCLUSIONS

Reinforced concrete beams with reinforcement work rendered Series Б-1 at all stages of working as a single monolithic structure. Methodology and measuring devices can get the necessary experimental data on carrying capacity, deformation and fracture samples. Used for the experiment measuring devices strain gauge, deflectometer can get detailed information about the deformation of samples at any time of the load and get a clear picture of how strains in cross-section, and in the area of the transverse force and bending moment. The distribution of longitudinal deformation on the height of the cross-section at almost all stages of the stress-strain state is close to linear, which allows the use in the calculation of the hypothesis of plane sections. The experimental results indicate that these constructs reliable in operation and exploitation and can be used in industrial and civil construction.

REFERENCES

Стороженко Л.І. Сталезалізобетонні конструкції: навчальний посібник / Л.І. Стороженко, О.В. Семко, В.Ф. Пенц . – Полтава, 2005. – 181 с.

Перспективи розвитку конструкцій із залізобетону / Стороженко Л.І., Муравльов В.В., Школяр С.П., Школяр Ф.С. // Сталезалізобетонні конструкції: дослідження, проектування, будівництво, експлуатація: збірник наукових статей. Вип. 9. – Кривий Ріг, 2011. – С. 185 – 189.

Стороженко Л.И. Сталезалізобетонные конструкции / Л.И. Стороженко, А.В. Семко, В.И. Ефименко. – К.: Четверта хвиля, 1997. – 158 с.

Стороженко Л.І. Результати експериментальних досліджень залізобетонних конструкцій з винесеним армуванням / Стороженко Л.І., Муравльов В.В., Мурза С.О., Школяр Ф.С. // Галузеве машинобудування, будівництво: збірник наукових праць. Вип. 4(33). – Полтава, 2013. – С. 260 – 265.

RETICULAR-STRETCHED THERMO-PROFILE: BUCKLING OF THE PERFORATED WEB

Nikolay I. Vatin

Saint-Petersburg State Polytechnical University, vatin@mail.ru

Jarmo Havula

HAMK University of Applied Sciences, jarmo.havula@hamk.fi

Lassi Martikainen

HAMK University of Applied Sciences, lassi.martikainen@hamk.fi

Alexey S. Sinelnikov

Saint-Petersburg State Polytechnical University, alexey_sinelnikov@mail.ru

Lidia L. Shurovkina

Saint-Petersburg State Polytechnical University, shurovkinalidia@yandex.ru

ABSTRACT

This paper is a continuation of reports that were contributed on international conferences in Moscow (Russia), Miskolc (Hungary), Tartu (Estonia), Lulea (Sweden), Riga (Latvia) and St.-Petersburg (Russia) [1]. St. Petersburg State Polytechnical University, HAMK University of Applied Sciences (Sheet Metal Centre) and Rautaruukki Oyj (Finland) were the fundamental engines of the research described in this paper.

Global science of thin-walled constructions took its place more than 50 years ago [2] and nowadays scientists [3, 4, 5, 6] achieved good results and developed more precise calculation methods [7, 8, 9, 10]. Thin-walled steel construction is comparatively new building construction technology that found its place in Russia. Russian scientists G.I. Belyy [11], A.R. Tusnin [12], E.L. Ajrumyan [13], I.V. Astahov [14], A.U. Kuznetsov [15] and others [16, 17] contributed a good deal to the theoretic fundamental development of thin-walled profile analysis. The base material used for thin-walled structure production – high-strength low-carbon steel. There are typical structural elements of load-bearing frame and walling that could be produced in according with the technology [18]: columns, beams, roof bearers [19] and also studs and racks of walling thermo-panels. The walling structural elements could execute the following functions [20]:

- 1) Bearing structural elements;
- 2) Non-bearing walling structural elements;
- 3) Dual function (bearing and walling) structural elements.

Design thermal conductivity value of walling thermo-panels is provided due to perforated web of the stud cross-section [21]. There are several methods of getting web perforation: slotting or cutting with following bending of

the cut part. These methods are implemented in production of thin-walled profiles classified as perforated [22]. New method of getting web perforation is based on sequential process of steel sheet cutting and followed spreading with creation of rhombic or triangular cuts [23]. Advantages of such method consist of steel waste material reduction and some strengthening of tensioned steel parts. This method is already implemented in production process and type of the profile is classified as reticular-stretched.

This paper includes buckling analysis of reticular-stretched profile web based on classical theory of elasticity and results of Jerki Kesti's research (Espoo, 2000) [24]. Numerical method used throughout the research was finite-element method (FEM) [25, 26]. Results of the research have good correlation with tests (Hämeenlinna, Finland) [23].

INTRODUCTION

Reticular-stretched thermo-profile – a new type of the thin-walled cold-formed profiles made of high-strength low-carbon steel and used as a bearing stud in wall constructions (see Figure 1). There is an intermediate stiffener between weakened by cuts zones in the web. This construction solution assumes increase of critical compressed stresses and web's local buckling in a whole cross-sections. Stress-strain behavior of the reticular-stretched thermo-profile is determined by functional usage as a part of building constructions. As mentioned above, reticular-stretched thermo-profile is used as a stud that defines its behavior as central and eccentric compressed element.

Studies undertaken by the authors have revealed that theoretical and laboratory research of the profile wasn't yet carried out [27, 28].

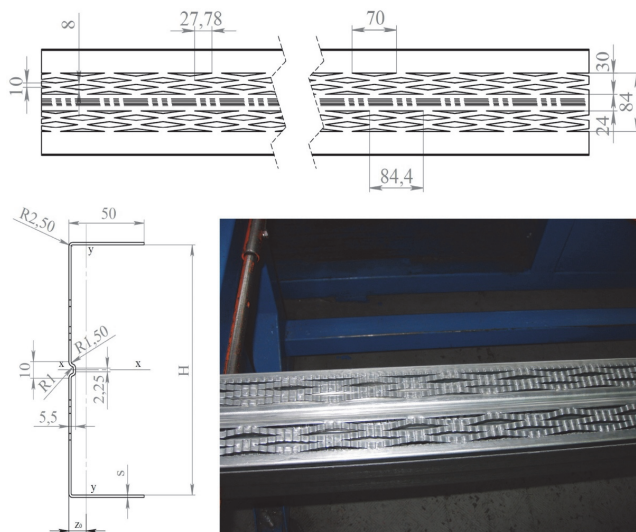


Figure 1. Reticular-stretched thermo-profile

GENERAL

The very core difference of the reticular-stretched thermo-profile from perforated one consists of the method of getting web perforation and existence of an intermediate stiffener in the cross-section's web. Web undergoes primary compressive forces and behaves as a compressed rectangular plate, supported along four sides. Wide-ranging research of the compressed rectangular plates' buckling was carried out by Timoshenko [29]. Different boundary conditions of the plate and stiffeners' influence were analyzed. Timoshenko found that force P_0 (1) had unchangeable value independent from boundary conditions for the plate with definitive width b and thickness t . Type of boundary conditions, relation of the plate's sides $\frac{a}{b}$, and also stiffeners' influence were included in buckling coefficient K_σ .

$$\sigma_{cr.w} = \frac{\pi^2 \cdot E}{12 \cdot (1 - \nu^2)} \cdot \left(\frac{t}{b}\right)^2 \cdot K_\sigma = P_0 \cdot K_\sigma \quad (1)$$

The plate, supported along four sides (case II), has $K_\sigma = 4$ and anticlastic buckling form (Figure 2, a). The plate, supported only along both transversely to the forces' direction sides (case I), buckles into cylindrical form like compressed paper sheet and has $K_\sigma = 1$ (Figure 2, b).

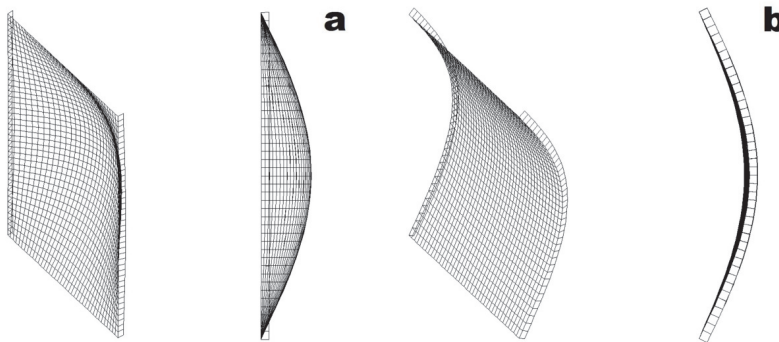


Figure 2. Buckling forms of compressed plate (a – anticlastic surface; b – cylindrical surface)

NUMERICAL INVESTIGATIONS

Classically, the web of a thin-walled cross-section is assumed as supported along four sides, i.e. flanges provide lengthwise sides with fixation into perpendicular to the web direction [29]. This assumption was analysed for the reticular-stretched thermo-profile throughout research undertaken by authors on the hypothesis that buckling form (anticlastic or cylindrical) of the rectangular compressed plate with edge stiffeners on both lengthwise sides and, that is supported only along transverse sides, depends on relation

$$\gamma = \frac{2 \cdot B}{C \cdot b}$$
 (B – flexural stiffness of an edge stiffener in relation to central plate's surface; C – cylindrical stiffness of a plate; b – plate's width).

Buckling analysis was carried out using finite element method (FEM) [30]. Geometrical parameters of the plate and edge stiffeners except for thickness were constant. Plate's form was chosen as four-square, $\frac{a}{b} = 1$ (200x200mm) for task's simplification and decreasing additional calculations. Dimensions of the edge stiffeners (200x5(t)mm) were defined in such a way as to minimize a web elastic rotation in relation to axis along lengthwise side. Parameter γ should be changed in necessary range with thickness values ($t = 0.092 \dots 9.2$ mm) likely real constructions. Boundary conditions were corresponded with defined task. Compressive load, $q=10$ N/mm, was uniformly applied to the plate's end. Buckling forms were evaluated based on the obtained values $K\sigma$. Results of analysis (see Table 1 and Figure 3) gave conclusion that compressed plate buckled into cylindrical surface for $\gamma \leq 1.0$ ($K\sigma = 1$), and into anticlastic surface for $\gamma \geq 100$ ($K\sigma = 4$).

Table 1. Buckling coefficients

№	B/Cb	t,mm	$K\sigma$	№	B/Cb	t, mm	$K\sigma$
1	Case I	2,00	0,93	19	8,0	0,727	3,48
2	0,05	9,20	1,04	20	9,0	0,686	3,54
3	0,1	6,50	1,10	21	10,0	0,650	3,59
4	0,2	4,60	1,22	22	20,0	0,460	3,83
5	0,3	3,75	1,33	23	30,0	0,375	3,92
6	0,4	3,25	1,43	24	40,0	0,325	3,96
7	0,5	2,91	1,53	25	50,0	0,291	3,99
8	0,6	2,65	1,62	26	60,0	0,265	4,01
9	0,7	2,46	1,71	27	70,0	0,246	4,02
10	0,8	2,30	1,79	28	80,0	0,230	4,03
11	0,9	2,17	1,87	29	90,0	0,217	4,03
12	1,0	2,06	1,94	30	100,0	0,206	4,05
13	2,0	1,58	2,35	31	200,0	0,158	4,07
14	3,0	1,29	2,68	32	300,0	0,129	4,08
15	4,0	1,03	3,04	33	400,0	0,103	4,09
16	5,0	0,920	3,20	34	500,0	0,092	4,09
17	6,0	0,840	3,32	35	1000,0	0,065	4,10
18	7,0	0,778	3,41	36	Case II	2,00	3,93

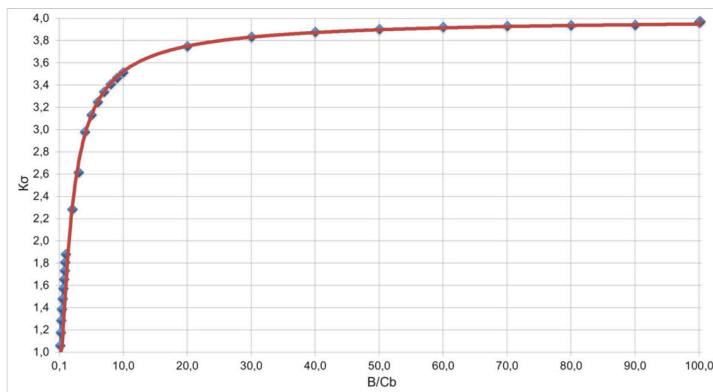


Figure 3 - Relation between buckling coefficient $K\sigma$ and parameter γ

For the reticular-stretched thermo-profile with cross-section thicknesses from 2 to 0.8mm relation γ are equal to 800...5000 accordingly. Thus, buckling analysis of compressed web as a plate supported along four sides could be applied. Buckling analysis of compressed plate (supported along four sides) that modelled behaviour of the reticular-stretched web (AI TCc 200-45-2.0) was carried out in comparison with perforated (AI TC 200-45-2.0), full and full plates with intermediate stiffener (see Figure 4).

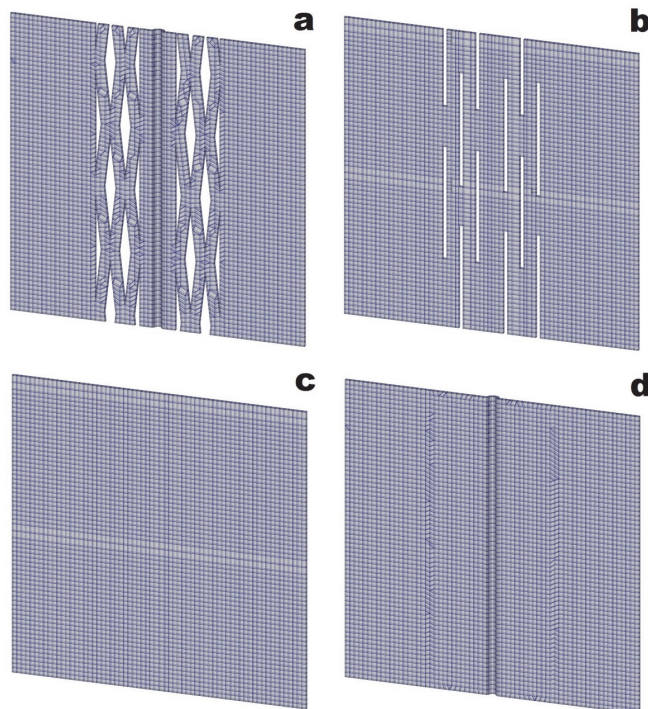


Figure 4. Types of plates (a – reticular-stretched; b – perforated; c – full; d – full with intermediate stiffener)

Geometrical plate dimensions were defined based on condition of sides' equality (198x198mm). Plate thicknesses were equal to 2.0mm. Compressive load, $q=10\text{N/mm}$, uniformly was applied to the plate's end. Obtained values of critical compressive stresses are presented in Table 2.

Critical compressive stress for web plate of reticular-stretched thermo-profile is equal to 85 N/mm^2 , which has satisfactory convergence with critical compressive stress obtained by experimental research. Normalized difference isn't more than 4,5%.

Comparative analysis of critical compressive stresses for four types of webs gave the following results:

- 1) Cuts on the reticular-stretched web decrease its buckling resistance by about 30%;
- 2) Web of the perforated profile has buckling resistance that is less than reticular-stretched one by about 40%;
- 3) Web of the profile without perforation has buckling resistance that is almost equal to reticular-stretched one. Normalized difference isn't more than 11%.

Table 2. Buckling coefficients for different plates

No	Element	Type of the web	P, N/mm ²	K _{buckl.}	P _{cr.} , N/mm ²	P ₀ , N/mm ²	K σ
1	Plate (cross-section's web)	Reticular-stretched	5.93	14.36	85.12	19.37	4.40
		Perforated	5.5	9.02	49.59		2.56
		Full	5.0	15.19	75.97		3.92
		Full with stiffener	5.18	21.62	112.07		5.79
2	Full cross-section	Reticular-stretched	5.93	16.97	100.59	19.37	5.19
		Perforated	5.5	10.91	60.02		3.10
		Full	5.0	19.23	96.15		4.97
		Full with stiffener	5.18	26.26	136.09		7.03

Buckling analysis of the compressed plate as a part of the cross-sections let to define more precisely critical stresses values taking into account more realistic web behaviour (see Figure 5).

Finite element models, which were built up for the previous task, were modified by addition of flanges (width, 43mm) with single edge folds (width, 14mm). Lengthwise sides were set free, transverse sides – supported.

Obtained values of critical compressive stresses (table 2) are more than classical values on 20%. This result is caused by elastic rotation of the web (due to torsional stiffness) in relation to its intersection with flanges. Qualitative results didn't change.

Today analytical calculations of centric and eccentric compressed thin-walled cold-formed profiles are carried out in accordance with Eurocode 3 (EN 1993-1-1, EN 1993-1-3, EN 1993-1-5) [19, 31, 32] and designers' manual (Ajrumyan E.L.) [33], based on the SNIIP II-23-81*[34]. These analytical methods are based on reduction of a gross cross-section to an effective cross-section that let one to take into account local and distortional buckling influences on bearing

capacity of the compressed element. There is no procedure in mentioned above methods that could take into account a perforation in the web.

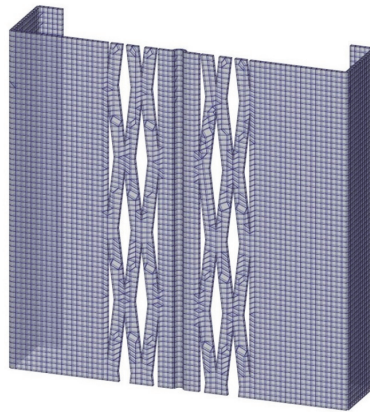


Figure 5. Finite element model of the reticular-stretched thermo-profile

Classical method of its consideration is based on replacement of the perforated web with full web that has reduced thickness. Reduction factor could be found on assumption that critical buckling stresses for perforated and reduced full compressed plates supported along four sides are equal. Solution of non-trivial equation (2) with known buckling coefficient of compressed perforated plate, $K_{perf.}$, gives necessary reduction factor. Buckling coefficient of compressed full plate supported along four sides is well known from classical task of its buckling analysis, $K_{gr.} = 4$.

$$k = \sqrt{\frac{K_{perf.}}{K_{gr.}}} \tag{2}$$

Table 3. Reduction factors for reticular-stretched plates

No	t,mm	P, N/mm ²	K _{buckl.}	P _{cr.} , N/mm ²	P ₀ , N/mm ²	K σ	K _{gr.}	k
1	0,75	15,2	2,14	32,6	11,7	2,79	4,0	0,835
2	0,85	13,5	2,96	39,9	15,0	2,65		0,814
3	0,95	12,0	3,97	47,8	18,8	2,55		0,798
4	1,05	10,9	5,19	56,6	22,9	2,47		0,785
5	1,15	9,9	6,65	66,1	27,5	2,40		0,775
6	1,25	9,1	8,37	76,5	32,5	2,35		0,767
7	1,35	8,5	10,37	87,8	37,9	2,32		0,761
8	1,45	7,9	12,68	100,0	43,8	2,28		0,756
9	1,55	7,4	15,32	113,0	50,0	2,26		0,752
10	1,65	6,9	18,31	126,9	56,7	2,24		0,748
11	1,75	6,5	21,69	141,7	63,7	2,22		0,746
12	1,85	6,2	25,46	157,4	71,2	2,21		0,743
13	1,95	5,9	29,66	173,9	79,1	2,20		0,741

Values K_{perf} for reticular-stretched thermo-profile were obtained by buckling analysis using finite element method (FEM) [35]. Geometrical dimensions of a plate (95.5x95.5mm) corresponded to reticular-stretched web part between flange and intermediate stiffener (AITCc 200-45-t). Cross-section thickness ranged from 0.75mm to 1.95mm with step 0.1mm ($t_{zinc} = 0.05\text{mm}$). Resulting reduction factor's values are within range from 0.74 to 0.84 (see Table 3).

FEM-analysis of compressed reticular-stretched thermo-profile and profile with reduced web thickness were carried out. Comparison of results showed that buckling resistance of reduced profile was less than buckling resistance of reticular-stretched thermo-profile by about 20%.

CONCLUSIONS

Taking into account above mentioned results the following conclusions could be made:

- 1) New type of thin-walled thermo-profile (reticular-stretched) were analyzed;
- 2) Numerical analysis of compressed reticular-stretched web showed that web cuts decrease its buckling resistance by about 30%. Comparative analysis of critical buckling stresses for reticular-stretched, perforated and full cross-section profiles gives a permission to conclude that intermediate stiffener is effective design solution;
- 3) Comparative analysis of experimental and calculative data for reticular-stretched profile and usual perforated profile showed that bearing capacity of the first one is more than the last one by about 80%.

ACKNOWLEDGEMENT

The experimental work was commented by Arto Ranta-Eskola, director of research, Rautaruukki Oyj (Finland). The authors also gratefully acknowledge the helpful comments and suggestions of the reviewers, which have improved the paper.

REFERENCES

- [1] Vatin, N.I. and Sinelnikov, A.S. Strength and Durability of Thin-Walled Cross-Sections, Design, Fabrication and Economy of Metal Structures. International Conference Proceedings, 2013, Miskolc, Hungary, April 24 – 26, Miskolc, 2013, pp. 165 – 170.

- [2] Winter, George. Light Gauge (Thin-Walled) Steel Structures for Building in the U.S.A. preliminary publication, 4th Congress of the International Association for Bridge and Engineering, 1952, 524 p.
- [3] Yu, Wei-Wen, Wolford, D. S. and Johnson, A. L. Golden Anniversary of the AISI Specification, 13 International specialty conference on Cold-Formed Steel Structures, St. Louis, MO, 1996, pp. 1–3, 5.
- [4] Schafer, W. and Pekoz, T. Computational modeling of cold-formed steel: characterizing geometric imperfections and residual stresses, *Journal of Constructional Steel Research*, Vol. 47, 1998, pp. 193–210.
- [5] Bayan Anwer Ali, Sariffuddin Saad and Mohd Hanim Osman, Finite Element Analysis of Cold-formed Steel Connections, *International Journal of Engineering (IJE)*, Vol. 5, №2, 2011, pp. 55–61.
- [6] Hartmut Pasternak and John Ermopoulos. Design of steel frames with slender joint-panels, *Journal of Constructional Steel Research*, Vol.35, Issue 2, 1995, pp. 165–187.
- [7] Cheng, Y., and Schafer, B.W. Simulation of cold-formed steel beams in local and distortional buckling with applications to the direct strength method, *Journal of Constructional Steel Research*, Vol. 63, Issue 5, 2007, pp. 581–590.
- [8] Hancock, G.J. Light gauge construction, *Progress in Structural Engineering and Materials*, 1997, pp.25–26.
- [9] Pekoz, T. Development of a Unified Approach to the Design of Cold-formed Steel Members, Research Report CF 87-1, American Iron and Steel Institute, 1987.
- [10] Gioncu, V. General theory of coupled instabilities, *Thin-Walled Structures*, 1994, pp.19 (2–4).
- [11] Belyi, G. I. Raschet uprugoplasticheskikh tonkostennykh sterzhnei poprostranstvenno-deformiruemoi scheme, *Stroitel'naiia mekhanika sooruzhenii: Mezhevuz. temat. sb. tr, LISI. №42*, 1983, pp. 40–48.
- [12] Tusnin, A. R. Chislennyi raschet konstruksii iz tonkostennykh sterzhnei otkrytogo profilja, Moscow: Izd-vo ASV, 2009, 143 p.
- [13] Ajrumyan E. L. Osobennosti rascheta konstruksij iz tonkostennykh gnutykh profilej, *Montazhnye i spetsial'nye raboty v stroitel'stve*, 2008, № 3, pp. 2–7.
- [14] Astakhov, I. V. Prostranstvennaia ustoichivost' elementov konstruksii iz kholodnognutykh profilei, Dissertation, St.-Petersburg, 2006, 123 p.

- [15] Kuznetsov, A. U. Prochnost' i prostranstvennaya ustojchivost' sostavnykh sterzhnevnykh ehlementov konstruksij iz kholodnogutykh profilej. Dissertation abstract, St.-Petersburg, 2013, 25 p.
- [16] Smaznov D.N. Konechno-elementnoe modelirovanie stoev zamknutogo secheniia iz kholodnogutykh profilei , Nauchno-tekhnicheskie vedomosti Sankt-Peterburgskogo gosudarstvennogo politekhnicheskogo universiteta, №123, 2011, pp. 334 – 337.
- [17] Kretinin, A. N. and Krylov, I. I. Osobennosti raboty tonkostennoi balki iz gnytykh otsinkovannykh profilei, Izvestiia vysshikh uchebnykh zavedenii, Stroitel'stvo, №6, 2008, pp. 1 – 11.
- [18] Zhmarin E.N. Mezhdunarodnaia assotsiatsiia legkogo stal'nogo stroitel'stva, Internet Journal "Construction of Unique Buildings and Structures", №2, 2012, pp. 27 – 30.
- [19] Tushina, O.A., Heinisuo, M. Method for analysis of thin-walled cold-formed purlins in roof based on the EUROCODE recommendations, Industrial and Civil Engineering, 11 (2012), pp. 67 – 70.
- [20] Kolesov, A. I., Lapshin, A. A. and Valov, A. V. Sovremennye metody issledovaniia tonkostennykh stal'nykh konstruksii, Privolzhskii nauchnyi zhurnal, №1, 2007, pp. 28 – 33.
- [21] Vatin, N.I. and Popova, E.N. Termoprofil' v legkikh stal'nykh stroitel'nykh konstruksiiakh, St.-Petersburg: Izd-vo SPbGPU, 2006, 63 p.
- [22] Vatin, N.I., Nazmeeva, T. and Guslinsky, R. Problems of cold-bent notched C-shaped profile members, Advanced Materials Research, Vols. 941 – 944, 2014, pp. 1871 – 1875.
- [23] Vatin, N.I., Havula, J., Martikainen, L., Aleksei Sinelnikov A.S., Orlova, A.V. and Salamakhin, S.V.. Thin-walled cross-sections and their joints: tests and FEM-modelling, Advanced Materials Research, Vols. 945 – 949, 2014, pp. 1211 – 1215.
- [24] Kesti, J. Local and distortional buckling of perforated steel wall studs, Dissertation for the degree of Doctor of Science in Technology, Espoo, 2000, 101p. + app.19p.
- [25] Perel'muter, A.V., Kriksunov, E.Z., Karpilovskii, V.S. and Maliarenkok A.A. Integrirovannaia sistema dlia rascheta i proektirovaniia nesushchikh konstruksii zdanii i sooruzhenii SCAD Office. Novaia versiia, novye vozmozhnosti, Magazine of Civil Engineering, №2, 2009, pp. 10 – 12.
- [26] Slivker, V. I. Stroitel'naia mekhanika. Moskow: ASV, 2005, 736 p.
- [27] Shatov, D. S. Magazine of Civil Engineering, №3(21), 2011, pp. 32 – 35.

- [28] Rasmussen, K. J. R. Experimental investigation of local-overall interaction buckling of stainless steel lipped channel columns, *Journal of Constructional Steel Research*, Vol. 65, Issues 8–9, 2009, pp. 1677–1684.
- [29] Timoshenko S.P. *Ustojchivost' sterzhnej, plastin i obolochek: Izbr. Raboty*, Moskow, Nauka, 1971, 807 p.
- [30] Gordeeva, A. O. and Vatin, N. I. *Magazine of Civil Engineering*, №3(21), 2011, pp. 36–46.
- [31] EN 1993-1-3, *Design of Steel Structures: Cold-formed thin gauge members and sheeting*.
- [32] Ungermann, D., Lübke, S. and Brune, B.. Tests and design approach for plain channels in local and coupled local-flexural buckling based on eurocode 3, *Thin-Walled Structures*, 2014, pp.108–120.
- [33] *Rekomendatsii po proektirovaniyu, izgotovleniyu i montazhu konstruksij karkasa malohtazhnykh zdaniy i mansard iz kholodnogutykh stal'nykh otsinkovannykh profilej proizvodstva OOO «BaltProfil'», TSNIIPSK im. Mel'nikova*, 2004, 69 p.
- [34] SP 16.13330.2011, *Steel structure*, M. Minregion razvitiya RF, 2011, 171 p.
- [35] Jurchenko V.V. *Proektirovanie karkasov zdaniy iz tonkostennykh holodnogutykh profilej v srede «SCADOffice» // Inzhenerno-stroitel'nyj zhurnal*. 2010. №8. pp. 38–46.

TUBULAR TRUSS JOINTS – HINGED OR RIGID?

Markku Heinisuo, Teemu Tiainen

Tampere University of Technology

ABSTRACT

Tubular steel trusses with welded joints are designed following standards, such as Eurocodes, supposing hinges to the joints between braces and chords. This is due to fact that the rotational stiffness of these welded joints has not been known until recently. In a recent study, the rotational stiffness of tubular welded joints using a comprehensive 3D finite element analysis was investigated. Corresponding buckling lengths for the members of the truss were defined by eigenmode analysis. Based on this work, in this paper it is briefly considered whether the widely used assumption of hinged joints is adequate or not.

TUBULAR STEEL TRUSS JOINT STIFFNESS

Tubular steel trusses (see Fig. 1) are widely used in many kinds of buildings. They are designed typically following standards such as EN 1993-1-1 supposing hinges in joints between chords and braces. This makes analysis procedure quite easy when simple node equilibrium equations can be used to solve member axial forces instead of more complex finite element model. Still, it is well-known that behavior of a welded joint is not hinged and probably not ideally rigid either, but somewhere in between.

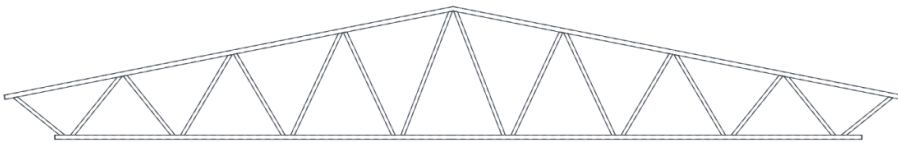


Figure 1. Typical tubular truss

The stiffness of such a joint was studied by Boel (2010) and Snijder et al (2011) by using comprehensive 3D finite element analysis. Based on previous literature they wrote the stiffness and buckling length as function of two parameters defined by

$$\beta = \frac{b_1}{b_0}$$
$$\gamma = \frac{b_0}{2t_0}$$
(1)

where b_1 is width of the brace, b_0 the width of the chord and t_0 the thickness of the chord wall.

The Eurocode standard EN 1993-1-8 gives limits for joint stiffness to tell if a joint can be considered ideally rigid or hinged:

$$\text{Hinged: } \frac{C_{in} \cdot L_{sys1}}{EI} < 0,5 \tag{2}$$

$$\text{Semi-rigid: } 0,5 \leq \frac{C_{in} \cdot L_{sys1}}{EI} \leq 8 \tag{3}$$

$$\text{Ideally rigid: } \frac{C_{in} \cdot L_{sys1}}{EI} > 8 \tag{4}$$

where EI is the bending stiffness of the brace, C_{in} the initial rotational stiffness of the joint and L_{sys1} the system length of the brace.

By using limits given by EN 1993-1-8 and stiffness formulas given by Boel (2010) curves in Figures 2 and 3 can be obtained. The length of bracing members in a tubular truss is typically between 1-6 metres. According to Fig. 2 the joint cannot be considered hinged. With low γ value – with relatively high wall thickness – the joint can always be considered rigid, if member length is over 2 metres.

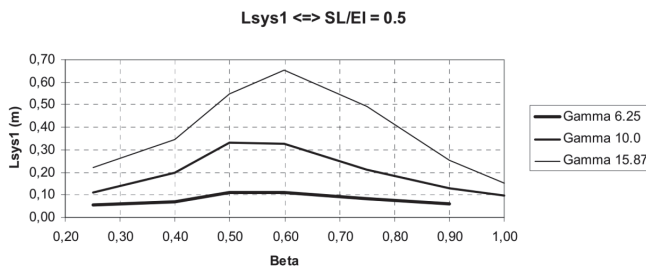


Figure 2. Limit length for hinged joint with different parameter values

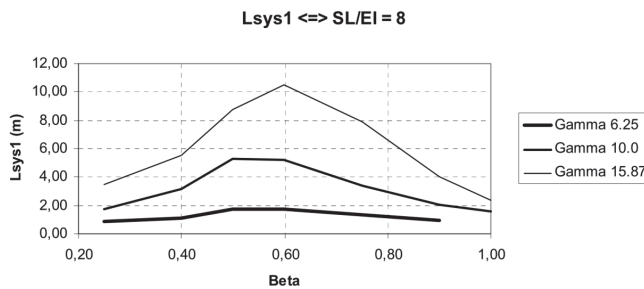


Figure 3. Limit length for ideally rigid joint with different parameter values

It was found that axial forces were basically the same regardless of the joint stiffness used in the model (Tiainen & Heinisuo, 2014). Still, joint stiffness has effect on bending moment distribution and buckling lengths of the members. Sneijder et al. (2011) gives formulas for buckling length as well. It seems that in most cases shorter buckling lengths than those proposed by EN 1993-1-1 could be used.

CONCLUSIONS

In this paper the problem of joint stiffness in welded tubular truss is considered. By using the most recent research information available it can be stated that - even though widely used - the assumption of hinges in brace ends seems unjustified. It seems that with typical dimensions, the joints should be considered either ideally rigid or semi-rigid. The problem of joint stiffness and buckling length is relevant not only in tubular trusses but steel frames as well.

REFERENCES

Harm Boel, *Buckling length factors of hollow section members in lattice girders*, Master's thesis, Eindhoven University, 2010

EN 1993-1-1, Eurocode 3: Design of steel structures, Part 1-1: General rules and rules for buildings, CEN, Brussels, 2005.

EN 1993-1-8, Eurocode 3: Design of steel structures, Part 1-8: Design of joints, CEN, Brussels, 2005.

Markku Heinisuo, Mikko Salminen, *Is welded joint in tubular truss hinged or rigid?* (onko putkiristikon hitsattu nurkkaliitos nivel vai jäykkä?), in Finnish.

Teemu Tiainen, Markku Heinisuo, *Tubular steel truss design using semi-rigid joints*, ICCCB 2014, Florida, USA.

Snijder, H.H., Boel, H.D., Hoenderkamp, J.C.D. & Spoorenberg, R.C. *Buckling length factors for welded lattice girders with hollow section braces and chords*. In L. Dunai, M. Iványi, K. Jármai, N. Kovács & L.G. Vigh (Eds.), *Proceedings of the 6th European Conference on Steel and Composite Structures (Eurosteel 2011), 31 August - 2 September 2011, Budapest, Hungary, (pp. 1881 - 1886)*

STEEL CONSUMPTION EFFICIENCY IMPROVEMENT IN HOLLOW UNITS MANUFACTURING

Devyatov V.V.^{1,a}, Vershinin V.V.^{1,b}

¹Moscow State University of Civil Engineering;
26 Yaroslavskoe shosse, Moscow 129337, Russia

^awitalijdeviatow3@gmail.com; ^bvlodya_91@mail.ru

Efficiency problems with rolled metal products usage in industry are always given high attention to. In the present article some efficiency improvement capabilities are considered. These capabilities relate to the use of round rolled metal products with solid and hollow cross-sections such as pipes and bars which are widely used as work pieces during manufacturing of various hollow and solid-section units like hydraulic and pneumatic cylinders, drill bars, sleeves, reducing fittings in pipelines, structural units and so on. In most cases during manufacturing of such products metal cutting is used to produce units with necessary shape and dimensions.

Metal cutting has the following advantages: a) it can be applied to almost any alloy and used to produce details of different shapes and dimensions with high accuracy and fine finish; b) necessary tools are low-cost; c) specific power capacity is low compare to other techniques. However it also has some disadvantages: a) large metal chip losses, especially during initial machining; b) high labor intensity when highest accuracy and finishing classes are necessary; c) large salaries expense; d) reduction of details load bearing capacity and their durability; e) relatively low productivity rate.

Metal machining wide use is necessary due to coarse work pieces, which are rather far from final products considering their shape and dimensions. If one provides manufacturing of work pieces with predefined dimensions, configuration and required finishing, further machining of such work pieces will be minimized. However, under current level of blank production this problem cannot be solved and metal cutting will be integral part of manufacturing procedure for a long time, especially at closing stage of finished-product output. Among main challenges are minimization of metal amount removed during cutting, productivity rate increase and cost reduction.

Mentioned problems can be solved through the use of pressure shaping techniques and its advantages. Pressure shaping techniques are believed to be among the most advanced. About 90% of all the steel smelted is subjected to pressure shaping: rolling, pressure molding, drafting, press forming, etc. When cutting is used, metal losses are about 30-40% of machined metal amount, while losses during processing on press-forging plant are 4-5 times lower. Using pressure shaping techniques also allows one to save 30 million

machine-hours and to free up to 10 000 production units per 1 million tons of metal machined.

One of the ways to improve efficiency of rolled metal products use is development and implementation of optimal flow processes, which have advantages of cutting and pressure shaping techniques. The lesser-used excess metal removal through cutting is, the higher steel consumption efficiency is. It is also essential when choosing processing technique to take into account cost of original mill products for a particular technique. It is known, that rolled tubular products are twice as more expensive as rolled solid-section round products of the same dimension and mechanical properties.

Let us compare alternative manufacturing techniques of hydraulic cylinder housings (see Figure 1). Among such prospective techniques are low-waste pressure shaping processing ones. The most prospective low-waste techniques are those, in which three dimensional metal strain state is implemented in deformation zone: mandreling, rotary extrusion, forward, backward and forward-and-backward differential hydrostatic and dynamic extrusion, etc. in solid or split dies. Extrusion techniques usage during manufacturing of details and work pieces ensures significant metal consumption reduction, high productivity rate, enhanced mechanical properties. In many cases machining operations with metal removing can be minimized or even excluded.

Let us consider two alternative hollow cylinder manufacturing techniques as an example of rolled tubular products utilization efficiency increase. In Figure 1 designs of hydraulic cylinders manufactured through traditional (Figure 1a, 1b, 1c) and low-waste pressure shaping (Figure 1d, 1e, 1f) techniques are shown.

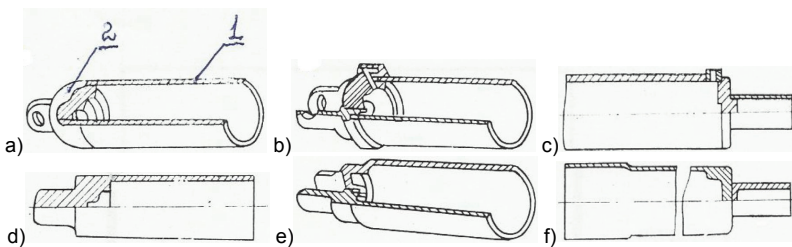


Figure 1. Designs of hydraulic cylinders, manufactured through traditional (a, b, c) and extrusion (d, e, f) techniques

In Figure 1 letters (a–c) refer to split-design cylinders which existed before, letters (d–f) – to the same cylinders manufactured through cold extrusion. Main parts of hydraulic cylinder housing are sleeve (1) and bottom (2) (see Figure 1a).

Low-pressure cylinder used in machine manufacturing is shown in Figure 1a. It has inner diameter equal to 88.9 mm, outer diameter equal to 98.43 mm and length of 682.65 mm. The cylinder weighs 7.7 kg. Cylinder of new design

(see Figure 1d) has no circumferential seal, so that scuffing doesn't occur; the new design is simpler than the old one, the cylinder is lighter and stronger.

In Figure 1b cylinder used in machinery with huge loads is shown. It required large amount of labor and time to manufacture such cylinders since cylinder operation under pressure of 2800 MPa would be impossible, if part processing was of poor quality. The cylinder had cast bottom. Mechanical processing of new design cylinder (see Figure 1e) is minimized. The cylinder design is made simpler, the cylinder has larger load-bearing capacity and requires minimal service.

Steering cylinders of old and new designs are shown in Figure 1c and Figure 1f, respectively. When manufactured through cold extrusion (Figure 1f), no welding was used. It is important when labor intensity, as well as strength at low temperature, is considered. Metal consumption reduction is achieved (Figure 1f) through cylinder open end expansion during extrusion instead of cylinder wall thickening and outer surface turning.

Main steps of traditional manufacturing techniques are work pieces preparation, sleeve mechanical processing with metal removing, hydraulic cylinder bottom (2) production through casting or press forming and welding of all these parts together.

Manufacturing of hydraulic cylinders through traditional techniques has several disadvantages:

- 1) Inefficient use of expensive rolled tubular products. It is reflected in the fact that metal industry produces limited amount of tube types which in most cases do not correspond to required standard dimensions of hydraulic cylinder parts. To obtain required sleeve dimensions one has to remove metal from inner and outer surfaces. As a result of such a technique employment metal utilization factor and labour intensity are low, sleeve strength characteristics decreases due to removal of tubular work piece surface layers hardened during rolling.
- 2) When the sleeve is welded to the bottom, sleeve dimensions obtained after mechanical processing change, so that additional finishing operations are necessary. Additionally, metal strength characteristics decrease due to effect of heat.

Rolled tubular products utilization efficiency can be improved via optimal coupling of metal cutting and pressure shaping techniques advantages in manufacturing processes. To make dimensions of tubular work pieces during hydraulic cylinder sleeve manufacturing closer to required in the drawings reduction or mandreling techniques can be used. Through the use of these techniques inner and outer diameters of tubular work pieces can be increased (mandreling) or decreased (reduction).

Hole mandreling provides high accuracy and fine surface finishing, increases durability, endurance and static strength. Mandreling can be performed with small and large interference i ($i = d_m - d_h$; d_m – mandrel diameter, d_h – diameter of a hole in a work piece) using free or confined schemes (see Figure 2).

During mandreling (see Figure 2) mandrel (2) with diameter d_m (index π in Figure 2) is pushed through the processing hole in tube (1) which has diameter d_h (index \exists in Figure 2). Hole diameter increases; height of the work piece decreases from L_w (index \exists in Figure 2) to L during free mandreling (Figure 2a) and increases from L_w (index \exists in Figure 2) to L during confined mandreling (Figure 2b).

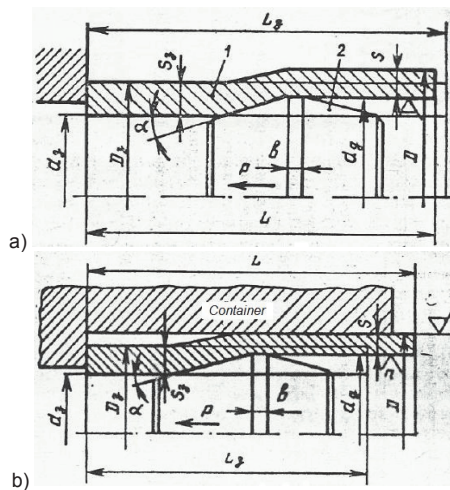


Figure 2. Sleeve mandreling with large interference: a – free mandreling; b – confined mandreling

Surface layer along the hole hardens, surface undulation decreases. During mandreling 3D stress-strain state exists in deformation zone, two principal stresses are compressive and the third one is tensile. Under low surface layer compression (small i) only crests burnishing takes place, no residual stresses occur. Under large hole expansion ratio plastic deformation can extend to a significant depth and even through the whole thickness of the tube wall. Due to distinct deformations of inner and outer surface layers of the tube after mandreling, residual stresses appears in the cylinder and their magnitude can reach yield strength.

It is known, that surface durability increases proportional to its micro hardness and magnitude of residual compressive stresses at the cylinder work surface. Residual stresses should not exceed particular values. High residual stresses can lead to hole dimensions and cylinder shape changes during its further processing and operation.

Presence of friction between mandrel and metal cause additional shear, which leads to uneven deformation within cross-section. Mandrel geometry also has an effect on cylinder wall properties and mandreling force.

Mandreling is utilized for hole making with high accuracy and fine surface finishing as well as for initial diameter enlargement and tubular work piece straightening prior to its mechanical processing. Large deformations can appear during processing of a work piece. Plastic deformations can take place not only in the surface layer, but in the whole deformation zone, which leads to metal mechanical properties changes through the whole detail thickness. This mandreling technique is sometimes called deforming traction.

Deforming traction technique spreads more and more. This process is facilitated by high labour intensity, possibility to process details up to 8 meters long, high dimension accuracy and mechanical properties.

Efficiency during hydraulic cylinder manufacturing can be increased through the use of mixed extrusion technique, which allows one to obtain hydraulic cylinder housing in one stroke of a press slide without production of hydraulic cylinder bottom and its further welding to hydraulic cylinder barrel.

Developed in [1–3] extrusion techniques allows one to obtain from round solid-section work pieces such products as barrels, cylinders with bottoms or flanges as well as with variable wall thickness along the barrel height. These techniques provide high labor intensity and quality of finished products.

Extrusion can be performed in cold, hot or warm states of the work pieces. Dependent on temperature regime during processing some details of a particular range can be manufactured with finished dimensions or finishing operations can be minimized compare to other techniques.

The basic problem during production of deep sleeves ($H/d > 2.5$), e.g. during making sleeves by backward extrusion, is that the punch operates under very difficult conditions (high temperature and high unit pressure), which cause reduction of its lifetime and frequent failures. For this reason deep sleeves are produced through at least two technological steps. This involves the necessity of building two technological stands (often two presses are used), which considerably increases the cost of production, its labor consumption and, above all, reduces productivity rate.

The new method of sleeve manufacturing proposed in [2] combines the known and specific pattern of metal flow in the extrusion process and aims at achieving the following: increased lifetime of working tools, productivity increase, manufacturing costs decrease, reduction of material losses and extrusion force magnitude decrease. This method includes two stages that are characterized by the following features (process scheme is illustrated in Figure 3):

- *Stage I* consists of simultaneous backward extrusion and mixed extrusion known schemes utilization, as a result of which a semi-finished product is obtained – a sleeve with a stem. Metal stream flows in two directions with part of the deformed perform volume flowing in the ring space and the remaining part flowing backward to the upper punch to form part of the sleeve already in the first stage.
- *Stage II* is the final step of deep sleeve forming and includes the deformation of the stem formed during the first stage of the process. The ring sliding down to form a free space in the container gradually releases the stem metal which, under the action of the punch, is carried towards the recipient walls and at the same time the sleeve wall of the preset thickness is formed. The sleeve bottom thickness depends on the setting of the punch distance from the movable ring.

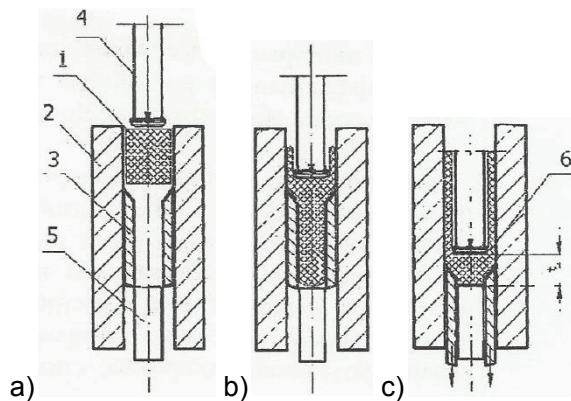


Figure 3. Schematic diagram of the sleeve manufacturing through the mixed extrusion technique using movable ring in the container 1) cylindrical work piece; 2) container; 3) ring; 4) punch; 5) pusher; 6) blank

The cylindrical work piece (1) is placed in the container (2) on the ring (3), which is fixed at the initial stage (see Figure 1a). Under punch action of the punch (4) metal of the cylindrical work piece (1) flows in two directions: into the gap between container wall (2) and the punch (4) and into the opening of the ring (3). At the moment of contact of the work piece metal with the face of the pusher (5) (see Figure 1b) the ring (3) starts moving down in accordance with the punch movement and at the same speed. The pusher (5) at this stage is fixed and the punch (4) keeps moving down (Figure 1b). The process is finished upon reaching the specified distance t between the face of the punch (4) and the pusher (5) equal to the sleeve bottom thickness. Then the blank (6) is removed from the container by the pusher (5) (see Figure 1c).

Results of theoretical and experimental study of the mixed extrusion technique with movable sleeve are presented below. Cylinders were made of 45 steel with outer diameter equal to 500 mm and wall thickness of 5 mm; squeezer yoke velocity was 50 mm/s and extrusion temperature varied from 850°C

to 1050°C. Influence of various extrusion process parameters on extrusion forces was analyzed through numerical simulation in FORGE® 2D. Initial temperature of the work piece, squeezer yoke velocity, punch dimensions and configuration were variable parameters.

Extrusion forces as a function of punch displacement for various work piece initial temperature are presented in Figure 4 for traditional backward extrusion (a) and new mixed extrusion with movable sleeve (b) techniques. Comparison of extrusion forces behaviour, as punch displacement increases, allows one to conclude that when new technique is used forces are significantly lower than during traditional backward extrusion. This results in economy of energy, punch durability increase and allows one to obtain through extrusion cylinders with large length

CONCLUSION

In conclusion it is worth emphasizing that presented in the article examples of effective use of new cylinder manufacturing techniques that facilitate metal consumption reduction, energy savings, labour intensity and product quality increase do not encompass all possible pressure shaping technique applications.

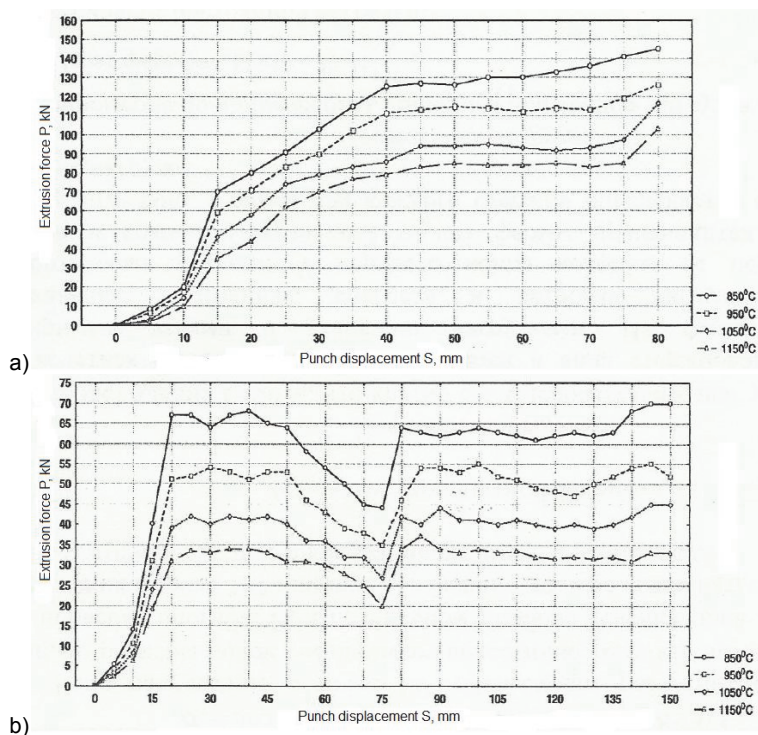


Figure 4. Extrusion forces as a function of punch displacement for various work piece initial temperature: a) traditional backward extrusion technique; b) new mixed extrusion with movable sleeve technique

REFERENCES

1. Devjatov V.V., Michalczyk J., Rajczyk J. Teoretyczne podstawy i technologia procesów wyciskania (*in Polish*). Częstochowa. Wyd.PCzęst. 2011.
2. Dewiatow W. W., Rajczyk J.: Sposób wytwarzania głębokich tulei z dnem (*in Polish*). Polski Patent P345424.
3. Dewiatow V. V., Dyja H. S., Stolbow V. Y. i in.: Matematyczne modelowanie i optymalizacja procesów wyciskania (*in Polish*). Seria Metalurgia nr. 38. Częstochowa 2004.

RELIABILITY ANALYSIS OF STEEL STRUCTURES

S.F. Pichugin

Poltava National Technical University named after Yuri Kondratyuk, Ukraine

INTRODUCTION

The steel structure reliability is the problem of high priority today. It can be treated like a scientific trend which doesn't need both material and financial expenses. The general probabilistic models of wind, snow and crane loads can be considered as a statistical basis of reliability estimation. However, these approaches lack both systematic analysis and model comparison which can cause different results in structural reliability design. The probabilistic computation of structures was not developed with regard to joint loads application, their real distributions and frequency characteristics. The assessment of a redundant structure safety is rather difficult task. In spite of many studies that have been done the problem of reliability analysis of these structures has not been solved yet. The exploitation experience demonstrated the existence of quite different reliability of various structures.

BASE OF RELIABILITY ESTIMATION

Researches of loads

The general algorithm of the method of reliability estimation of steel building structures is illustrated in Figure 1. This method is based on experimental researches, pooling and integration of load statistic data. The results of regular snow measurements for 15 – 40 years at 62 Ukrainian meteorological stations have been taken as reference statistical material for ground snow load. The systematic information about the wind velocity measurements done with ten minutes average at 70 Ukrainian and CIS (The Commonwealth of Independent States) meteorological stations were used as a initial data. The wind force values were analyzed with the help of a certain quadratic transformation of the wind velocity without the account of its direction. The crane load experimental studies were performed at several metallurgical plants in different shops from 10 to 30 years of service. Vertical and horizontal loads of bridge cranes with rigid or flexible hanged cargo were analyzed.

In accordance with obtained results the following load features were determined. Ground snow and wind loads for Ukraine and Russian south regions are of a quasi-stationary origin. Their mathematical expectations and standards have a seasonal trend. At the same time snow and wind frequent characteristics and normalized ordinate distributions remain constant during the season (Pichugin 1997, 2000). The crane load is stationary; its density distribution corresponds well to the normal distribution law (Pichugin

1998). Taking into account the bimodal character of Ukrainian snow density distributions so-called polynomial-exponential law was used:

$$f(\gamma) = \exp(C_0 + C_1\gamma + C_2\gamma^2 + C_3\gamma^3), \quad (1)$$

where $\gamma = (x - \bar{X}) / \hat{X}$ – normalized deviation of snow load; C_0, \dots, C_3 – parameters which are determined by the values of load mathematical expectations \bar{X} , standard \hat{X} and relative skew. Wind density distribution is well approximated by Veibull's law or distributions (1).

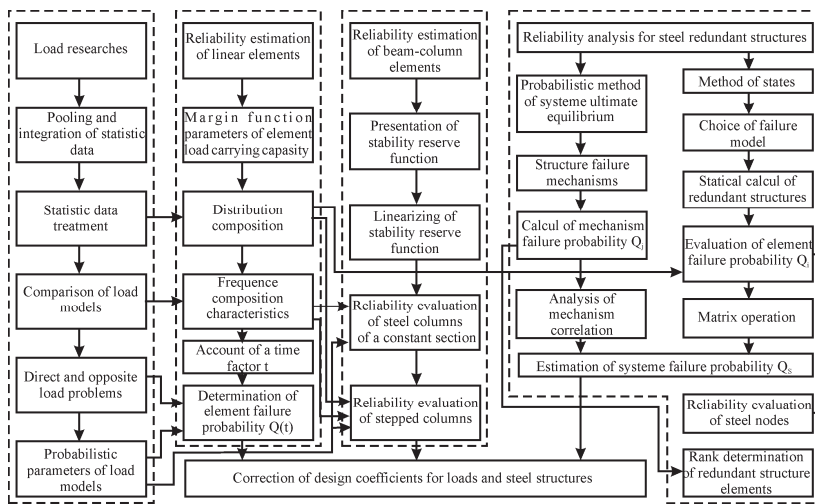


Figure 1. General algorithm of reliability estimation of steel building structures.

Probabilistic Load Models

The systematic analysis of random loads was realized for the five most commonly used probabilistic models. The main one is presented in the form of a stationary (crane load) or quasi-stationary (wind and snow loads) random processes; their parameters are an effective frequency ω and the coefficient of trend K_{lr} which accounts the atmospheric load season change.

The absolute maxima of random processes are one of simpler model; they are determined by the tail part of the distribution of outliers and are higher then characteristic maximum level γ_0 . The latter is a solution of the following equation $N_+(\gamma_0; 0 \leq \tau \leq t) = 1$, where $N_+(\cdot)$ – the number of outliers of random process.

The model in the form of a random sequence of independent random loads with the intensity λ is widely spread (λ – the number of loads in per-unit

time t_λ). For discrete presentation of loads the frequent parameter of which is the mean duration of overloading $\bar{\Delta}$ connected with the intensity by the ratio $\Delta = t_\lambda / \lambda$.

The analysis of the problem has demonstrated that the load values sampling can be classified as the exponential type. That is why their maximum values can be presented correctly by the extreme double exponential Gumbel distributions of a normalized type (Gumbel 1967):

$$y = \alpha_n (\gamma - u_n), \tag{2}$$

where u_n – characteristic extremum; α_n – extreme intensity; $y = -\ln[-\ln F(t)]$ – Gumbel distribution argument; $F(t)$ – integral distribution function.

Comparison of Load Models

The choice of models of loads depends on a specific of solving probabilistic problems: the more complicated ones are solved in the manner of random processes which, however, are difficult to describe and take much more computation time. More accessible and simple models, mentioned earlier, are based on the random values and corresponding frequency characteristics and provide no less exact solution if they are properly based. In particular, all the examined models are close to its sense of the following evaluation:

$$Q(t) \cong N_+(\gamma, t) = \omega t K_r f(\gamma) / \sqrt{2\pi} = f(\gamma) / f(\gamma_0) = \lambda t [1 - F(t)] = t [1 - F(\gamma)] / \bar{\Delta}, \tag{3}$$

where $Q(t)$ – probability of exceeding γ – level during t .

The first formula is based on the expression of frequency of quasi-stationary random process which has the general distribution of ordinate and normal distribution of a derivative (Bolotin 1969).

Provided with Equation (3) the formulae which connect the parameters of different probabilistic load models were derived in author’s papers (Pichugin 1995, 2011).

Load probabilistic comparison can be well performed at the extreme scale (Gumbel 1967) which is illustrated in Figure 2. On the axis of ordinate of a scale the standardized load is set, on the axis of abscissa the Gumbel’s distribution argument is set which is connected with the load return period T . Gumbel’s distribution (2) is described on the scale in the form of straight lines. The models of a random process, a random sequence of independent loads and discrete presentation are introduced as different curves. The main advantage of this scale is its visual effect of the tail parts of the load distributions which

have rather small distinctions in the usual form of presentation. It enables to present the visual comparison and correspondence of parameters of different load models.

All necessary mean wind and snow probabilistic parameters of Ukrainian districts were introduced in our works (Pichugin and Makhinko 2005, 2012). The worked out parameters give possibility to develop the reliability estimation of building structures.

RELIABILITY OF STEEL ELEMENTS UNDER DIFFERENT STEEL LOADS

General Approach

The principal ideas of applied method were developed in works (Pichugin 1995, 2011). The failure of an element takes place when a stochastic stress under the joint applied loads $\tilde{S}(t)$ exceeds the random limit of a steel yielding state (resistance of an element \tilde{R}).

The failure of the element is defined by the equation

$$\tilde{Y}(t) = \tilde{R} - \tilde{S}(t) < 0, \quad (4)$$

where $\tilde{Y}(t)$ – margin function of load carrying capacity.

The safety characteristics is of great importance and is derived from equation

$$\beta = \bar{Y} / \hat{Y} = (\bar{R} - \bar{S}) / (\hat{R}^2 + \hat{S}^2)^{1/2}, \quad (5)$$

where $\bar{Y}, \bar{R}, \bar{S}$ – the corresponding mathematical expectations; $\hat{Y}, \hat{R}, \hat{S}$ – the corresponding standard mean deviations.

The probability of failure $Q(t)$ is estimated from Equation (3). The solution of this problem demands the presentation of joint distributions and the characteristics of $\tilde{Y}(t)$ frequency. The compositions or differences of load and strength distributions should be done for design of margin of carrying capacity (5). Convolution formulae are used for this purpose; their analytical expressions were represented in our book (Pichugin 2011). The examples of joint distributions based on the proposed formulae are presented on the Figure 3. They can be non-symmetrical and differ considerably from the normal distribution in solutions of structural reliability problems.

Correlation functions and effective frequencies of random processes of various loads differ considerably. Therefore the joint action of several loads becomes multi-frequency. This peculiarity can be defined in the formula (3) by the structure complexity coefficient β_{ω} which equals the ratio of mean frequency on maximum to the effective frequency on zero.

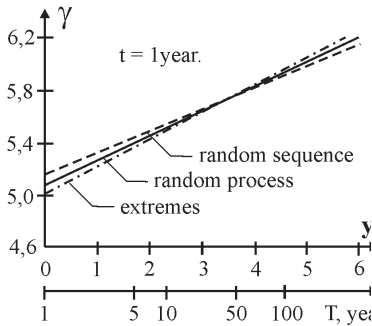


Fig.2. Comparison of crane load models. F

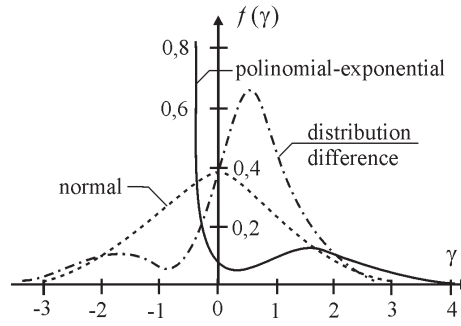


Fig.3. Difference of distributions.

Analysis of Reliability of Steel Elements

Some of the buildings consist of numerous structures, roofs or ceilings. The dead load of structures like these is a sum of normal random values describing the weight of every layer. It is established that decreasing coefficient of combination $\psi = 0,60 - 0,95$ can be applied to a dead load in this case.

Crane beams as well as crane trestle structure can be treated like elements under only crane load. We'll examine general stress of these elements without local effects and fatigue. In this case the probability of structure failure $Q(t)$ depends on the ratio of a load stress of one bridge crane X_{M1} to the load stress of two bridge cranes X_{M2} , then on the ratio of a load carrying capacity of cranes to their mass and it also depends on crane work condition. The analysis showed that steel elements have a deficient reliability if they are under 4-wheeled crane load when $X_{M1}/X_{M2} \geq 0.8$ i.e. in the case of the one crane load dominance. In the rest cases steel elements reliability determined on the base of general stress state criteria under crane loads is sufficient. In some cases the design crane load on steel structures can be decreased when their reliability is preserved. For example, in the case if the approach of a loaded crane trolley to a crane track is limited or if the structure service term T is also limited. For the last case the design crane load may be multiplied by temporary coefficient $\gamma_T = 0.93 - 1.0$ for $T = 1 - 50$ years (Pichugin 2014).

The reliability of steel structures (beams, trusses) under snow load was estimated by a developed method. These structures are of different mass roofs and snow loads for all Ukrainian districts. The calculation demonstrated the lack of reliability of rafter structures. That justifies the idea of understating of existed snow loads Code in Ukraine. Besides, this fact validates the causes

of steel truss failures. It applies to steel structures with light weight roofs in the southern districts of Ukraine when there is much snow in winter. The increasing of snow design load for 1.5-2 times for our region can solve the reliability problem of steel structures under snow load.

Steel elements under wind load designed in accordance with the existing code (glass elements, wind protection screens etc) are of sufficient reliability. So if the service term of these elements will be limited it is possible to introduce the temporary coefficient $\gamma_T=0.46-1.0$ for $T=1-50$ years for the design wind load. The obtained results allow decreasing considerably the design wind load for the conditions of structure erection. It is recommended to introduce the increasing coefficients of combination $\psi = 0,7 - 0,9$ into the steel structure design under snow, wind and crane loads.

Reliability of Steel Beam-Column Structures

Time factor, existing loads, random steel strength were taken into account during computation process of these elements (Pichugin 2011). For that reason the statistic stability of steel beam column elements was investigated; the function of stability reserve has been offered; the possibility of its linearisation has been suggested; some approaches with regard to geometrical and physical non-linearity have been worked out. Existing steel columns of industrial buildings in a broad range of parameters were examined: when the truss and column connection is rigid or hinged; if the building span is 24-36 m, column step is 6-12 m: if the roof is with steel profile flooring or reinforced concrete panels, with bridge cranes of 30 to 125 tons and different conditions of work. It is applicable for all snow and wind districts of Ukraine. All the columns were designed in accordance with existing Code. The analysis of obtained results demonstrated the failure probability of steel column of a constant section as well as the upper parts of stepped columns. The failure period of mentioned above elements is 100-250 years. So the general conclusion is as follows: the reliability of steel columns of industrial buildings is quite sufficient. Besides, the reliability of lower parts of the stepped columns appeared to be much higher than upper ones. That is the result of applying additional random crane force to the lower part of a column. Taking into account these facts and using the criteria of equal reliability of upper and lower parts it is recommended to introduce the additional coefficient of work condition $\gamma_C=1.15$ in the calculation of lower parts of stepped columns. The introduction of this coefficient will allow decreasing steel column weight.

Reliability Analysis of Steel Structure Joints

The logic and probabilistic methodology was used for analysis. It was founded out that reliability of typical steel joints could be compared with the schemes of successive connections of correlated elements. Thus, the joint reliability depends upon the number of engaged independent load carrying elements. It is obvious that if the number of elements is increased the joint reliability will

decrease. The reliability of joints with less number of elements is higher. As a result of this the joints can be less reliable than the structure itself (column rods, span parts of beams and so on). The reliability of existing structures has to be examined together with the reliability of elements (sections) as well as joints.

Probabilistic Estimation of Redundant Steel Structures

Some beams and simple frames, as well as multi-storey and multi-span structures of industrial and residential buildings present this type of structures. The failures of these systems are various. This paper attacks the problem which concern is only steel structures with the loss of carrying load capacity. Redundant structure failures occur after some member failures in the form of transmission to different workable states. These states match different designing schemes with various probabilistic parameters. Thus, the redundant structure failure estimation is a very complicated problem as depends upon the system complexity. The method of states, probabilistic method of ultimate equilibrium and logic and probabilistic method were developed for solving this problem. The main attention was paid to the redundant structures with bending dominance (beams, frames). Corresponding formulae are derived; the algorithms and computing programs are developed. The estimation of a wide range of industrial redundant structures with different degree of redundancy was obtained on the base of this approach. It gave possibility to evaluate the safety level of redundant structures in comparison with separate members and statically determined structures. This level can be taken into account introducing the additional coefficient of work condition $\gamma_C = 1.1 \dots 1.4$. The minimum values of this coefficient correspond to the least number of appeared plastic hinges (two or three for so called "partial" mechanism of structure failure). The largest coefficient γ_C values have to do with failure scheme with the largest number of hinges of plasticity close to the degree of redundancy ("full" failure mechanism).

CONCLUSION

The general probabilistic models of wind, snow and crane loads were designed and taken as a statistic basis of reliability estimation. These models are as follows: stationary and quasi-stationary random processes, its absolute maxima, random sequence of independent loads, discrete presentation and extreme model. The practical method of reliability analysis of steel structure elements is proposed. Load real distributions and frequency characteristics are taken into account. Using the worked out method the reliability analysis of wide range of steel structures designed in accordance with existing Codes was examined. This analysis showed that the structures have rather different level of reliability. In particular the light roof structures are not reliable enough being under great influence of snow load for Ukraine. At the same time the Building Code allows over-estimation of reliability for steel columns. With regard to mentioned above it's proposed to correct some load factors,

a combination factor and a factor for model uncertainties of Design Codes of steel structures and loads. In addition the numeric computations offer to introduce a design coefficient which takes into account the specific character of work and failure of redundant structures.

REFERENCES

- [1] Bolotin V.V., *Statistic Methods in Structural Mechanics*, Holden Day, San Francisco, 1969, 250 p.p.
- [2] Gumbel E.I., *Statistics of Extremes*, Columbia University Press, New York, 1967, 320 p.p.
- [3] Gordeev V.N., Lantukh-Lyaschenko A.A., Pashinskii V.A., Perelmuter A.V., Pichugin S.F., *Loads and Actions on Building Structures*, Publishing House C, Moscow, 2009, 528 p.p. (in Russian).
- [4] Pichugin S.F., Probabilistic Presentation of Load Actings on Building Structures, *News for High Educational Establishments. Construction*, No. 4, 1995, p.p. 12 – 18 (in Russian).
- [5] Pichugin S.F., Reliability Estimation of Steel Elements under Variable Loads, *XLI Konf. Naukowa KILIW PAN i KN PZITB "Krynica 1995"*, Tom III, Politechnika Krakowska, Krakow – Krynica 1995, p.p. 151 – 156.
- [6] Pichugin S.F., Probabilistic Analysis of Wind Load and Reliability of Structures, *Proc. 2-nd European and African Conf. Wind Eng.*, Genova, Italy, Vol. 2, SGEEditoriali, Padova, 1997, p.p. 1883 – 1890.
- [7] Pichugin S.F., Analysis of Bridge Crane Loads on Industrial Buildings, *XLIV Konf. Naukowa KILIW PAN i KN PZITB "Krynica 1998"*, Tom VII, Politechnika Poznanska, Poznan – Krynica 1998, p.p. 41 – 47
- [8] Pichugin S.F., Probabilistic Description of Ground Snow Loads for Ukraine, *Snow Engineering. Recent Advanced and Developments.* – A.A.Balkema, Rotterdam, 2000. – p.p. 251 – 256.
- [9] Pichugin S.F., Makhinko A.V. *Wind Loads on Building Structures*, Publishing House ASMI, Poltava, 2005, 456 p.p. (in Russian).
- [10] Pichugin S.F. *Reliability of Industrial Buildings Steel Structures*, Publishing House ASV, Moscow, 2011, 456 p.p. (in Russian).
- [11] Pichugin S.F., Makhinko A.V. *Snow and Ice Load on Building Structures*, Publishing House ASMI, Poltava, 2012, 460 p.p. (in Russian).
- [12] Pichugin S.F. *Crane Load on Building Structures*, Publishing House ASMI, Poltava, 2014, 504 p.p. (in Russian).

SYSTEM ENGINEERING OF OPTIMAL DESIGN OF BUILDING CONSTRUCTIONS ELEMENTS

Vasilkin A.A.

Assistant Professor, Candidate of Science
Moscow State University of Civil Engineering (MGSU), Russia

ABSTRACT

The article shows the possibility of using mathematical programming methods to obtain optimal solutions of building structures. As an optimization algorithm used the method optimization, based on the property of monotonic nature of used dependencies. The paper emphasizes the usefulness of mathematical modelling methods, in providing integrated security of construction projects and to reduce the risk of the onset of failure.

The experience of use of system engineering in various areas of engineering activities, as well as the experience of formation of system engineering of construction allows you to define the study of design problems as one of the main spheres of its application. All modern problems of construction are purely system engineering problems, and they can be divided into the following groups: technical, organizational, economic, planning, and management [1]. One of the technical problems of design includes the optimal design selection problem.

Design optimization is one of the elements of technical design. This procedure allows engineers either to find the optimal geometrical and technical characteristics of the object under the specified conditions, or to get the general relations and arrange the necessary methods of calculation, if they not exist [2]. At that, the process of optimal selection of main characteristics of the designed object to will become a part of the appropriate method for solving the problem, and the designs optimization will continue to be the conceptual basis of design.

When solving construction design practical problems, the selection of design decisions are often based on the engineering experience and intuition. However, when solving design problems is based on a numerical optimization algorithm, the engineering problem can be considered as purely mathematical. At that, the selection of design decisions relies on an iteration optimization process of numerical data.

The optimization process proposed by Wilde [2] for solving engineering problems, when in the problem there are several variables, is based on using a method of successive separate optimization. The principle of method is that several variables are operated alternately, not simultaneously, i.e. at each stage only one of the variables is used.

In the presented work the optimization process is based on using the monotonic property of functions that prevails in the engineering problems on structural optimization. We will solve the problem of selection of optimal sizes for horizontal cylindrical pressure tank for liquefied gas storage.

Let us assume that the volume of the tank $V = 100\text{m}^3$, the internal pressure

$$p = 0.18 \frac{\text{kN}}{\text{cm}^2};$$

We have the following variables:

S - wall thickness;
 r - inner radius;
 l - tank length;
 t - base thickness.

At the first stage of the problem solving we will determine how the cost of the base t will vary depending on the variables S, r, l .

The total cost of manufacturing of the tank depends on S, r, l, t , i.e. it is necessary to minimize the function of the cost $C(t, S, r, l)$.

Let us consider t and determine what varies in the object cost depending on variation in t . It is obvious that first of all the base cost varies. Since the base cost depends on the steel volume V multiplied by the steel cost, and the steel cost is taken as constant, the cost of the base varies depending on the steel volume V or variables r and t . Therefore, we have the cost of the base $C(t, r)$ – the function of radius and thickness.

Since the total cost of the tank reaches its minimum when the base minimized in t , therefore we do not consider possible values of other variables at this stage of optimization.

We assume that the lower bound for the function $C(t, r)$ at constant r can be determined as $\min C(t, r)$, i.e. $C(t, r) \geq \min_t C(t, r)$ – partial function minimum in t , we change only t . The process of determination of $\min_t C(t, r)$ is called partial optimization in variable t .

Let us represent the total cost of the tank as a sum of the cost of the base $C(t, r)$ and the cost of the wall $C(S, r, L)$, while the cost of the wall does not depend on t .

Let us consider the whole object with respect to the first variable t . The sequential partial optimization of the total cost of the tank with respect to t is to find

$$\min_t [C(t, r) + C(S, r, L)] = \min_t C(t, r) + \min_{S, r, L} C(S, r, L) = \min_t C(t, r) + C(S, r, L)$$

since the function $C(S, r, L)$ does not depend on t .

In the presented equation the partial minimum of the total cost depends on all the variables of the problem, except t , because t is a variable to be minimised and the value of this variable is being optimized out of the function of the total cost.

Ultimately we are interested in the minimization of the total cost of the tank in all four variables that can be written as:

$$\min_{t, S, r, L} [C(t, r) + C(S, r, L)] \quad (1)$$

We can achieve the required result by determining partial minimum in t and minimizing the obtained function in all other variables. The sequence of these operations is presented as:

$$\min_{S, r, L} (\min_t (C(t, r) + C(S, r, L))) = \min_{S, r, L} (\min_t C(t, r) + C(S, r, L)) \quad (2)$$

Two minima of the function of general expenses (1) and (2) must be equal.

$$\min_{t, S, r, L} [C(t, r) + C(S, r, L)] = \min_{S, r, L} [\min_t C(t, r) + C(S, r, L)]$$

The right part of the equation refers to the fact that the original problem consisting of four variables should be solved at the first stage by partial optimization in t . For this purpose it is enough to examine the function characterizing the cost of the base and set a limit in t of the form $t \geq H \cdot r$.

According to the Designer's Reference. Metal structures. T2. Ed. V.V. Kuznetsov [3], spherical bases are analyzed for stress and strains by:

$$\sigma = \frac{\gamma_f}{2 \cdot h} \leq \gamma_c \cdot R, \text{ from which } t = \frac{p \cdot \gamma_f \cdot r}{2 \cdot R \cdot \gamma_c}$$

We assume

then

$$H = \frac{p \cdot \gamma_f}{2 \cdot R_y \cdot \gamma_c}$$

for steel 09Г2С-15 (С345) at a thickness $t = 20 \div 40$ mm;

$$R_y = 29 \frac{kN}{cm^2};$$

$\gamma_c = 0.8$ is a working condition ratio

$\gamma_f = 1.2$ is a partial safety factor for load for internal pressure.

We will receive

$$H = \frac{0,18 \cdot 1.2}{2 \cdot 29 \cdot 0.8} = 4.7 \cdot 10^{-3}$$

The problem of the sequential partial optimization is to determine $\min_t C(t, r)$ taking into account constraints (strength conditions for the base). At that the radius r is temporarily assumed as a constant value, and H as parameter that may take on appropriate values for various design characteristics.

The cost of the base is proportional to the volume of metal and is an increasing function of t , which is as follows.

The steel volume of the base is $V = 2 \cdot \pi \cdot r^2 \cdot t$. Let us set the constant 2π as a parameter of the cost of the base C_t ,

$$\text{Thus, } C(t, r) = C_t \cdot r^2 \cdot t,$$

Therefore, $\min_t C(t, r) = C_t \cdot r^2 (\min_t t)$, so to minimize the cost of the base it is necessary to make its thickness t as small as possible, i.e. as close to the lower bound $t \geq H \cdot r$ as possible.

Thus, the minimum cost of the base is:

$$\min_t C(t, r) = C_t \cdot r^2 \cdot H \cdot r = (C_t \cdot H) \cdot r^3,$$

where $(C_t \cdot H)$ is a parameter.

At the next stage of solving of the problem we will make a partial optimization of the total cost of the tank in the wall thickness S .

Other factors being equal (t, r, l are constant) the cost of manufacturing of the tank wall increases as S increases. Therefore, the value S should be made as small as possible. Let us set the restriction for the strength of the tank wall. According to the Designer's Reference [3] the voltage in the tank wall will be:

$$\sigma = \frac{\gamma_f \cdot p \cdot r}{S} \leq R_{wy} \cdot \frac{\gamma_c}{\gamma_n},$$

where,

$R_{wy} = R_y$ is a rated design resistance of a weld at physical monitoring methods;

$\gamma_c = 0.8$ is a working condition factor;

$\gamma_n = 1.1$ is a safety factor for the purpose;

$\gamma_f = 1.2$ is a partial safety factor for the load for internal pressure;

S = wall thickness;

$$S = \frac{\gamma_f \cdot p \cdot \gamma_n}{R_y \cdot \gamma_c} \cdot r$$

Let us assume the imposed restrictions in the form $S \geq K_s \cdot r$, where

$$K_s = \frac{\gamma_f \cdot p \cdot \gamma_n}{R_y \cdot \gamma_c} = \frac{1.2 \cdot 1.1 \cdot 0.18}{29 \cdot 0.8} = 10.2 \cdot 10^{-3}$$

The function of the cost of the tank wall will reach its minimum, when the value S corresponds to the exact lower bound, i.e. $S_{min} = K_s \cdot r$.

Therefore,

$$\min_{S, r, l} [C(S, r, l)] = \min_{r, l} [\min_S C(S, r, l)] = \min_{r, l} [C(S_{min}, r, l)] = \min_{r, l} [C(K_s r, r, l)]$$

The cost of the wall material is proportional to its volume, which is equal to $2\pi r \cdot l \cdot s$. Let us denote 2π as C_s as a parameter of the wall cost.

We have $C(S, r, l) = C_s \cdot r \cdot l \cdot S$,

To minimize S , we substitute $S_{min} = K_s \cdot r$, then the cost of the tank is minimized in S and will be

$$C(S, r, l) = C_s \cdot r \cdot l \cdot K_s \cdot r = (C_s \cdot K_s) \cdot r^2 \cdot l$$

which is an increasing function of r and l .

The result of partial optimization of two variables will be as follows:

$$\begin{aligned} \min_{t, S, r, l} [C(t, r) + C(S, r, l)] &= \min_{r, l} [\min_{t \geq H \cdot r} C(t, r) + \min_{S \geq K_s \cdot r} C(S, r, l)] = \\ &= \min_{r, l} [(C_h \cdot H) \cdot r^3 + (C_s \cdot K_s) \cdot r^2 \cdot l] \end{aligned}$$

(3)

For minimization in r and in l , it is necessary to consider the remaining constraints.

The tank volume will be:

$$V = \pi \cdot r^2 \cdot l \quad (4)$$

One can see that the functions (3) and (4) are increased as r and l increase. Thus, the greater is the tank volume, the greater is its cost. The tank with minimum permissible volume $V = \pi \cdot r^2 \cdot l$ corresponds to the minimum cost.

From the equation of the tank volume you can obtain an explicit expression for l , at that r is unknown.

$$l = \frac{V}{\pi \cdot r^2}$$

The elimination of l from the relation (3) will lead to the dependence:

$$C = \min_{r,l} \left[(C_t \cdot H) \cdot r^3 + (C_s \cdot K_s) \cdot r^2 \cdot \frac{V}{\pi \cdot r^2} \right] = (C_t \cdot H) \cdot r^3 + \frac{V}{\pi} \cdot (C_s \cdot K_s),$$

we obtained an equation with r in the first summand.

Since the factor $(C_t \cdot H) \cdot r^3$ is positive, and the factor $\frac{V}{\pi} \cdot (C_s \cdot K_s)$ does not depend on r , the total cost of the tank is an increasing function of r . Thus, the radius of the tank should be as small as possible. At the same time from the formula of the tank volume $V = \pi \cdot r^2 \cdot l$ it is seen that the value of the radius is bounded from below, because there is an upper bound of the wall length - the maximum value L_{max} .

$$r = \sqrt{\frac{V}{\pi \cdot l}}; \quad l = \frac{V}{\pi \cdot r^2} \leq L_{max}$$

Therefore, we assume $l_* = L_{max}$, where l_* is the value of this variable at which a minimum of the function being optimized is achieved. We have two constraints on the base thickness t , the lower bound is determined by the strength condition, the upper bound – by the limitation of the total tank length L_{max} . As the cost of the base is increased with a rise of t , at the minimum point as an active constraint there should be used the greatest lower bound, i.e. $t_* = H \cdot r_*$. For partial optimization in r it is necessary to use a limiting value of the tank volume V as an active constraint.

Thus, there are four constraints:

For wall thickness $S \geq K_s \cdot r$

For base thickness $t \geq H \cdot r$

For the dimensions, which determine the volume $V = \pi \cdot r^2 \cdot l$
 For the overall length of tank $l \leq L_{max}$

Finally we have that the definition of an optimum design is ensured by using the following equations:

$l_* = L_{max}$ - the optimal value of the length of the tank l ;

$r_* = \sqrt{\frac{V}{\pi \cdot L_{max}}}$ - the optimal value of the radius of the wall r ;

$t_* = H \cdot r_*$ - the optimal value of the base thickness t ;

$S_* = K_s \cdot r_*$ - the optimal value of the wall thickness.

The following main design characteristics are set in this example

$L = 1200$ cm; $V = 100$ m³, $H = 4.7 \cdot 10^{-3}$; $K_s = 10.2 \cdot 10^{-3}$,

Then the variables have the following optimal values.

$l_* = 1200$ cm;

$$r_* = \sqrt{\frac{100 \cdot 10^6}{3.14 \cdot 1200}} = 163 \text{ cm.}$$

That corresponds to $D = 326$ cm ≈ 3.25 m - therefore a constraint on the observance of transport dimensions is performed.

$t_* = 4.7 \cdot 163 = 0.76$ cm = 8 mm;

$S_* = 10.2 \cdot 10^{-3} \cdot 163 = 17$ mm.

CONCLUSION

The considered in this article method of partial optimization by Wilde, is based on the monotonic nature of the dependencies, which is a quite simple and at the same time reliable theoretical basis of the method.

We have designed the tank on the basis that its length must correspond to the maximum permissible value determined by the overall constraints, and the other dimensions are determined by the requirements of design standards, and each constraint is considered as a strict equality. At designing of building structures, which are fully conditioned by the constraints, you can use the inherent property, allowing you to solve the problem without detailed information on the economic characteristics of the designed construction - the monotonic property of the function.

REFERENCES

1. Gusakov, A.A., System engineering. M.: Fund New Millennium, 2002, 768 pages.
2. Wilde, D., Optimal design: Translation from English, M.: Mir, 1981, 272 pages.
3. Kuznetsov, V.V., Metal structures. In 3 volumes. Designer's Reference. M.: ASV, 1998, 576 pages.

ON THE CHOICE OF EVALUATION ASPECTS IN UNDERSTANDING UNIVERSITY-BUSINESS COOPERATION (UBC) RESULTS

Tenhunen, Lauri

HAMK University of Applied Sciences, Finland

Ranta-Eskola, Arto

SSAB, Finland

ABSTRACT

In European countries, the social impact of higher education units is typically estimated in such a way that the focus has been on the produced services and direct benefit to the units rather than on the interests of the sectorial or functional co-operation and / or the economic results of joint arrangements.

The main tasks of universities are education, research as well as transfer of information and know-how (mm. Chatterton & Goddard, 2000; Etzkowitz & Leydesdorff, 2000). Most authors agree these.

In theory it would be easy to operationalize the measurement of achieving the main task of higher education units. However, evaluation results differ much based on the ways of different evaluation aspects, including dimensions such like “qualitative – quantitative”, “real – mental”, “cooperation – independent activities”, “explicit know-how – tacit know-how” and especially “evaluation by cooperative partners – self-evaluation”.

This paper points out some evaluation aspects of the social impacts of universities and especially university-business cooperation. The main result of the paper is that choosing those evaluation aspects which are acceptable from the point of view of all relevant cooperation partners, leads to best ways in university-business cooperation. In that case also the social impacts of universities are best possible from the point of view of the cooperation partners and the public and private financiers of higher education units.

The paper utilizes Finnish experiences.

BACKGROUND

The concept of “the social impacts of higher education units” can be found from many laws in Finland. It has been used as precondition to have a license for having government funded higher education, to determine the quantity of financing or to determine the unit prices in higher education. The regulations of the government budget in Finland have partly been founded on the concept

of the social impacts of the administrative sectors. The administrative sectors have to set targets on the social impacts in their budgets and the level of attaining these targets is also measured.

According to the evaluation report of higher education institutions (HEIs) in Finland (KKA 2013), some 90 % of those who answered the questionnaire agreed with the argument that "... the utilizing of research results and the social interactions of HEIs" should be used when developing the financing models of HEIs in Finland.

In the program of impressiveness and productivity, launched by the ministry of economy and finance in Finland (2012), the social impact of a public institution is defined to be a so called entrenched concept, which can be interpreted to form one part of the productivity of an organization.

Productivity			
Internal		External	
Cost efficiency	Performance	Service ability	Social impacts

Figure 1. The structure of the productivity of an organization (The program of impressiveness and productivity, launched by The ministry of economy and finance in Finland, 2012)

In the above mentioned program, the social impacts are defined to include the level of performance of the organization, the stage of accomplishing the targets of social conditions and the targets of social impacts based on the activities, results, products and services for the citizens and society.

Causality seems to be the fundamental concept when analyzing and evaluating social impacts. The impacts are assumed to depend on activities and processes of an organization. When analyzing the social impacts of HEIs, the causality aspects need to be evaluated as well. The dependence of the results and impacts on the accomplished activities and processes is not absolutely clear, because social impacts are connected to many complicated social, economic and cultural processes. Also the dependence is indirect in many cases.

One of the analyzing possibilities is based on the method of the Logic Model (Frechtling, 2007; Davey & Plewa & Muros, 2014). The Logic Model shows the theoretical causality between resources, activities, results, products and impacts. Typically the social impacts of universities and higher education units have been evaluated by analyzing the utilities produced by the institutions themselves. In the analyses, the utilities which can only be reached in functional cooperation or in industrial cooperation are neglected.

This rules out also such development arrangements which are possible only in cooperation. In some case these are equal, but in some cases they differ a lot.

When using the Logic Model (Figure 2), the base of planning is formed on the aimed products of the activities. Then results, activities and resources are derived from the products. Setting the targets is mostly based on the products and their impacts.

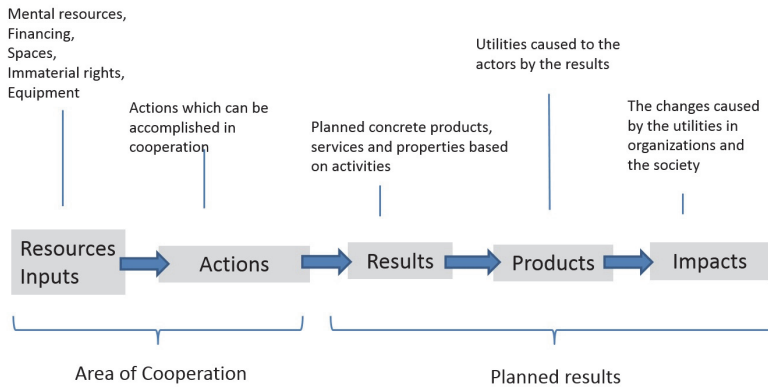


Figure 2. The Logic Model (modified and visualised)

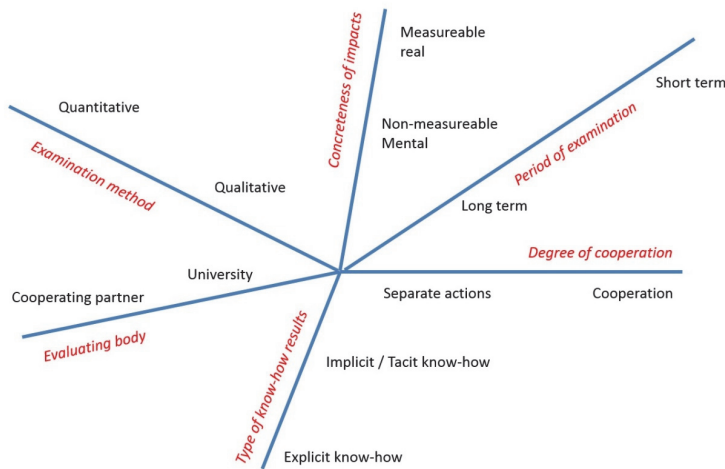


Figure 3. Framework for examining and analysing the results and Social impacts of higher education institutions

Social impacts can be rather complicated both conceptually and causally. Based on the literature (Davey et al, Perkmann et al (I) and (II), Liyanage et al) it is possible to distinguish some elements which help in evaluating the impacts. These are e.g. period of examination, concreteness of impacts and degree of cooperation. On the one hand it is also essential whether the social impacts are examined only from the point of view of the university, or whether

they are analyzed from the point of view of the cooperating organization (Davey et al). On the other hand it is essential, whether the produced new pieces of knowledge are tacit know-how or are they explicit know-how which can be indicated e.g. by exams and credits quantitatively and by degree.

In Figure 3, we have collected such points of view which help in examining and analyzing operative targets, results and social impacts of HEIs.

SOME CONTENT-RELATED DIMENSIONS

Content-related dimensions get highlighted when setting targets at the universities. These can be analyzed using the framework presented in Picture 3. The dimensions may vary based on the points of view in the analyses. For example, analyzing the university as a part of the regional innovation system or the regional innovation environment, new meaningful content-related dimensions can be revealed by using statistical multivariate methods.

It is also apparent that the potential social impacts of universities in the long run are more qualitative and mental than in the short run. However, the need for measuring and setting exact targets require more concrete and explicit concepts.

Below we have listed content-related dimensions and target areas connected to regional innovation environments (Caniëls & Bosch; Sotarauta & Mustikkamäki). Some of these elements are also important in producing regional competitiveness (Sotarauta & Mustikkamäki):

- Social welfare of the region
- Quality of environment
- Development of regional administration
- Jobs in the region
- Living standards and its development in the area
- Regional infrastructure
- Organizations in regional networks
- Development of human resources in the region
- Functionality of the regional innovation systems
- Image of the region
- Investments in the region

The roles of universities differ. Based on the differences, the content-related dimensions of their social impacts and target areas can be analyzed (Caniëls, M. C. & van den Bosch, H. 2011) with the following concepts e.g.:

- Activities in forming the regional image
- Strengthening of the regional culture
- Deepening the media conversation
- Serving as a critical counterforce

- To variegate thought patterns
- Increasing the freedom of thinking
- Increasing the civilization"
- Strengthening human resources
- Serving as a channel to global knowledge and know-how
- Networking
- Founding and strengthening new businesses
- Training people
- Transferring know-how and technology
- Generating cooperation and forums for information exchange
- Inspire people in work and cooperation

The university can accomplish many kinds of roles within its regional environment. The various assignments of the university depend on the chosen roles (Ministry of education of Finland).

The content-related dimensions and target areas of university-business cooperation (UBC) include (Drucker & Goldstein) e.g.:

- Cooperation projects
- External financing
- Quantitative leverage
- New jobs
- New businesses
- Broader market areas of enterprises
- Growth based on innovations
- Student practicing in enterprises in the region, country and abroad
- Change of researches and teachers abroad
- Resources reserved for producing forecasts to businesses
- Taylor made training to businesses
- Cooperation processes and problem solving
- New businesses based on know-how
- New patents, licenses and innovations
- New publications
- Development of entrepreneurship, SMEs and spin-off companies
- New commercial solutions, products and services

According to the evaluation report of higher education institutions (HEIs) in Finland (KKA 2013), in Finnish universities of applied sciences most answerers think that the strategies, target impacts, and main activities of the university should be defined in cooperation with partnering enterprises and other institutions. On the other hand, in Finnish classical universities the answers were mostly "university defines its strategies independently". Answerers from enterprises and public organizations thought it is important to have cooperation in choosing the strategic targets and focus areas of the university.

Such content-related dimensions which are connected to human life and society in general, can be effected by the activities of the university, are e.g.:

- Impact on the warming of the climate
- Impact on availability and quality of energy, water and food
- Impact on multicultural development
- Impact on the stability of financial market
- Impact on structure of population
- Impact on the health of the nation
- Impact on pandemics
- Impact on safety of the society

The differences of regions and the variety of universities make it challenging to evaluate the social impacts of the universities. Within any organization, the best strategic solutions are usually based on the strengths of the organization. These strengths are defined in relation to other institutions and bodies in the region. This forms a kind of multivariate situation, where causal effects are difficult to distinguish and the productivities of several universities are challenging to compare.

UNIVERSITY-BUSINESS COOPERATION UBC

Potentially, the best results based of university-business cooperation can be achieved, when the university aims to develop its strengths and direct its products, services and cooperation to those areas of industries and to those phenomenon of society, which are significant on its region.

One of the group work reports of the ministry of education in Finland (Opetusministeriö 2007) suggests that universities should be evaluated within the following evaluation baskets:

- Integration to innovation activities (commercial innovations and system innovations)
- Integration to labor markets
- Integration to social-ecological development
- Integration to regional environment
- Integration to social discussion (incl. social planning and decision-making)

Tens of different indicators within each of the above mentioned baskets are collected in the report (Opetusministeriö 2007). We may conclude based on this basket analyses that it points out implicitly the relative importance of university-business cooperation UBC within the strategies of universities.

The main tasks of universities are education, research as well as transfer of information and know-how (mm. Chatterton & Goddard, 2000; Etkowitz

& Leydesdorff, 2000). Most authors agree these. University-business cooperation can successfully be utilized when accomplishing any of these tasks.

The above mentioned report describes a cooperation model which successfully integrates the traditional university activities and active cooperation activities. This is visualized in Figure 4.

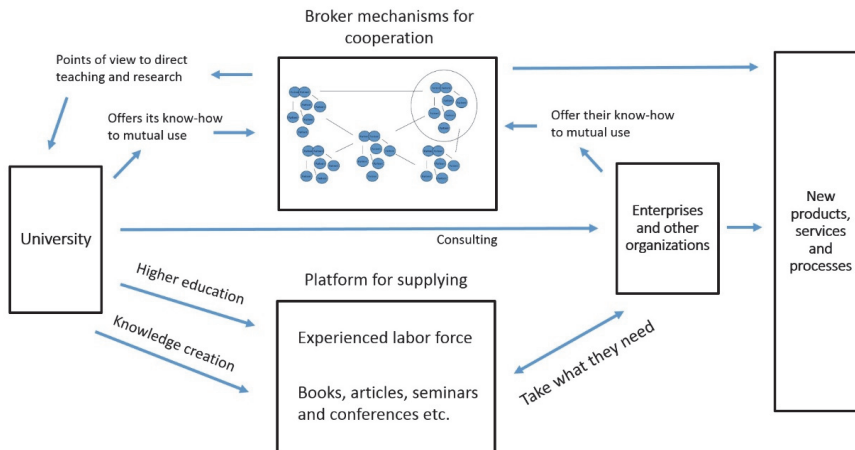


Figure 4. Cooperation model for universities and other organisations

Mead (Mead 1994) has defined “strong organizational culture” as follows:

- (1) it is convergent which means that all individuals of the organization have equal enough values, beliefs and opinions
- (2) it is easy to communicate within the organization and
- (3) individuals in the organization are more or less depending on each other.

Tenhunen (Tenhunen 1996) has pointed out that strong organizational culture can exist only when there are enough essential pieces of information available for all individuals in the organization.

Individuals as well as their organizations tend to behave rationally. Based on the theory of measurement, on the financial guidance of organizations and on the behavioral implications of available information, people act responsibly and rationally (Tenhunen 1996). Especially in expert organizations and know-how based organizations, information guidance is a good operative management method for leading people in the organization.

Rationality in organizational behavior means that people and the organization will accomplish the organizational targets and plans voluntarily and following

the available guidance information. This is based on mutual understanding of the plans and strategies. However, there always exist limits to the rationality. Full rationality would require almost complete knowledge and anticipation what will follow on each choice (compare with Miner 2006). That is one of the reasons, why causes and effects (causalities) in multivariate situations are sometimes unclear.

People need to rely on the strategy and targets involved. That is why the used evaluation aspects should not be often changed.

In the following table we have considered the meaning of different evaluation aspects (Figure 3) in university-business cooperation UBC.

Table 1. How the choice of evaluation aspects affect the results and social impacts of business - university cooperation (UBC)

Measurement points of view	Variation limits	Effect on results and impacts of UBC
Examination method	Quantitative - Qualitative	<p><i>Quantitative:</i></p> <ul style="list-style-type: none"> Operational measures regionally in use Better UBC results in case measures are chosen in cooperation (uni – business – other org) Measures pointed out by ministry alone not necessary best for developing UBC <p><i>Qualitative:</i></p> <ul style="list-style-type: none"> Ministry point out the planned impacts Freedom for universities Universities would describe their understanding of causal reasons and effects
Concreteness of impacts	Measurable real – Non-measurable mental	<p><i>Measurable evaluation:</i></p> <ul style="list-style-type: none"> Not necessary the same measures to be used by different universities Universities can point out their strengths in UBC in the region <p><i>Non-measurable mental evaluation:</i></p> <ul style="list-style-type: none"> Impacts and on the other hand the activities are described smoothly Causal effects cannot be identified in a satisfying way
Period of examination	Short term – Long term	<p>Short term:</p> <ul style="list-style-type: none"> The faster the results, the better the investment economically Many enterprises within university-business cooperation are waiting short-term results for their development needs <p>Long term:</p> <ul style="list-style-type: none"> In general, the society in general waits for the results of the university activities to be utilized in the future by citizens as well as organizations Creating knowledge, know-how and higher education results are long-term processes
Degree of cooperation	Cooperation – Separate actions	<p><i>Cooperation:</i></p> <ul style="list-style-type: none"> Leads to better and productive use of social resources Matches different interests, causes and effects <p><i>Separate actions:</i></p> <ul style="list-style-type: none"> Separate actions do not necessarily match with each other The information used should be harmonized and available for institutions and organizations within the region Strategic targets in the region need to be agreed

Type of know-how results	Explicit know-how – Implicit / tacit know-how	<p><i>Explicit Know-how:</i></p> <ul style="list-style-type: none"> Created by publications, reports, seminars, cooperation projects, development projects, dialog and discussion between institutions and citizens <p><i>Implicit know-how:</i></p> <ul style="list-style-type: none"> Traditional higher education creates a lot on tacit information for the students as well as the teachers and researchers in the university. The level of education in the society is increased. Such research results, which are not published, cause pieces of implicit know-how.
Evaluating body	Cooperating partner – University	<p><i>Cooperating partner:</i></p> <ul style="list-style-type: none"> Realistic evaluations by external partners Especially evaluations of university-business cooperation UBC results and impacts necessitate the external organizations to take part in the evaluation process Separate evaluation reports from other organizations form proper bases of future development. <p><i>University alone:</i></p> <ul style="list-style-type: none"> Separate actions are proper when evaluating internal development results in the university and when using limited points of view in purpose for given reasons Outcomes would be evaluated somewhat more positively than in cooperation

CONCLUSIONS

Above we have discussed the meaning of different evaluation aspects and how they affect the results and social impacts of business - university cooperation (UBC). From the analyses, it can be seen that the evaluation results differ much based on the selection of different evaluation aspects.

The main result of this paper is that choosing those evaluation aspects, which are acceptable from the point of view of all relevant cooperation partners leads to best ways in execution of university-business cooperation. In that case, also the social impacts of universities are best possible from the point of view of the cooperation partners and the public and private financiers of higher education units.

REFERENCES

- Caniëls, M. C. & van den Bosch, H. (2011). The role of higher education institutions in building regional innovation systems. In: Papers in Regional Science, 90(2), pp. 271–286.
- Chatterton, P. & Goddard, J. (2000). The Response of Higher Education Institutions to Regional Needs. In: European Journal of Education, 35(4), pp. 475–496.
- Davey T. & Plewa C. & Muros V. G. (2014). University-Business Cooperation Outcomes and Impacts – A European Perspective. Teoksessa Moderne

Konzepte des organisationalen Marketing, Thorsten Kliewe, Tobias Kesting (Editors). Springer Verlag, 2014.

Drucker, J. & Goldstein, H. (2007). Assessing the regional economic development impacts of universities: a review of current approaches. In: *International regional science review*, 30(1), pp. 20 – 46.

Etzkowitz, H. & Leydesdorff, L. (2000). The dynamics of innovation: from National Systems and “Mode 2” to a Triple Helix of university–industry–government relations. In: *Research Policy*, 29(2), pp. 109 – 123.

Frechtling, J. A. (2007). *Logic Modelling methods in program evaluation*, Jossey-Bass: San Francisco.

Kellogg Foundation (2004). W.K. Kellogg Foundation Logic Model Development Guide, 10. maaliskuuta 2014 osoitteessa <http://www.wkkf.org/resource-directory/resource/2006/02/wk-kellogg-foundation-logic-model-development-guide>.

Korkeakoulujen arviointineuvosto KKA (2013). Korkeakoulut yhteiskunnan kehittäjinä. Korkeakoulujen arviointineuvostonjulkaisuja 5:2013. Yhteiskunnallisen ja alueellisen vaikuttavuuden arviointiryhmän loppuraportti. KehittäjinäVeijo Ilmavirta, Hannele Salminen, Markku Ikävalko, Heikki Kaisto, Päivi Myllykangas, Eero Pekkarinen, Hannele Seppälä, Touko Apajalahti.

Liyanage, C. & Elhag, T. & Ballal, T. & Li, Q. (2009). Knowledge communication and translation—a knowledge transfer model. In: *Journal of Knowledge management*, 13(3), pp. 118 – 131.

Mead, Richard (1994). *International Management – Cross-Cultural Dimensions*. Cambridge: Blackwell Publishers. *Asia Pacific Journal of Human Resources*, Volume 34, Issue 2, December 1996, Pages: 126–128, Martin Simms.

Miner, J.B. (2006). *Organizational Behavior 2: Essential Theories of Process and Structure*. M.E. Sharpe Inc. USA 2006.

Opetusministeriö (2007). Yliopistojen yhteiskunnallinen vuorovaikutus. Arviointimalli ja näkemyksiä yliopistojen rooleihin. Opetusministeriön työryhmämuistioita ja selvityksiä 2007:22. Jari Ritsilä & Mika Nieminen & Markku Sotarauta

Perkmann, M. & King, Z. & Pavelin, S. (2011). Engaging excellence? Effects of faculty quality on university engagement with industry. In: *Research Policy*, 40(4), pp. 539 – 552.

Perkmann, M. & Neely, A. & Walsh, K. (2011). How should firms evaluate success in university–industry alliances? A performance measurement system. In: *R&D Management*, 41(2), pp. 202 – 216.

Sotarauta, M. & Mustikkamäki, N. (2001). Alueiden kilpailukyvyyn kahdeksan elementtiä. Suomen Kuntaliitto Acta-sarja nro.137. Helsinki (ISBN 951-755-496-6).

Stähle P. & Sotarauta M. (2003). Alueellisen innovaatiotoiminnan tila, merkitys ja kehityshaasteet Suomessa. Eduskunnan kanslian julkaisu 3 / 2003. Tulevaisuusvaliokunta, Teknologian arviointeja 15.

Tenhunen, Lauri (1996). Yrityksen taloudellinen ohjaus. Teoriaa ja käytäntöä (Financial Guidance of an enterprise. Theory and Practice). Yrityksen taloustieteen ja yksityisoikeuden laitos. Tampereen yliopisto. Sarja A2: Tutkielmia ja raportteja. Tampere 1996.

Valtiovarainministeriö (2012). Vaikuttavuus- ja tuloksellisuusohjelma. 13. maaliskuuta 2014 osoitteessa http://www.vm.fi/vm/fi/05_hankkeet/0108_vaikuttavuus_tuloksellisuus/index.jsp

Chatterton, P. & Goddard, J. (2000). The Response of Higher Education Institutions to Regional Needs. In: *European Journal of Education*, 35(4), pp. 475 – 496.

Etzkowitz, H. & Leydesdorff, L. (2000). The dynamics of innovation: from National Systems and “Mode 2” to a Triple Helix of university–industry–government relations. In: *Research Policy*, 29(2), pp. 109 – 123.

DESIGN FRAMEWORK OF A ROBOT SYSTEM FOR CLEANING EXTERNAL GLASS WALLS OF MODERN BUILDINGS

Bogdan MOCAN, Stelian BRAD and Mircea FULEA

**Technical University of Cluj-Napoca,
Memorandumului Street no 28, Cluj-Napoca, Romania
bogdan.mocan@muri.utcluj.ro, stelian.brad@staff.utcluj.ro,
mircea.fulea@staff.utcluj.ro,**

Keywords: cleaning robot, novel concept, modern class walls buildings

ABSTRACT

Cleaning the curtain walls of high-rise buildings is always very dangerous and strenuous. This paper is based on the previous authors' research in the field robotic systems for cleaning or periodical inspection, used on external glass walls of modern buildings that are made from modular glass panels. The designed robot is simple in construction and serves for glass wall. The system is composed from mechanical system with light structure, power system formed, and command moving in conformity with predictable software. To identify the most efficient solution for cleaning a study was conducted to guarantee the completeness of window cleaning.

INTRODUCTION

Nowadays robotics is one of the most dynamic field of scientific researches. The shift of robotics researches from manufacturing to services applications is undeniable [1]. During the last decades interest in studying climbing and walking robots has been increased [1,2].

In the past decades a large number of high-rise buildings with glass walls are developing in modern cities. The shape of these buildings varies greatly from classical facades with straight edges to modern facades with tight bends or even spherical curtains [3,4]. A curtain wall system is an outer covering of a building in which the outer walls are non-structural, but merely keep the weather out and the occupants in. Cleaning the outer surface of these buildings is dangerous and laborious work [3].

Currently, most buildings are still cleaned manually with the help of a nacelle system operated by workers with simple cleaning tools or resorting to utilitarian alpinists. The number of modern buildings with complex shapes is increasing worldwide [3]. Even skilled utilitarian alpinists with specific safety systems have difficulties in climbing and cleaning those buildings.

The development of robotic systems capable of walking and climbing on glass walls offers an immediate solution to the above-mentioned problems. Because of the current lack of uniform building structures, wall cleaning of high-rise buildings is becoming one of the most appropriate field for robotization [5,6,7,8,9,10].

Wall climbing robots are special robots that can be used in a variety of application like cleaning, inspection and maintenance of surfaces of sea vessels; oil tanks, glass slabs of high rise building, etc. A wall climbing robot should not only be light, but also have large payload, so that it may reduce excessive adhesion forces and carry instrumentations during navigation [6,7,8,9,10,11]. These machines should be capable of travelling over different types of surfaces, with different inclinations, such as floors, walls, or ceilings, and to walk between such surfaces [12]. Furthermore, they should be able of adapting and reconfiguring for various environment conditions and to be self-contained [13].

In order to automate the cleaning tasks of external glass walls, a gondola-based climbing service robot has been designed. In the next section the previous researches published in the literature has been overviewed. Third Section highlight the problem and Forth Section describes the proposed approach and design methodology, and the proposed framework is successfully applied to a case study in Fifth Section. Finally, the conclusion has been discussed in Sixth Section.

RELATED RESEARCH

The interest in the development of climbing robots has grown rapidly in the last years. So far, considerable research was devoted to these service robots and various types of experimental models were already proposed, [14]. However, we have to notice that the application of climbing robots is still limited. Apart from a couple successful industrialized products, most are only prototypes and few of them can be found in common use due to unsatisfactory performance in on-site tests (regarding aspects such as their speed, cost, reliability, and most of them can only deal with uniformly shaped planes glass) [11,14,15].

Recently, several robots using various locomotion mechanisms have been proposed. Locomotion mechanisms can be classified by four types: legged type, translation type, wheeled type, and track-wheel type. Each type shows different performance in payload capacity, transition ability, and control complexity.

Table 1.I shows the legged-type climbing robot. Table 1. I(a) shows the robot named the Treebot [9], which is composed of two grippers and a continuum manipulator. The locomotion of the Treebot is similar to that of an inchworm, which is a kind of biped locomotion. This robot is designed for climbing trees, but its mechanism has also been used in the wall-climbing robot. The continuum manipulator is actively maneuverable, so this robot can transit

from one tree to another. It has a payload capability of 1.75 kg, which is nearly three times its own weight. However, a locomotion strategy is too complex, and thus it needs a complex control system, such as the calculating kinematics of the continuum manipulator. Reference [10] suggested a two legged climbing robot with foot segments using hot melt adhesion (HMA), as shown in Table 1. I(b). The locomotion strategy of this robot is similar to that of the Treebot, and, therefore, with it, good transition ability for various targets can be achieved. However, this locomotion also required complex control, making its application to real sites difficult [9].

The translation-type climbing robot is shown in Table 1.II. The Sky cleaner robot [3] is representative for translation climbing robots. It is one of the simplest forms of locomotion and it uses a translational mechanism with an appropriate attachment device. These types of robot do not require any complex control during locomotion. In addition, the payload capacity of these robots is high, due to their high stability of locomotion. However, these robots have no transitioning ability, because of their limited maneuverability [3,4].


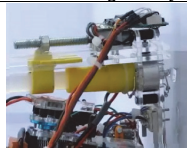






I. Legged type		II. Translation type	
a. Treebot [9]	b. HMA climbing robot [10]	Sky cleaner robot 1-3 [3]	
			
III. Wheeled type		IV. Track-wheel type	
a. Two-magnet robot [12]	b. Waalbot II [13]	a. Tank-like robot [8]	b. Transformable robot [15]
			

Table 1. Types of locomotion mechanism

Table 1.III shows the wheeled-type climbing robot. The Magne-bike [12], which is suggested by Tache et al., is a compact robot with two magnetic wheels in a motorbike arrangement. Murphy et al. [13] proposed a two-leg-wheeled-type climbing robot, named Waalbot II. These two robots showed great performance in transition ability. The Magnebike could transit almost all kind of surface, and the Waalbot II achieved various internal transitioning abilities. Further, the locomotion strategy of these robots is simple; thus, the control complexity of these robots is low. In contrast, the adhesion area of this mechanism type is only line contact, and thus the payload capacity of these types of robot is small compared to that of other locomotion types [13].

Table 1.IV shows the track-wheel-type climbing robot. A tank-like climbing robot, developed by Seo and Sitti [8], is shown in Table 1.IV(a). The robot is

designed as a modular track-wheel type climbing robot connected by two passive compliant joints and featuring one active tail. This robot showed great flexibility in transition ability, since, with it, transitions are achieved without complex control. In addition, this robot achieved three internal transitions and two external transitions. Moreover, it has a large adhesion area; thereby the payload capacity was tested as 500 g (weight ratio 1.82). Reference [15] proposed a transformable track-wheel climbing robot with five rotatable passive compliance joints, as shown in Table 1.IV(b). The robot showed a 3 kg payload capacity through a wide adhesion area. Moreover, a track-wheel system makes control of driving simple, and the passive compliance joints allow for flexible locomotion of transitioning. In addition, the robot showed one internal transition ability and one external transition ability. However, the transitioning abilities of the robots are limited to relatively simple transitions [16].

Locomotion mechanism	Legged	Translation	Wheeled	Track-wheel
<i>Payload capacity</i>	High	High	Low	High
<i>Transition ability</i>	High	Low	High	Middle
<i>Control simplicity</i>	Low	Middle	High	High

Table 2. Qualitative analysis of locomotion mechanisms

Each locomotion mechanism has different characteristic; therefore there are different pros and cons associated with each locomotion mechanism. Qualitative analysis of the payload capacity, transition ability, and control complexity on each locomotion mechanism is summarized in Table 2.

PROBLEM DEFINITION

An issue that have to be managed very well within the development process of such a robotic system for cleaning the high-rise buildings with glass walls is the competitiveness of such a system. These climbing robots for cleaning the glass walls are built in a low number of units or very often, in a single customized unit. This requires low development costs in order to obtain economic justifiable solutions. For increasing the competitiveness of the robotic cleaning system, a key objective for designers should be to maximize the “performance/cost” ratio for the customer. Considering the current rules on environmental protection such a robotic system must be environmentally friendly, and having the capability of recycling the washing solution.

Within this scenario, the focus of this paper is to develop a competitive robotic system for cleaning glass walls. The main feature of the robotic system is that it is multifunctional and to a small degree reconfigurable in terms of its functionalities (could be easily adapted for inspection). Also, the objective of this research is to demonstrate that such robotic systems can be competitive in terms of price if it is considered an affordable approach from beginning. For this purpose it was developed a methodology that integrates tools and

methods for prioritizing customer requirements (e.g. AHP), and product performance planning (e.g. QFD with fuzzy logic)

METHODOLOGY

To execute the desired cleaning tasks, climbing robots have to fulfill certain requirements. Of course, the requirements and their importance and focus depend on the individual application need. In order to minimize the “performance/cost” ratio for the customer we have to should best possible matching the following objective functions: cleanliness and velocity, reliability and safety, usability. Also an affordable approach have to be taken into account in order to be competitive in term of proce. The proposed framework integrates three objective functions that have to be met:

1. Cleanliness and velocity: The robot clean ability and speed are two main aspects in this field. Also, the system should be able to handle steps or protrude structures to be able to reach all positions at the building [17,18].

2. Reliability and safety: A further important non-functional aspect is the robustness of the system. If the climbing robot fails often during one cleaning task it would not be usable in practice. The requirements reliability and safety include robust hardware, optimal controllers and methods to detect and handle hazardous situations and to recover from them [19].

3. Usability: Cleanliness, velocity, manoeuvrability are important, but, they are only the basis of the general operability of the system. To bring a robotic system into application it has to be more powerful, more efficient and less dangerous than common approaches e.g. manually cleaning the glass walls. Therefore, the spare parts need to be easily replaceable, and the operation must be faster and less complicated compared to existing approaches. Additionally, also aspects like energy consumption, weight or dimension of the system can be important [20,21,22].

Based on the specific tasks and needs of the cleaning and inspection process, a robot developer has to decide the rank of the objective functions and how to implement them into practice to fulfill individual requirements. For that we proposed, figure 1, a framework that has to be followed for design and develop a competitive cleaning robotic system.

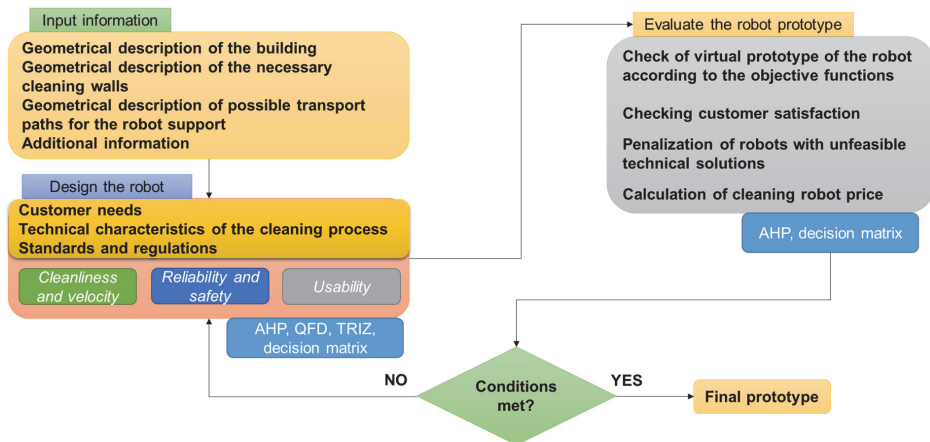


Figure 1. The proposed framework

This framework concurrently takes into account knowledge of experts with regard to weights obtained by the AHP (Analytical Hierarchy Process) for qualitative criteria and by QFD (Quality Function Deployment) for planning the performance of the robotic system within the design phase (Figure 1). The results may differ from project to project depending on project objectives. A more detailed presentation of the proposed framework can be seen in Figure 1.

CASE STUDY

An automatic gondola for cleaning glass windows was design using the proposed framework, which takes the World Trade Center of Bucharest as its operation target. Having in mind the three objective functions: Cleanliness and velocity, Reliability and safety, Usability and using competitive tools like AHP, QFD, decision matrix and TRIZ, which are not detailed here due to the limited space of the paper, for planning the performance of the robotic system we developed a robotic system which has the main specifications summarized below:

1. High reliability, due to the simplified system and the reliability of the suspending sub-system.
2. Because of the gondola solution and cleaning solution, the cleaning robot can be attached not only to glass, but also to a wall with tile, aluminium-boards.
3. High cleaning efficiency and good quality, which are realized by using brushes, rubber scraper and demineralized water and special detergent.

4. As it reclaims, purifies and recycles the sewage, the robot is water saving cleaning device.
5. Remote control mode, easy to use and low cost.

The development of the cleaning robotic system concept was made by an affordable approach. Thus, the resulting robot concept is 1.4 meters high, 1.2 meters wide and 0.4 meters thick. The automatic cleaning gondola system can fulfill the work of attaching on the wall, cleaning the glass window, reclaiming, purifying and recycling the sewage. A remote control device and a wireless CCD camera are adopted for the robotic system which is pre-programmed to run in an autonomous and supervisory control mode for making a minimum inspection tasks.

The robotic system includes a sub-system on the roof of the building which is used for suspending and hauling the robot to move vertically and horizontally, and the robot (automatic gondola) which is responsible for cleaning (Figure 2). The weight and payload of the robot are no longer limited by the vacuum cups because its weight is completely supported by the cables (Figure 2).

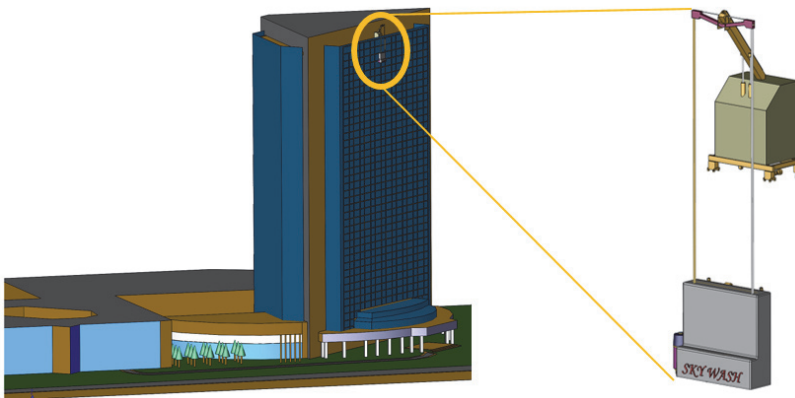


Figure 2. Automatic cleaning robot

The cleaning robotic consists of a main frame, attachment devices, a water-recycling device, a cleaning system, and a control system. The main frame serves as a carrier for all the other devices. The cleaning system is the core part of the robotic gondola and is developed to satisfy the dexterity cleaning requirements.

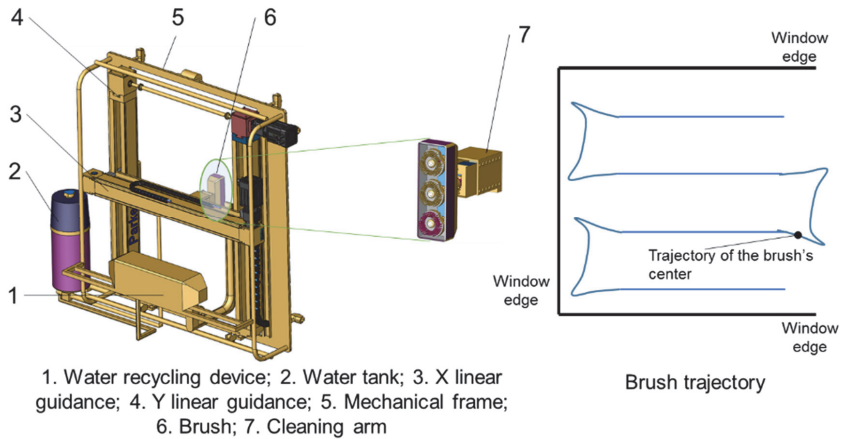


Figure 3. Robotic cleaning system and brush trajectory

Two parallel Y linear guidance and a X linear guidance compose the crossed cleaning mechanical frame. The X linear guidance with a cleaning arm can move horizontally along the X linear guidance. The cleaning arm has the ability to be rotated to touch the window surfaces and accomplish the cleaning task. It can move vertically along the Y linear guidance itself. So the movement of this arm in vertical and horizontal directions is controlled by the X and Y linear guidance together. At the ends of the cleaning arm is an adaptive cleaning head. A turning joint like a wrist is mounted on the tip of the arm and connects the cleaning arm and the brush (Figure 3).

The cleaning efficiency of the robotic system is planned to be over 150 m²/hour. To determine the best method of cleaning we conducted a study. For this study we used circular brushes like “AIB glass washing” and soft cleaning rags “Microstrip” and demineralized water (distilled) with cleaning additives (detergent). Interpretation of the results was done empirically, without the use of statistical methods of differentiation.

Table 3. Studies on cleaning a window

Method of working	Graphical representation	Results
Sweeping the glass on horizontal direction with rubber scraper		<i>Unsatisfactory</i> result (the surface thus cleaned is still stained).
Sweeping the glass on horizontal direction with rotating brush		<i>Unsatisfactory</i> result (the surface thus cleaned is still stained).
Sweeping the glass on horizontal direction with rotating brush and wiping the surface with a soft rubber scraper		<i>Excellent</i> result (the surface thus cleaned remains clean, dry and bright, if using demineralized water).
Sweeping the glass on vertical direction with rotating brush and wiping the surface with a soft rubber scraper		<i>Excellent</i> result (the surface thus cleaned remains clean, dry and bright, if using demineralized water).

The conclusions of the study for identifying the best method for the cleaning were that cleaning the surface by combining circular brush and soft rubber scraper, regardless of the method of working used (sweeping glass horizontally, vertically or after a random curve) yielded excellent results (thus cleaned surface remains clean, dry and bright, if used water was demineralised).

CONCLUSION

Different aspects regarding design of a robotic system for cleaning external glass walls of modern buildings, are presented. Combining the three objective functions in a unique manner by affordable approach we demonstrate that that it is possible to robotized the cleaning process of the World Trade Center of Bucharest. An optimal cleaning velocity, and at the same time, a high quality cleaning process is ensured. The introduction of video system within the cleaning robotic this facilitate performing video inspection without any risk to human operators. Further activities will be carried on to improve control using a microcontroller developed within RESIN Research Center from Technical University of Cluj-Napoca as well as strategy to work around obstacles by using multiple ultrasonic sensors.

ACKNOWLEDGEMENT

Support within the project POSDRU/159/1.5/S/137516 PARTING is acknowledged with gratitude.

REFERENCES

- [1] T.-K. Lee, S. Baek, S.-Y. Oh, Sector-based maximal online coverage of unknown environments for cleaning robots with limited sensing, *Robotics and Autonomous Systems* 59 (10) 698–710, 2011.
- [2] D. Lee, N. Ku, T.-W. Kim, J. Kim, K.-Y. Lee, Y.-S. Son, Development and application of an intelligent welding robot systems for shipbuilding, *Robotics and Computer-Integrated Manufacturing* 27 (2), pp. 377–388, 2011.
- [3] H. Zhang, J. Zhang, G. Zong, W. Wang, R. Liu, Sky cleaner 3: a real pneumatic climbing robot for glass-wall cleaning, *IEEE Robotics & Automation Magazine* 13 (1), pp. 32–41, 2006.
- [4] V.-G. Loc, S.-G. Roh, I.M. Koo, D.T. Tran, H.M. Kim, H. Moon, H.R. Choi, Sensing and gait planning of quadruped walking and climbing robot for traversing in complex environment, *Robotics and Autonomous Systems* 58 (5), pp. 666–675, 2010.
- [5] A. Gimenez, M. Abderrahim, C. Balaguer, “Lessons from the Roma I inspection robot development experience“, *Proceedings of the 5th*

International Conference on Climbing and Walking Robots, pp. 913-920, Karlsruhe, Germany 2001.

[6] C. Balaguer, A. Gimenez, J. M. V. Pastor, M. Padron, M. Abderrahim, "Climbing autonomous robot for inspection applications in 3D complex environments". *Robotica*, Vol. 18, No. 3, pp. 287–297, pp. 4116–4121, 2000.

[7] A. Sintov, T. Avramovich, A. Shapiro, Design and motion planning of an autonomous climbing robot with claws, *Robotics and Autonomous Systems* 59 (11), pp. 1008–1019, 2011.

[8] T. Seo, M. Sitti, Tank-like module-based climbing robot using passive compliant joints, *IEEE/ASME Transaction on Mechatronics*, in press (<http://dx.doi.org/10.1109/TMECH.2011.2182617>), 2012.

[9] T. Lam, Y. Xu, A flexible tree climbing robot: Treebot-design and implementation, in: *International Conference on Intelligent Robots and Systems*, pp. 5849–5854, 2011.

[10] M. Osswald, F. Iida, A climbing robot based on hot melt adhesion, in: *Int. Conf. on Intelligent Robots and Systems*, pp. 5107–5111, 2011.

[11] H. Zhang, J. Zhang, W. Wang, R. Liu, G. Zong, A series of pneumatic glass wall cleaning robots for high-rise buildings, *Industrial Robot: An International Journal* 34 (2), pp. 150–160, 2007.

[12] F. Tache, W. Fischer, G. Caprari, R. Siegwart, Magnebike: a magnetic wheeled robot with high mobility for inspecting complex-shaped structures, *Journal of Field Robotics* 26 (5), pp. 453–476, 2009.

[13] M. Murphy, C. Kute, Y. Menguc, M. Sitti, Waalbot II: adhesion recovery and improved performance of a climbing robot using fibrillar adhesives, *International Journal of Robotics Research* 30 (1), pp. 118–133, 2011.

[14] B. Chu, K. Jung, C.-S. Han, D. Hong, A survey of climbing robots: locomotion and adhesion, *International Journal of Precision Engineering and Manufacturing* 11 (4), pp. 633–647, 2010.

[15] G. Lee, K. Seo, S. Lee, J. Park, H. Kim, J. Kim, T. Seo, Compliant track-wheeled climbing robot with transitioning ability and high-payload capacity, in: *IEEE Int. Conf. on Robotics and Biomimetics*, Phuket, Thailand, Dec. 7–11, pp. 2020–2024, 2011.

[16] W. Wang, G. Zong, "Controlling and Sensing Strategy for Window Cleaning Robot", *Hydraulics & Pneumatics*, No. 1, pp. 4–7, 2001.

[17] F.E.H. Ta, "A software framework for an automated wall cleaning robot" *Robotics and Mechatronics Congress*, Singapore, 6–8 June 2001.

- [18] H. Zhang, J. Zhang, R. Liu, W. Wang, G. Zong, “Pneumatic Climbing Robots for Glass Wall Cleaning”, Proceedings of the CLAWAR 2004, Madrid, Spain, September, pp.1061 – 1069, 2004.
- [19] T. Miyake, H. Ishihara, “Mechanisms and Basic Properties of Window Cleaning Robot”, Proceedings of the 2003 IEEE/ASME International Conference on Advanced Intelligent Mechatronics, pp. 1372 – 1377, 2003.
- [20] T.P. Sattar, B. Bridge, S. Chen and Z. Zhao, “Development of CLAWER System that Combines the Tasks of Monitoring, Mobility, Manipulation, and Measurement for Industrial Inspection Tasks”, Proceedings of CLAWAR 2003, Catania, Italy, pp.699 – 706, 2003.
- [21] H. Zhang, J. Zhang, G. Zong, “Realization of a Service Climbing Robot for Glass-wall Cleaning”, Proceedings of the 2004 IEEE International Conference on Intelligent Mechatronics and Automation, Chengdu, China, August 26 – 31, pp. 101 – 106, 2004.
- [22] H. Zhang, J. Zhang, W. Wang, G. Zong, “Design of a Pneumatic Glass Wall Cleaning Robot for High-Rise Buildings”, Proceedings of the ASER '04 2nd International Workshop on Advances in Service Robotics Stuttgart, Germany, May 21, pp. 21 – 26, 2004.

DESIGN, ENGINEERING AND MANUFACTURING OF BEARING ELEMENTS OF THE LOW STEEL WEIGHT

Fridkin V.M.

**Doctor Techn. Sc., Professor, Moscow State University of
Railway Engineering (MIET), Moscow, Russia**

Kouzmenko I.M.

Cand. Techn. Sc., associate professor, «Belarusian-Russian University», Mogilev, Belarus

Sysa N.S.

Holding «Protos Companies Group», Mogilev, Belarus

Kuzmenka D.O.

Master of Techn. Sc., «Belarusian-Russian University»

Bogdanov S.V.

Cand. Techn. Sc., «Belarusian-Russian University»

INTRODUCTION

Efficiency of projected and erected constructions is directly connected with a structure and features of distribution of stress and deformations of bearing elements. One of the primary goals at projecting is reduction of cost of building, first of all, at the expense of decrease in steel intensity of constructions at the maintenance of their high bearing ability.

In constructions of civil, public and industrial buildings, bridges, platforms, crane beams of production buildings and other constructions, the beams, i.e. the bearing elements receiving action of the bending moments are widely applied.

Bearing elements of solid columns: columns of uniform cross-section on height and over crane parts of stepped columns represent a core subject to compression with a bend.

Sections of bearing elements traditionally accept in the form of compound I-girder. They are made by welded, riveted connections or with application of frictional bolted connections.

Beams of compound section are applied in cases when rolled beam sections do not satisfy conditions of resistance, rigidity, general stability, i.e. under long spans and large bending moments. The beam height is defined by economic reasons, permissible deflection, and in some cases, building height. The construction height of such sections reaches 1500 - 1800 mm and more.

Symmetric sections are usually applied to columns, for example, circular sections. Under large loads, use asymmetrical sections, with the prevailing unilateral bending moment.

PERFORATION AS A WAY OF REDUCTION OF MATERIAL CONSUMPTION

Traditional production techniques of a compound I-girder

Among many productions, the classical approach to manufacturing of bearing elements lowered materials consumptions is known: perforation of a wall of a solid rolling or a welded I-girder. However such technology does not always allow an I-girder of large height or to project cores of optimum section. Besides, unification of the constructive elements which are original assembly units on which base projecting of various constructions is possible is practically excluded.

Manufacturing of I-girders of the large height is carried out with application of welding technologies and special equipment. In particular, such special line of automatic welding under a flux material successfully works at the Holding «Protos Companies Group» in the Mogilev district. However the height of the I-girder on this line is limited 1500 mm.

Requirements to resistance, rigidity and to projecting of steel constructions in Belarus and Russia are regulated by Building specifications and rules (BS and R), for example [1, 11].

Perforation of an I-girder wall

Resistance of beams and columns with cutouts (with the perforated wall), updating of methods of their calculation and rationality of application at different times has been considered by A.R.Rzhanitsyn, A.I.Skljadnev, V.M.Dobrachev, V.M.Daripasko, E.V.Litvinov, A.A.Jurchenko, T.M.Rogatovsky, A.I.Pritykin and other authors. Among foreign authors, it is possible to note works of F. Faltus, R.Nalleuh, I.E. Gibson, Century S. Jenkins, N.J. Gardner, M.Ngabok, A.Vazile and others.

Usually I-girders with perforated wall manufacture in a following order. The wall of a rolled section (figure 1) is cut on a zigzag broken line with a regular step by means of gas cutting or in powerful presses, and then both halves of the cut beam are joined by welding in the flanges of the wall combined among themselves. As a result, from the original rolled section, a beam with windows in the wall is formed.

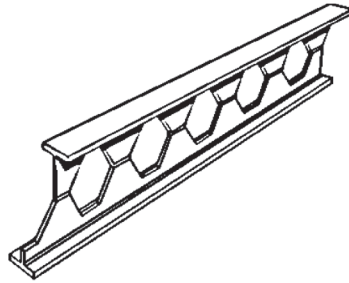


Figure 1. Compound I-girder with a perforated wall

Such an approach is not essentially new. It already has had time to prove its advantages: rationality of distribution of a material in the section at perception of operational loadings, decrease in weight and steel usage.

Constructive decisions of beams and columns with the perforated wall differ in a large variety, defined by variability of patterns of a wall cutting.

Most often the perforated bearing elements apply with regular cutting and identical height of zone I-girders (cores of symmetric section). At the Belarussian-Russian university the design of a column of the ring cross-section [2] made by a way of cutting, separation and welding of a wall of a pipe is offered and investigated.

Some features of manufacturing of the perforated elements

The perforated I-girder is made using standard technology, appears more difficult in structure and geometry, than a classical I-girder. If it is a question of sections in height from 0,7 m to 2,2 m for factories metal constructions, manufacture of the perforated products becomes rather unprofitable in connection with occurrence of considerable welding deformations and necessity of performance of special constructive-technological actions for their minimization.

The increase in height of I-girder, without serious reorganization of technological process of their manufacturing, is possible at use of the new technical decision offered in given work [3, 4].

BEARING ELEMENT OF METAL CONSTRUCTIONS AND METAL CONSTRUCTION ON IT'S BASE

The basic bearing element

Many constructions of perforated I-girders and design procedures of their resistance and the stability are offered, allowing considering the geometrical

form of perforation, their relative positioning and levels of concentration of tension near them [5–10].

Thus there is not solved a question of simplification of manufacture and installation of perforated I-girders with the big building height.

At the Belarussian-Russian University, in the co-authorship with “MIET” and Holding «Protos Companies Group», the constructive-technological decisions directed on simplification of a design and manufacturing techniques of the bearing element of metal constructions are offered: basic bearing element of metal construction (Figure 2). These offers are issued as demands for delivery of patents [3, 4] on the invention in the Republic of Belarus and in the Russian Federation.

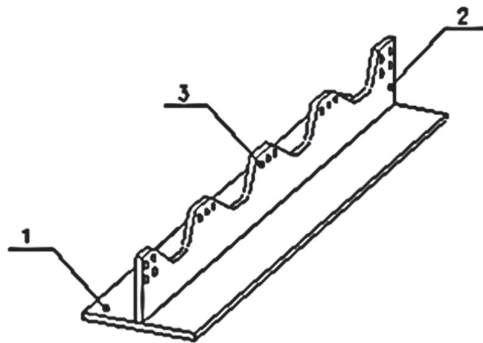


Figure 2. Basic bearing element of metal construction

Basic bearing element of metal construction represents a construction of a beam type of an I-girder. It consists of actually bearing element 1 and a wall 2 which are rigidly connected to each other. The wall 2 is carried out from sheet product with a variable height.

Metal construction based on bearing element of metal construction

Depending on the design diagram and features of the constructive form of a construction, its function and conditions of loading and the maintenance, projected metal construction gathers from separate bearing element of metal construction. Elements, in turn, can install on a miscellaneous conditions in relation to each other and to other constructive elements of metal construction.

Connection of bearing elements of metal construction among themselves can be carried out by both welding, and frictional high-strength bolts with use of covers, plates and (or) braces. For this purpose, depending on the height of a part of an I-girder (Figure 2) one or several apertures of type 3 are carried out.

Thus, on the basis of bearing elements of metal construction structures of the various form and function can be created. Their description is resulted in the text of above mentioned applications. Simplicity of manufacturing, high bearing ability, the optimum constructive form, and optimum steel intensity is thus provided.

Order of manufacturing of compound I-girder based on bearing element of metal construction

The compound I-girder on the basis of base bearing element of metal construction is shown in Figure 3 on which are marked:

the sizes of parent sheet of a wall: h – height, t – a thickness;

the sizes of a window: h_{wind} – window height, a_{wind} – width of a window, w_{wind} – distance between windows;

h_{perf} – height of the perforated I-girder, b – width of a flange of an I-girder.

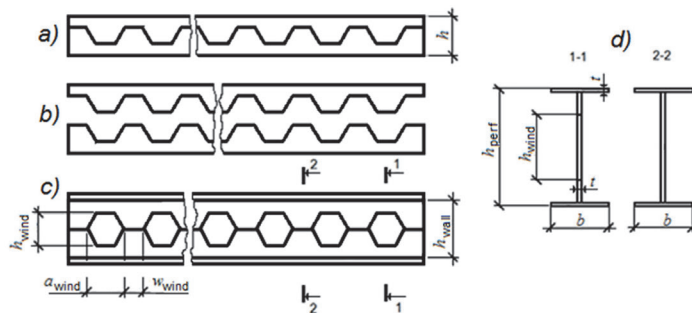


Figure 3. The order of manufacturing perforated girders on the basis of basic bearing element of metal construction (the technology is developed together with "Holding").

The following order of manufacturing is applied:

- a wall by means of welding connect to with flange sample: receive an I-girder, that is a base of bearing element of the metal construction (see Figure 2);
- parent sheet is cut (loosen) on the broken line which geometrical parameters should correspond the certain project to the form and the sizes of windows in wall of bearing element of metal construction (Figure 3 a). Two samples for a wall of an I-girder (Figure 3 b) receive. The cut geometry represents, for example, an isosceles trapezium with the rounded corners for reduction of influence of concentrators of pressure;

- for receiving of the perforated I-girder (Figure 3 c, section 1-1) manufacture two basic element of the metal construction, connect I-girders with their displacement from each other (Figure 3 d) with welding application, or connect covers on frictional high-precision bolts.

It is possible to manufacture various constructions from the basic bearing element of the metal construction having T-section which basis is made by beams and racks (column).

TECHNIQUES OF THEORETICAL AND EXPERIMENTAL RESEARCHES OF WELDED I-GIRDERS OF THE NEW CONSTRUCTION

Calculation techniques

In the given work techniques were used:

- engineering design procedures of beams and columns with a solid wall on the first and second limiting states, recommended by Steel Constructions [1, 11];
- calculation of beams with the perforated wall by a technique of the Kazan State University of Architecture and Engineering [12];
- calculation of columns by E.U.Fomenko's technique [13]: the perforated wall was replaced with solid by reduction of a thickness of the wall counted from equality of the moments of inertia of walls;
- calculations on the basis of platform ANSYS (software package ANSYS® Workbench). At creation of models of I-girders and columns, for definition of distributions of force and deformation fields, following types of final elements [14] were used: SOLID 186 – a three-dimensional element of the volume deflected mode with twenty knots; CONTA 174 - a three-dimensional contact element of type «a surface with a surface» with eight units; TARGER 170 – the three-dimensional reciprocal element having in the units mechanical degrees of freedom.

Techniques of experimental researches

Reliability of results of calculations was estimated by their comparison with the data of measurements of stress and deformations with the subsequent definition of errors between them. In experiments samples of welded I-girders of the identical height, made on technology of Holding «Protos Companies Group» (Figure 4 a) were used.

In Figure 4 b the section A (0,471 m) is shown, in which normal stresses were defined, and in Figure 4 c - section K, in which the flexure of a column (0,724 m) was measured.

In Figure 5, for an example, the general view of the sample with the perforated wall before test is shown. Supporting elements on which beams were established, had on distance of 50 mm from end faces of the sample. Test samples were loaded with the concentrated force with step 10 kN, applied in the middle of span.

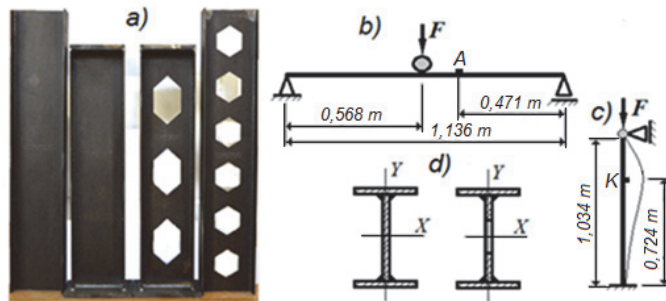
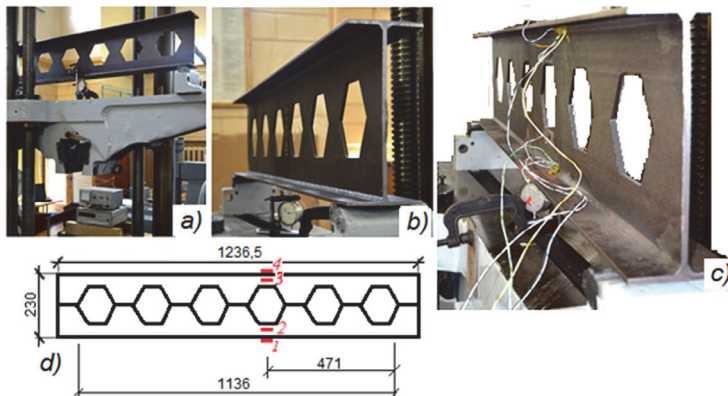


Figure 4. The Experimental samples made on technology of Holding «Protos Companies Group» (a) and test patterns of a bar (b, c)

Flexure was measured by the indicator of hour type «indicating gage-5» with the scale interval of 0,01 mm. Pressure was measured by means of wire resistance strain gages type of 2FPK-10-100-B in accordance with State Standard 21616-76 with resistance 105,34 - 105,66 ohm. They were established according to the pattern (Figure 5 d).



a) – the front view, b) - a side view, c) – a view from outside of resistance strain gages, d) – the installation pattern of resistance strain gages 1 – 4.

Figure 5. The General view of the perforated beam before test for a bend

STRESS AND DEFORMATIONS OF BEARING ELEMENTS I-GIRDER SECTION

Bending experiment

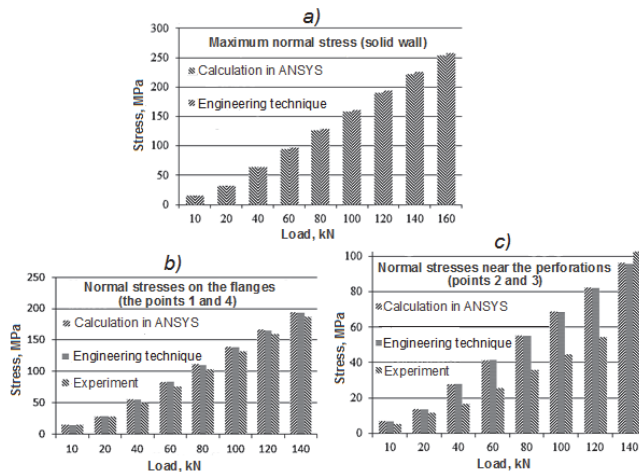
Results of experiments are stated in detail in [15]. According to calculation of bearing ability of samples on the first limiting state at a bend, the maximum rated loading makes: for an I-girder with a solid wall is 167,3 kN, with the perforated wall is 162,3 kN.

In Figure 6 results of calculation of the normal pressure, executed in ANSYS and by engineering technique, and also the experiment data (strain gauging) for a beam with the perforated wall are shown. Stresses were defined by their average values. The accuracy of results of calculations practically is absent. The error of measurements of the stress on flanges (the points 1 and 4) makes: with engineering calculation is 5,3 %, with calculation in ANSYS is 5,7 %. In the perforated wall (points 2 and 3) an accuracy above – accordingly 31,9 % and 32,4 %.

Sufficiently high convergence of calculations by applied techniques and experiments allows using confidently enough finite element method on the basis of complex ANSYS for the analysis of the deflected mode of constructions without carrying out of additional experimental researches.

Stability experiment of a core

Columns in height of 1,075 m with solid and with the perforated wall were investigated. The test arrangement is presented in Figure 4c.



a) – maximum normal stress in the solid wall (midspan of the beam); b), c) – normal stresses in the perforated wall (layers of cross section of the beam weakened by perforation, see figure 5d): the points 1 --4 (b) and points 2 and 3 (c)

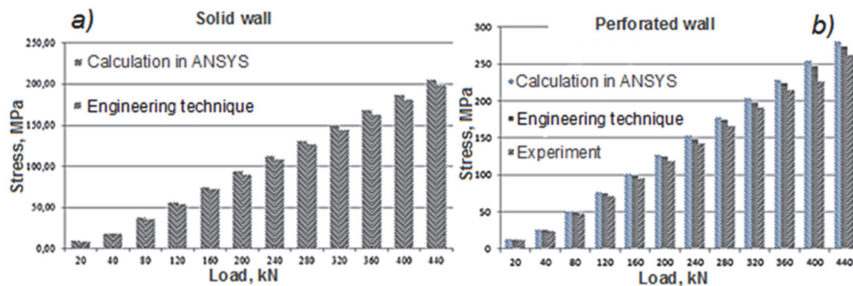
Figure 6. Normal stresses depending on loading

Measurement of normal stresses was spending in section of the perforated wall. Resistance strain gages at the height 0,537 m were symmetrized on either side of a window.

In the section of a column weakened by perforation, engineering calculation gives critical load 466,01 kN, in ANSYS – 460,82 kN. Critical load, by results of experiment, makes 440 kN.

In Figure 7 distribution diagram of normal stresses along an axis of columns with solid and with the perforated wall are presented.

The calculation error in ANSYS and results of experiment makes 4,73 %, engineering calculation on the resulted thickness and results of experiment is 24,5 %, engineering calculation in the section weakened by perforation and results of experiment is 5,9 %.



the column with a solid wall (a) and with perforated wall (b)

Figure 7. Distribution of normal stress along an axis of a column depending on loading

COMPARISON OF BEARING ABILITY OF I-GIRDERS OF IDENTICAL STEEL INTENSITY

Bearing ability was estimated on the first (on the maximum normal stresses) and to the second (on the maximum deflections) limiting states. Steel intensity of the I-girder beam at a bend, at identical thickness of applied sheet product h and width of flanges is defined by height of a wall of an I-girder.

For comparison of bearing ability the I-girder in height of 200 mm is considered. At a thickness of sheet product of 4 mm and width of flanges of 100 mm, height of a solid wall is 192 mm.

The compound I-girder with the perforated wall from basic welded sections (on technology of bearing element of metal construction) is received by dissolution of sheet in height of 192 mm, with the subsequent welding of walls with flanges. Two sections gather with shift on flexures, and then their welding is carried out. The height of the received I-girder is 264 mm at height of a wall

of 256 mm. Thus, the height of an I-girder has increased in 1,33 times. Steel intensity has not changed.

By calculations in ANSYS the maximum normal stresses (figure 8) and flexures in the midspan (figure 8 b) in the I-girder with a solid wall and in compound I-girder and with the perforated wall are defined.

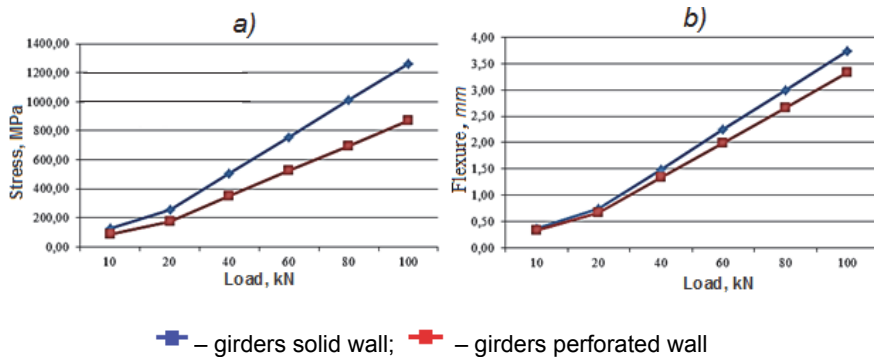


Figure 8. The maximum normal stresses and flexures in the midspan in the I-girder of identical steel intensity with the solid and perforated wall

The perforated construction on the basis of bearing element of metal construction (welded sections) wins not only on flexures (the difference in favour of the perforated wall makes 12,29 %), but also substantially on the maximum normal stresses in the flange (decrease on 44,75 % also in favour of the perforated wall).

The economy of metal of I-girder with the perforated wall in comparison with the I-girder with a solid wall, at their identical height, will make, depending on accepted geometrical parameters of dissolution of a wall, from 10 to 25 %.

CONCLUSION

The new constructive-technological decision of forming of the constructive elements with the optimum geometrical parameters is offered, allowing reducing steel intensity of projected designs without decrease of their bearing ability.

The basis of constructive elements is the base bearing element of metal construction, which make by dissolution of sheet sample on the broken line which geometrical parameters should correspond to the form and the sizes of windows in wall bearing element of the metal construction, defined by the project. Two samples for a wall of an I-girder receive. The wall, by means of welding, incorporates to flange sample: receive an I-girder that is a base of bearing element of metal construction.

Sufficiently high convergence of calculations by various techniques with the data of calculation in the ANSYS is proved that allows using finite element method on the basis of complex ANSYS for the analysis of the deflected mode of constructions without carrying out of additional experimental researches.

Offered constructive-technological decisions allow to lower steel intensity of beams at least on 25 % (at identical height of a wall standard of I-girder sections and received on offered technology). Steel intensity of columns can be lowered on 15–25 % in comparison with the expense of metal on columns from rolling I-girders.

LITERATURE

- [1] Building specifications and rules (SNiP) II-23-81* Steel structures (1990). State construction engineering of the USSR. Moscow: Central Design Company for Standard Design and Urban Development of the State construction engineering of the USSR, 96 p. (*in Russian*)
- [2] Semenov A V, Kuzmenko I M (1997) Economic constructive forms of welded metal columns: *Collection of scientific works of young scientists; new technologies and equipment in the industry*: Mogilev, MGTU, pp. 140–143 (*in Russian*)
- [3] Fridkin V M, Kuzmenko I M, Markov S N, Basharymova V N, Sysa N S, Kuzmenko D O, Bogdanov S V (2012) The bearing element of the metal constructions and metal construction on its basis. Application No a20121717, International patent classification 04B1/00; the applicant is the Belarusian-Russian University; a priority dd 07/12/2012 (*in Russian*)
- [4] Fridkin V M, Kuzmenko I M, Markov S N, Basharymova V N, Sysa N S, Kuzmenko D O, Bogdanov S V (2013) The bearing element of the metal constructions and metal construction on its basis. Application No a2013150386, International patent classification 04B1/00; the applicant is the Belarusian-Russian University; a priority dd, 12.11.2013 (*in Russian*)
- [5] Daripasko V M (2000) Resistance and stability of the I-girder elements with the perforated wall at the general case of the loading; author's abstract of dissertation of the candidate of technical sciences: S.-Petersburg, 23 p. (*in Russian*)
- [6] Mitchin R B (2003) Local stability of a wall and optimization of the steel perforated beam: author's abstract of dissertation of the candidate of technical sciences: Lipetsk, 26 p. (*in Russian*)
- [7] Litvinov E V (2006) Resistance and stability of a wall in the linearly-perforated elements of steel constructions with regular apertures: author's abstract of the dissertation of the candidate of technical sciences: Novosibirsk, 24 p. (*in Russian*)

[8] Pritikin A I (2008) Calculation of perforated beams: Publishing house KGTU: Kaliningrad, 308 p. (*in Russian*)

[9] Kuzmenko D O, Tarasenko D S, Kovalev M I, Kuzmenko I M (2013) Optimization of the geometrical form of I-girders of the lowered material consumption: *48th student's scientific and technical conference of the Belarusian-Russian University*: Mogilev, the Belarusian-Russian University, p. 116 (*in Russian*)

[10] Kuzmenko D O, Bogdanov S V, Kuzmenko I M (2014) Modern ways and methods of decrease of metal consumption of I-girders (columns). *Materials, equipment and energy saving technologies*: Mogilev, the Belarusian-Russian University, pp 278 – 279 (*in Russian*)

[11] Building specifications and rules (SNiP) 2.01.07-85* Loadings and stresses (1987). State construction engineering of the USSR. Moscow: Central Design Company for Standard Design and Urban Development of the State construction engineering of the USSR, 36 p. (*in Russian*)

[12] Dymolazov M A, Efimov O I (2012) Designing of a beam with the perforated wall. Methodical instructions for course designing of students of correspondence mode of study of a specialty 2903 on discipline «Metal constructions. A special course»: Kazan, 26p.

[13] Fomenko E J (2008) Flexural-torsional form of loss of stability of the eccentric-compressed steel i-girders with the perforated wall: author's abstract of the dissertation of the candidate of technical sciences: Krasnoyarsk, 26 p. (*in Russian*)

[14] Basov K A (2005) ANSYS: Users directory: DMK Press Moscow, 640 p. (*in Russian*)

[15] Kuzmenko D O (2014) Bearing designs of buildings and constructions with improved structurally-technical characteristics: MPhil. Mogilev, the Belarusian-Russian University, 82 p. (*in Russian*)

SCIENTIFIC RESEARCH ECONOMICAL, SOCIAL-PSYCHOLOGICAL AND TECHNICAL FACTORS OF QUALITY IMPROVEMENT OF BUILDING WELD-FABRICATED CONSTRUCTIONS

Parlashcevich Valentina

**Moscow State University of Civil Engineering (MGSU)
129337, Russia, Moscow, Yaroslavskoe shosse, 26
vs91144@mail.ru,**

ABSTRACT

This article contains investigation of methods of quality improvement of weld-fabricated building constructions. Improvement of accuracy and quality of welded building steel constructions is a multitask challenge. This problem may be addressed in different directions - accounting technical and economic factors and accounting social and psychological questions. This article contains the results of studies of residual welding stresses and strains that largely affect the quality of designs. On the basis of these studies are given allowances for the size of blanks designs. Also indicated that the decrease legs fillet welds and the number of welds reduces the amount of welding stresses and strains.

INTRODUCTION

Operability, reliability and durability of the welded metal constructions are largely dependent on the quality of their production. Insufficient quality of manufacture of welded metal structures and their elements also make difficult the technology of mounting. Consequently, the problem of improving the quality of manufacture of welded structures is important.

ANALYSIS OF RESERVES TO IMPROVE THE QUALITY OF CONSTRUCTION

The problem of improving the quality of welded structures requires big material expenditures. Manufacturing techniques used in different plants depend on their financial resources and manufacturing standards, which leads to different qualities of welded structures.

Modernization and retooling of production is the basis for improving the quality of the welded structure. The process of production of welded structures, must have a high level of mechanization and automation of technological processes [1]. The manufacturing process must be based on the

use of modern equipment for assembly and welding of stainless and the most modern technology of welding.

The problem of improving the quality of manufacture of welded metal structures also includes the creation of environmentally friendly jobs, with elements of aesthetics favorable for work.

Improving quality also depends on the solution of social and psychological problems. Social and psychological problems can be solved by promoting greater social and personal status of staff and awareness of their personal contribution to the success of the joint mission of manufacturing design [2, 3].

Workers need to know and appreciate their contribution to the making welded construction. Workers are the creator of welded construction. Workers are important part of the production process [2, 3].

Quality of welded structures is impossible without the use of scientific advances and discoveries. All modern scientific achievements and discoveries should be used in the production of designs.

The quality of welded construction depends heavily on welded processes and welding stresses and strains. [4]. Reducing welding stresses and strains will greatly enhance the quality of designs.

RESULTS OF RESEARCH ON PERMISSIBLE SHRINKAGE

The fabrication process begins with the preparation of the metal, marking and cutting work-pieces design. Marking and cutting of metals must be carried out taking into account shrinkage allowances when welding. Normalized value of the shrinkage allowance is approximate and often does not correspond to the actual forms of the designs and technology of its manufacture.

For example, allowance for shrinkage of the longitudinal weld seam is 0.1 mm per 1 m length of the structure. Allowance in length due to the formation of transverse shrinkage is equal to 1 mm on the seam. In fact, shrinkage of the structure of the weld depends on a large number of structural and technological factors.

Element size, type of steel, heat input welding; the leg fillet weld, the number of passes, gaps, etc. have an effect on the shrinkage during welding [4]. Our research conducting in MGSU, allows you to assign a more precise value of the shrinkage allowance [4, 5, 6, 7]. The recommended value of the shrinkage allowance depends on many structural and technological factors.

Shrinkage allowance of the element I-section, from the longitudinal shrinkage and transverse shrinkage is presented in tables 1 and 3

Table 1: Allowance (mm) per 1 m length of the element I-section, compensating shrinkage of the fillet weld on the one hand wall

Height wall, mm	Width shelves, mm	Yield (MPa)			
		230	300	400	500
300	300	0,12	0,13	0,6	0,17
400	400	0,08	0,09	0,11	0,13
500	500	0,06	0,07	0,08	0,09
800	200	0,10	0,11	0,13	0,15
	300	0,08	0,09	0,11	0,13
	400	0,07	0,08	0,09	0,11
1000	200	0,09	0,10	0,12	0,14
	300	0,07	0,08	0,09	0,10
	400	0,06	0,07	0,08	0,09
1200	200	0,08	0,09	0,11	0,12
	300	0,06	0,07	0,08	0,09
	400	0,05	0,06	0,07	0,08
1400	300	0,06	0,07	0,08	0,09
	400	0,05	0,06	0,07	0,08
	500	0,04	0,05	0,05	0,06
1600	300	0,05	0,06	0,07	0,08
	400	0,04	0,04	0,05	0,06
	500	0,03	0,04	0,04	0,05
1800	300	0,05	0,06	0,07	0,07
	500	0,03	0,04	0,04	0,05

Shrinkage allowance for the length of the element ($A.S$) is determined by the formula

$$A.S_1 = A.S_{i1} \cdot L \cdot k_1 \cdot k_2, \tag{1}$$

where: $A.S_{i1}$ – allowance (mm) per 1 m length of the element I-section, compensating shrinkage of the fillet weld on the one hand wall (see table 1);

L – length element;

k_1 – coefficient taking into account the effect of the second fillet weld on the other hand wall;

k_2 – coefficient taking into account the effect of the gaps.

Table 2: Allowance (mm) 1 transverse butt weld in the element of I-section, compensating transverse shrinkage

	Welding heat input divided by the thickness q_{ef}/t					
	4000	8000	12000	16000	20000	24000
Allowance 1 seam mm	0,12	0,32	0,46	0,57	0,68	0,77

Shrinkage allowance for the length of the element ($A.S$) is determined by the formula

$$A.S_2 = A.S_{i2} \cdot n \cdot k_3 \cdot k_4, \quad (2)$$

where: $A.S_{i2}$ – Allowance (mm) on 1 transverse butt weld, compensating transverse shrinkage;

n – quantity butt weld;

k_3 – coefficient taking into account the effect of the second pass weld;

k_4 – coefficient taking into account the effect of the gaps.

Table 3: Allowance (mm) per 1 transverse fillet weld of rib in the element I-section, compensating transverse shrinkage

Thickness wall, mm	Thickness shelves, mm	Leg length, mm	Welding heat Input J/sm	shrinkage from welding one rib welding, mm
6	8-18	5	8500	0,34-0,20
8	11-24	5	8500	0,25-0,15
10	12-30	5	8500	0,19-0,12
12	12-36	6	12500	0,24-0,16
14	14-40	6	12500	0,20-0,14

Shrinkage allowance for the length of the element I-section per 1 transverse fillet weld of rib is determined by the formula

$$A.S_3 = A.S_{i3} \cdot k_5 \cdot n_r, \quad (3)$$

where: $A.S_{i3}$ – Allowance (mm) per 1 transverse fillet weld of rib in the element I-section,

compensating transverse shrinkage on the one hand wall;

k_5 – coefficient taking into account the effect of the second fillet weld on the other hand of rib;

n_r – quantity of rib.

The total allowance for shrinkage in the element of I-section compensates for shorten when welding waist longitudinal fillet welds, transverse butt welds and fillet welds from the welding ribs is determined by the formula:

$$A.S_{\Sigma} = A.S_{i1} + A.S_{i2} + A.S_{i3}. \quad (4)$$

IMPROVING THE QUALITY OF ASSEMBLED STRUCTURES

The next step - assembly whole design of the individual pieces. Blanks should be assembled and welded as a whole construction. Stage assembly structures from blanks are also significantly influences the quality. The greatest effect is the assembling and welding of constructions in hard jigs.

Welding residual stresses and strains are inevitably formed in the structural elements during welding. However, residual welding deformations shortening in structural elements are reduced when welding in hard jigs.

Various manufacturing techniques exist in plants and, therefore, there is a different accuracy and quality of construction. Availability of modern assembly equipment depends on the culture of production and material resources of the plant.

Assembly and welding whole design of the individual pieces in rigid jigs attachment greatly improve the quality of weld construction.

REDUCTION OF RESIDUAL WELDING STRESSES AND STRAINS

Welding is the most basic and most fundamental operation of manufacturing of metal structures and welding have the maximum impact on construction quality.

As was already noted, welding gives development big temporary and residual welding stresses and strains in the metal. And shrinkage during welding deforms structure changes it sizes and shape. Welding residual stresses are added to the load voltage and reduce the efficiency and quality of construction. Residual welding deformation changes in the sizes and the shapes of constructions and also greatly reduces the quality of designs.

Welding stresses and strains can not be fully rid! We can only reduce their value! Welding stresses and deformations are due to uneven heating of the metal during the welding [4, 5, 6, 7, 9, 10]. Heating from the welding depends upon the effective heat input during the welding and thermal properties of the metal [8].

Quantity of welding heat input is calculated by to the following formula

$$q_n = q_{eff} / v = 0,24 \cdot I \cdot U \cdot \eta / v. \quad (5)$$

where: I – welding arc current;
 U – welding arc voltage;
 v – speed of welding.

A value of welding heat input is proportional to the value of a leg of fillet weld specified by a design engineers or technologists.

Design engineers and technologists often unreasonably inflate the legs of fillet welds and weld used on both sides. It is often assumed that the larger the legs of fillet welds and more weld seams quantity, the better. But the big legs are welded at high heat input welding. And the welding stresses and deformations have a large value in compounds with large legs of the fillet weld and with a large number of welds.

Scientific research the conditions of manufacture given the average values of the welding heat input fillet weld leg with various sizes (Figure 1). In addition investigations were carried out at different welding methods are widely used in the manufacture of welded steel building structures. The following welding methods were investigated: manual metal arc (MMA), metal active gas (MAG), and submerged arc welding (SAW).

The graph (see Figure1) shows that the maximum amount of heat input is transferred to a work-piece in the process of manual metal arc (MMA Welding). The minimum amount of heat is transferred in the process of mechanized (Mig/Mag Welding).

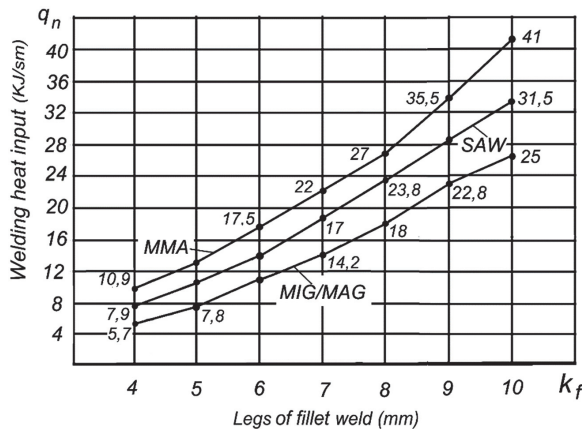


Figure 1. Welding heat input for manual (MMA Welding), mechanized (Mig/Mag Welding) and automatic welding (SAB Welding)

Therefore, production of welded structures is recommended to perform mechanized types of welding.

Studies conducted on work-pieces natural structures confirmed that lowering of the leg fillet reduces the heat input welding and lowers the welding deformations (Figure 2). Deformations fillet weld joints and butt welds is reduced proportionally to the value heat input welding or quantity the fillet weld leg [4. 5] (see Figure 2).

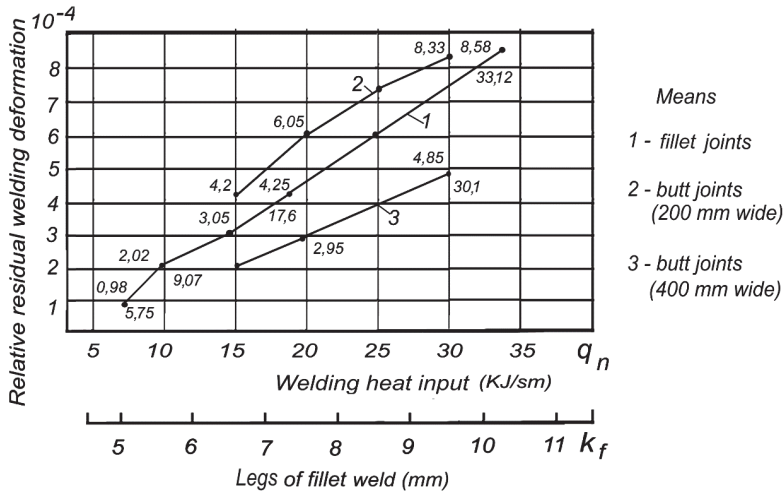


Figure 2. Relative residual deformation resulted from metal active gas welding

Accounting of welding stresses and deformations in the design and manufacture of structures will improve accuracy, quality and reliability.

SUMMARY

Improve the quality of manufacturing structures promote:

1. Modernization and technical re-equipment of production is the basis for improving the quality of construction. The process of production of welded structures should have a high level of mechanization and automation of all processing steps.
2. The solution to all social and psychological problems, increasing social and personal significance of the worker and awareness of its necessity in the manufacture of structures.
3. The focus should be temporary and residual welding stresses and strains that will inevitably arise in the manufacture of welded steel structures.
4. Residual welding deformation should be considered when cutting workpieces. Allowances compensate for shrinkage welding.
5. To use seams with the minimum legs fillet welds (3 – 4 mm) in unstrained and low-loaded joints.
6. Assembly and welding of constructions in hard devices significantly increases the quality of the products.
7. Manufacturing of welded structures perform better mechanized types of welding.

REFERENCES

1. Oboturov V.I., Danilov A.I. Welding in construction: innovative technological processes and equipment // Industrial and civil construction. 2013. № 5. Pp. 60–62.
2. Yuri Irkhin. Psychology of Success: How to Influence People and to Govern Themselves. M.: Publishing House of the Rus. Univ. Peoples' Friendship. 1992. 40 p.
3. James Borg. The power of persuasion. The Art of Influence People. In the book of On the Table for the Head. № 11. 2012. Pp. 23–31.
4. V. Parlashkevich, V. Belov., A. Vasilkin. Ways to improve the quality of welded metal constructions // Industrial and civil construction. 2014. № 9. Pp. 69–72.
5. Ignatyeva V.S. Method of "Fictive Temperatures" as the Basis of Research in the Field of Strain-Stress Distribution in Welded Connections. In the book of "Metal structures in the building". Moscow. Moscow Institute of Civil Engineering, Collected Works, No. 152, 1979. Pp. 71–88.
6. Parlashkevich V. Welding voltage and deformation of elements of construction metal structures. European Science and Technology: materials of the VI international research and practice conference vol.II. Munich, Germany. December 27–28, 2013. c. 321–326.
7. Belov V.A., Vershinin V.P., Parlashkevich V.S. Resource Saving Technologies of Weld-Fabricated Constructions. In the book of "Modern technologies in construction. Education, science and practice". Moscow, 2001.
8. Rykalin N.N. Calculation of Thermal Processes in Welding. Moscow, Mashgiz Publishing House, 1951. 296 p.
9. Kulikov V.P., Decyatnik V.V., Logvina Ye.V. Determination of welding stresses and deformations in the butt welding of thin plates. Vestnik of Belarusian-Russian University. 2007. No. 3. Pp. 48–56.
10. Sleptsova E.A., Pavlov A.R. Calculation of Welding Stresses and Deformation in Butt Welding of Thin Plates. Vestnik of Samara State University. Samara. 2008. No. 61. Pp. 273–287.

DETERMINATION OF INITIAL FORCES IN TWO-LAYER LARGE SPAN METAL DOMES DUE TO ASSEMBLING ERRORS

Evgeny Lebed
Dozent

Artyom Grigoryan
Phd-student

Moscow State University of Civil Engineering (MGSU), Russia

ABSTRACT

The paper describes the dependence of errors occurring in the frames of large-span metal domes as a result of inaccuracy of actual dimensions of assembly elements. The imperfections in joints are considered as sources for initial forces (stresses) in the elements. Different types of adjustment operations are used to eliminate imperfections. This enforced fitting creates initial forces (stresses) in the elements of the dome. A method is proposed for determining initial internal forces in two-layer metal large-span domes by computer analysis. It is based on a special computational model of the frame of the dome and on special technique for applying loads to this model.

Key words: metal dome, assembly errors, connections of structural elements, adjustment operations.

INTRODUCTION

The imperfections in joints in space frames that initiate from assemblage process are considered as sources for initial forces (stresses) in the elements. Erection of large-span metal domes is accompanied by inevitable errors that are accumulated during the assemblage of a large number of individual units (assembly blocks).

It is important to note that imperfections in metal structures that initiate from assemblage process are found out during the analysis of failures of buildings and structures [1]. Besides factors connected with durability of metal and corrosion, the following defects are described by most sources:

- Discrepancies between the project and actual sizes of the elements of the structure;
- Bending of particular elements of the structure;
- Appearance of gaps between the connected elements in joints;

- Displacements of bars' axis from the centers of their connections;
- Changes in the geometry of the dome in general.

Changes in geometry of the spatial system of bars of the dome are most noticeable. They are caused by significant displacements of the joints of the dome comparing to the project mode. These displacements might be as big as several centimeters. It is confirmed that the analysis taking into consideration of changes in the geometry of the dome demonstrates significant differences of its stressed and strained condition in comparison with the project that does not include the changes [2].

It is often indicated that the most common causes of imperfections in metal domes are:

- Violations in the assemblage process prescribed by the project;
- Fixation of geometric shape of the metal assembly blocks before they are installed in the required position;
- Using additional units in the joint connections.

However, this is not exactly correct. The main reasons of imperfections of geometric shape of domes, of bar bending, and of gaps in the joints are caused by objective laws of Physics, Mathematics, and Probability Theory. It is impossible to produce metal units and, moreover, metal structures that would be made in complete accordance with the project values. The actual values always differ from the model, and those deviations are by themselves insignificant. However when a complex metal dome is being assembled they can cause the problem of assemble ability of structures [3].

Frames of metal domes form spatial lattices that are characterized by mutual dependency of distances between nodes in different directions. Change in distances in one direction due to imperfection in the length of the bar, causes the necessity of adjusting distances in other directions that can be done only by applying forces in these directions. These effects result in the use of different types of adjustment operations [4]. These fitting operations are needed at the stage of connecting all assembly blocks of the dome into a single structure. The enforced fitting during the assemblage process inevitably creates initial forces (stresses) in the elements of the dome.

METHODOLOGY

A method is proposed by the authors for determining initial internal forces in two-layer metal large-span domes by computer analysis. It is based on a special computational model of the frame of the dome and on special technique for applying loads to this model. To demonstrate the method the authors present the results of the stress-strain analysis of the two-layer metal dome

with rib-ring frame system. The frame has a spherical form with the radius of curvature of 48 meters, with 16 trussed ribs and 8 rings not accounting for the support ring. The distance between layers is 3 meters (Figure 1).

Assessment of possible errors of assembly was performed by the software MONTAG developed earlier by E. Lebed [5] and based on the computer statistical modeling of frames by Monte-Carlo method. The authors considered the erection with the temporary central pillar under the top ring, which served as a support for the space sectors of the dome frame. The sectors were pre-assembled from 3-D blocks formed by the bars of top and bottom layers of single cell of the lattice.

The model of dome frame with rib-ring frame system was performed by LIRA in accordance with the geometric layout presented above. The elements of the dome are made of double angles. All elements were dimensioned according to the results of static analysis of the dome for the self-weight load of load-bearing and envelope structures and for snow and wind loads (Figure 2). This allowed modeling all required conditions for the analysis of initial forces (stresses) created by the enforced fitting during the assembly process.

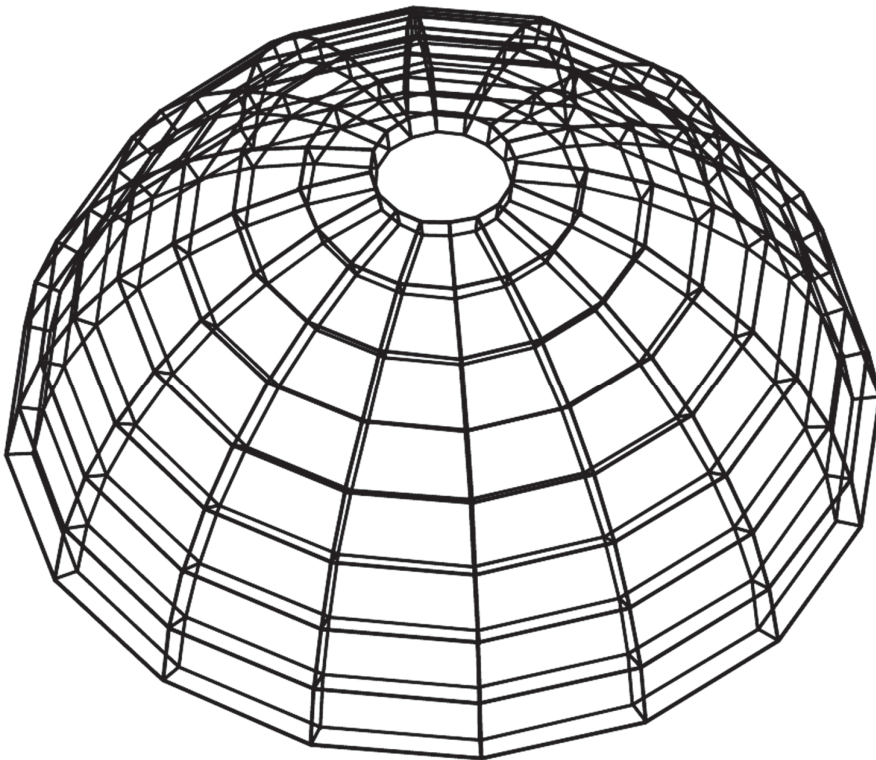


Figure 1. Geometric layout of two-layer dome with rib-ring frame system.

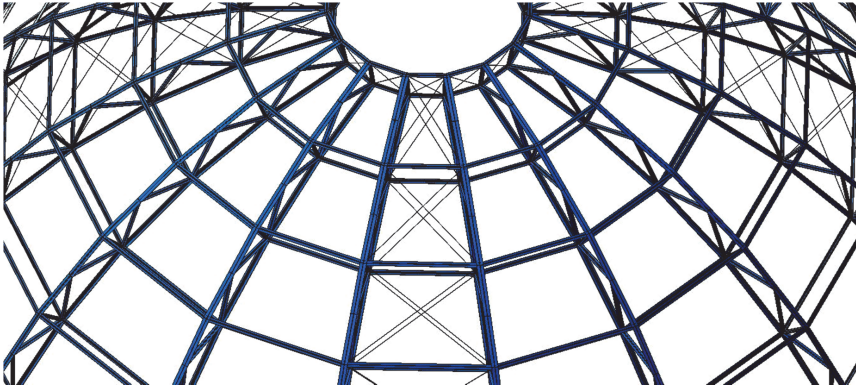


Figure 2. Design of the frame of the analyzed dome with rib-ring frame system.

The data for the possible errors thus obtained enabled to define the priority directions for applying forces for the assembly of space sectors to provide their adequate connection and insure the space action of the frame as a whole. A special computer model was developed that accounted for the geometry of the frame during assembly process. The assembly of the frame of the dome by meridional sectors with temporary central pier under the upper ring was investigated. It was assumed that every spatial meridional sector assembled from 3-D units is installed on the upper and lower rings. After that, the joints of meridional ribs of adjacent sectors are connected together. Since the actual geometric shape of every spatial sector of the dome frame is formed independently from the other sectors, it is enough to consider only two sectors of the frame (Figure 3).

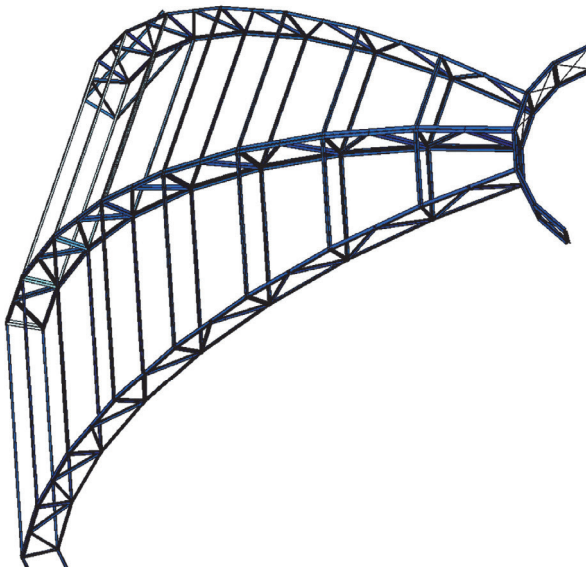


Figure 3. Model for the analysis of initial forces (stresses) created by the enforced fitting.

In the process of assemblage of the sectors from the assemblage blocks their actual geometric shape in projection on to a vertical plane is deformed. Since the sectors are assembled onto the top and the bottom layer, their actual geometric shape due to the variable value of extreme deviations at different joints $[\delta_i]$ acquires a shape of an arch above or below the project shape, as shown.

To connect the joints of adjacent meridional ribs of different sectors it is necessary to apply counter directed forces along the radius of curvature (along the normal) (Figure 4). Since these forces cannot be applied at two places simultaneously, we have to first connect the joints in the middle of meridional rib F_2 , and later – in the quarters: F_1 и F_3 .

The actual geometric shape of the meridional ribs of different sectors are deformed both in the direction of the rings (on the plane) and along the ribs (along the meridian). Instead of a straight line, a projection of each of the adjacent meridional ribs on to the plane acquires a shape of a curve; and the projections of the nodes' centers on the layers' axis will not coincide. Accordingly, the external forces were applied to the model in the directions that were defined by the displacements of the nodes, thus eliminating the occurring errors.

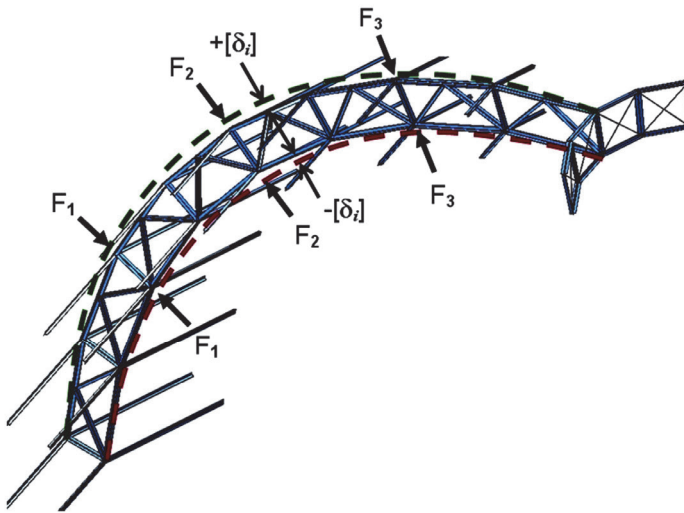


Figure 4. Realization of enforced fitting of meridional ribs for normal deviations.

The errors caused dislocations of nodes of the frame in normal, meridian and ring directions at the same time. Therefore the forces were applied either in every direction separately, or in a chosen main direction for the given case.

The goal for applying forces was to change the location of nodes of adjacent sectors in space in such a manner that they would merge in the same point.

Accounting for different values of mutual displacements of connected joints, the applied forces had different absolute values. To balance the system of forces, step-wise analyses for unit forces were performed, and the system of coefficients was introduced on a later step.

CONCLUSIONS

The results of the analysis demonstrate that the step-wise static analysis allows to determine the initial internal forces and stresses in the bars of the dome during the erection period. Taking into consideration the initial forces (stresses) when designing metal dome frames will increase stability of two-layer large-span metal domes and will allow for change the technology of the assembly process and the principles of blocks connecting.

REFERENCES

1. Dobromyslov A.N. Oshibki proektirovaniya stroitel'nyh konstruksiy: Nauchnoe izdanie – M: Izdatel'stvo ASV, 2007. – 184 s.
2. Tur V.I. Kupol'nye konstruksii: formoobrazovanie, raschet, konstruirovaniye, povysheniye effektivnosti. – M: Izdatel'stvo ASV, 2004. – 96 s.
3. Lebed E.V. Tochnost' vozvedeniya sterzhnevyyh prostranstvennyh metallicheskih pokrytiy i ee prognozirovaniye // Nauchnyy zhurnal Vestnik RUDN (Moskva). Seriya: Inzhenernyye issledovaniya. 2013. № 4. S. 5–12.
4. Ishchenko I.I. Montazh stal'nyh i zhelezobetonnykh konstrukziy. – M.: Vyssh. shk., 1991. – 287 s.
5. Lebed E.V. Komp'yuternoe modelirovaniye tochnosti vozvedeniya dvuhpojasnyh metallicheskih kupolov // Promyshlennoe i grazhdanskoe stroitel'stvo. 2013. № 12. S. 89–92.

MODERN STADIA. TECHNICAL AND ECONOMIC PROBLEMS OF DESIGN AND OPERATION

P.G. Yeremeyev

**D. Tech. Sci., Prof., Department Head in
Kucherenko Central Research Institute for Building Structures
(part of OJSC SRC Stroitelstvo)**

ABSTRACT

Modern stadia are complex multilevel structures. Stadia should comply with the requirements set by FIFA and UEFA for international competitions as regards safety, strength and operational reliability of structures as well as spectators' and contestants' safety. Problems of construction are resolved by developing new materials and technologies, creating more advanced, faster and safer construction techniques and using light roofs. Heavy structural elements are replaced with spatial truss or tensile systems. Various modern materials are used such as high-strength steels, steel ropes and polymer membranes. Unique wide-span structures have high criticality rating and their failures can have severe economic and social consequences. Therefore, there are additional requirements for the scope and types of necessary surveys and design activities as well as acceptance and operation procedures of such structures that should be taken into consideration. Stadium design and construction require an integrated approach to the selection of optimum structural solutions and materials, manufacture and installation techniques, operating conditions as well as close supervision throughout all stages of construction. Failure to observe any of the above conditions will reduce the system reliability and may result in accidents (malfunctions). The article gives examples of accidents with stadium roofs. The article also poses stadium safety problems and proposes possible solutions. Environmental issues play increasingly important role. FIFA proposed the Green Goal Program aiming at environmental optimization of stadium construction.

A boom in sports facility and stadium construction is occurring around the world. This includes arenas with roofed stands. Such facilities have always been and still are landmarks in their cities. Modern stadia are complex tiered structures whose architecture, design solutions, materials, manufacture and installation technologies are ahead of their time and define future construction trends [6].

Their design, construction and operation require a comprehensive approach to various, often conflicting issues, including the following:

- ensuring safety, strength and operating reliability of structures;
- selecting optimum design solutions and materials;
- reducing labor requirement for manufacture and installation;
- ensuring safety and comfort of spectators and athletes;
- minimizing the stadium construction and operation costs;
- complying with increasing environmental requirements of FIFA and UEFA.

Roofs are the most important element that defines the stadium's appearance [7]. In northern countries, roofs protect stands from rain and wind; in southern, from sun and high temperature. It fully applies to the Russian climate with a lot of precipitation, long winters and inclement weather in spring and fall.

PROBLEMS OF CONSTRUCTION

These are resolved by developing new materials and technologies as well as more advanced, faster and safer construction methods. Heavy structural elements are replaced with spatial truss or tensile systems. Various modern materials are used such as high-strength steels, ropes, cast steel and polymer membranes. Spatial truss systems, rope nets, various cable, suspended, hybrid and tent systems, etc. are common in stadia. Their advantages include long spans, adaptability to various plan and surface shapes as well as aesthetic qualities. Transformable roofs that protect spectators against inclement weather, expand the structure's functionality to cover multiple uses and improve the facility's bottom line are becoming more common.

Selection of roof design should take into account wind suction which, aside from creating forces opposite to roof's own weight and snow load, can also create roof vibration. Increasing the roof's own weight to solve the problem is costly. An alternative approach would be maximum use of spatial forces within the roof structure or utilization of shell elements (wall or lining panels, etc.). With the above contradictory factors, sound decisions require detailed aerodynamic studies with scale models, taking into account the following parameters:

- prevailing wind direction and speed;
- prevalent air temperature;
- probability of precipitation (rain or snow);
- local peculiarities of wind flow turbulences caused by surrounding buildings and the stadium features.

For cost reduction, such studies can be combined with studies aiming to create comfortable conditions for spectators and determine wind impact on grass growth.

Selection of materials for load-bearing structures takes into account the fact that steel structures are lighter and cheaper than reinforced concrete, can be prefabricated and afford plenty of opportunity for creating aesthetic, refined systems. Fire safety rules require that fireproofing materials be applied to steel elements which reduces the cost benefits of steel. But fire safety rules are changing, new technologies allow unprotected steel structures through the use of fire-resistant steels or sprinkler systems (permitted by new fire safety regulations abroad). It should be kept in mind that the main hazard in case of a fire in a stadium is not structural failure but suffocation by smoke, so provisions are made to permit evacuation of people from the stadium in minimum time, long before any structural failure begins.

SAFETY OF STRUCTURES

Stadia have high criticality rating and their failures can have severe economic and social consequences. Therefore there are additional requirements for the scope and types of necessary surveys and design activities, for fabrication and installation of structures and for acceptance and operation procedures. Design of such structures involves problems not covered in regulatory documentation. Novelty of technical solutions requires the engineer to have deep specialized knowledge and experience in designing similar structures. At the same time, engineers should not be overwhelmed by the growing volume and details of modern regulations but should have a clear understanding of underlying factors. Construction safety and efficiency is best achieved by personnel capable of seeing overall picture. Large quantities of data can potentially create greater opportunity for errors [8].

Human safety is the foremost requirement that should be clearly understood and observed by everybody involved in planning, engineering, design, construction and management. Ensuring safety means protecting the structure and people from various external threats. The threats can arise from criminal actions, accidents or human errors, such as errors in facility design, operation or management. Stadium safety is ensured by both adequate design solutions and proper facility management and operation. Good management cannot compensate for design errors and vice versa. Safety of a facility cannot be achieved by solving individual problems but requires a comprehensive, integrated approach. Design should include a consideration of all possible safety measures. It is recommended to start with preventive measures that will rule out, preclude or minimize possible impact of accidents, human errors, etc.

Operating safety of a facility should be achieved by complying with the following requirements:

- observing the provisions of Russian rules and regulations that ensure safe operation of the facility; producing and updating a technical certificate of the facility;
- making sure that the facility's operating mode conforms to its purpose and that its actual operating environment, loads and influences match their design or regulatory values;
- planning, preparing and conducting maintenance and periodic inspections;
- timely detection, assessment and rectifying defects in building structures, making repairs and taking remedial actions;
- creating conditions for safe presence of people and their evacuation in case of emergency;
- maintenance of the facility by competent personnel.

ACCIDENTS AND EMERGENCIES

Violation of any one or more of the above requirements reduces the system reliability and may lead to an accident (malfunction). By accident is meant structural failure of or damage to the whole structure, its part or an individual structural member or deformation thereof in excess of maximum allowable values. Malfunction is a loss of the facility functions due to an excessive change of its parameters or properties caused by internal processes and/or external influences. Malfunction does not always lead to structural failure (loss of structural reliability) with threats to people or material damage. Malfunction can prevent normal use of the facility.

Various authors [1, 3, 4] identified main causes of malfunctions in construction which obviously can be applied to sports facilities: design errors (20 ÷ 55%), violation of manufacture and installation technologies (17.5 ÷ 53%), misuse (5 ÷ 33%), low quality of materials (6 ÷ 14.5%), regulatory shortcomings (up to 4%), other causes and their combinations (up to 25%). Variations in figures given by different authors can likely be explained by insufficient statistical data, differences and imperfections of techniques used to establish causes of accidents, etc. Anyhow, a large percentage of errors in design, construction and use is alarming. An analysis of causes of structural failures shows that most catastrophic situations are caused by a combination of factors.

Available data were generalized to identify some main supposed causes of the problem:

1. Growing volumes of construction, including the construction of technically complex structures, which increases the absolute number of failures while relative quantities are constant.
2. Development of technologies resulting in novel design solutions and techniques, materials and construction methods giving rise to complex problems yet to be resolved. Malfunctions are brought about by individual or combined unprecedented causes when even the most fundamental principles of conventional building design and construction practices are changing.
3. Growing number of people that are involved in construction without adequate qualifications. Standards of workmanship in construction are generally much lower now. Design and construction work is often done by people without practical experience whatsoever.
4. Ignorance, bad faith or negligence leading to noncompliance with regulatory requirements, design documentation and operating procedures, failures to monitor operations throughout all design, construction and acceptance stages, unwarrantedly tight deadlines for design, manufacture and installation, even in case of technically complex structures.
5. Failure to use structures in accordance with the design and regulatory documentation. Failure to conduct full scope of instrumental monitoring whose results could be used to assess actual bearing capacity of structures, forecast remaining life of the building and thus make sound decisions on extending their safe operation periods.

There are certain key conditions and measures that are necessary for mitigating the risk of accidents (malfunctions) in construction and increasing the reliability of technically complex and unique facilities.

1. Theoretical and experimental research of new building materials and structural forms; design quality improvement; learning and application of foreign best practices.
2. Development and improvement of regulatory and technical documentation, alignment with international building codes.
3. Broad communication of discovered causes of accidents and measures for their prevention to builders and operators; use of accident cause analysis to amend regulatory and design documentation.

4. Stricter monitoring throughout all stages of design, including the expert review and approval stages. Unfortunately, design shortcomings only become obvious after accidents.
5. Actual complex structure will inevitably differ from design. Re-calculations taking into account the actual geometry and characteristics of structural elements and junctions are recommended. Results of such re-calculations can be used to bring the computational model as close to reality as possible and thus determine with a better accuracy the structure's proximity to its limit state and its actual long-term reliability.

According to [5], the most common types of accidents in sports facilities are structural failures of roofs (48%), stands (31%) and building envelopes (21%). Below are some well-known accidents with stadium roofs:

In 2001, the roof of Mottaqi Stadium in Sari, Iran collapsed due to a violation of its safe operation rules; there were 25,000 fans in the stadium designed to hold 15,000 people. Some people climbed the roof which caved in under their weight. Two people died and 290 were injured.

In 2002, two strong typhoons hit Jeju Province (South Korea). The first one with a maximum wind speed of 28.7 m/s tore three panels of membrane roof off the Jeju World Cup Stadium. The second typhoon with a maximum wind speed of 40.8 m/s destroyed another three panels.

Montreal's Olympic Stadium was damaged for a similar reason in 1988 and 1991 when aerodynamic instability lead to a local rupture of its transformable Kevlar roof.

In 2009, the roof of Stadium Southland in Invercargill, New Zealand, collapsed. The roof structure was a spatial truss system in the form of a lattice. The collapse was caused by a combination of factors including heavy snowfall with rain, design shortcomings and installation defects (major deviations from the design and building codes, including welding deficiencies), lack of competent personnel to perform and supervise construction, etc.

Multi-purpose Sultan Mizan Zainal Abidin in Kuala Terengganu, Malaysia, capable of holding 50,000 people collapsed one year after its official opening in 2008. The roof structure was a two-layer grid made of MERO steel members. The roof collapsed in normal weather. Design errors, major deviations of bearing member from their design positions during installation, lack of competent supervision during construction, nonconformity of materials and manufacturing to building codes were identified as possible causes.

In 2010, work began on De Grolsch Veste Stadium in Enschede, Netherlands, to increase its capacity by more than 30,000 people and install roof over the stands. A large section of the roof collapsed on the upper rows of the stands during construction killing two people and injuring more than a dozen. Loss of stability of two bearing trusses was one of identified causes.

Strong snowfall collapsed part of the roof of Veltins-Arena in Gelsenkirchen, Germany in 2010. Three sections of fibreglass canvas were damaged.

In 2010, the giant inflatable roof of the Metrodome Stadium in Minnesota, USA, collapsed after strong snowstorm (snow thickness reached 50 cm and temperature dropped to -18°C).

General redevelopment of Mercedes-Benz Arena in Stuttgart, Germany, began in 2011 to modernize the stadium and increase its capacity. A building crane working on one of the stands fell onto the stadium roof tearing a large hole in it with some roof elements falling down.

In 2013, a small section of the membrane roof of Arena Fonte Nova was ruptured. The stadium capable of holding 56,000 spectators was built to host 2014 FIFA World Cup games in Salvador, Brazil. The collapse occurred due to an overload of a sagging section of PTFE membrane by water accumulation after heavy rain.

MAINTENANCE

Maintenance of bearing structures includes monitoring their condition, keeping them in good order and preparing them for seasonal operation. No changes should be made to the structural system of a building during its use, and maximum loads specified in design and regulatory documentation should never be exceeded. Any deficiencies in building structures should be timely identified and remedied. There should be no wear preventing safe operation of the facility. Maintenance and overhaul should be scheduled and carried out to maintain and restore its technical and operating characteristics and should be based on inspection and monitoring of the facility's condition. Reinforcement of structures is mandatory if their bearing capacity is reduced by 15% or more.

TECHNICAL AND ECONOMIC ISSUES

Stadium design should consider not only capital investments but operational expenses too. The key to success of any stadium is maximizing its economic performance while striking the right balance between the capital costs of construction, operating expenses and profits. Capital expenditures are estimated through an analysis of the following factors: site costs; stadium capacity; configuration of its stands; configuration and dimensions of roofs; mechanical, electrical and plumbing systems; construction techniques; quality of interior and exterior finish; parking lot capacity; landscaping quality and scope.

Stadium construction expenses are one of the main factors, with the cost of building structures being the largest part of the total cost of the stadium, larger than in buildings of other types. Cost structure does not depend much on the total capacity of the stadium [2]: foundations account for 10% of costs;

bearing structures, 20 ÷ 25%; exterior and interior walls and finishing, 10 ÷ 20%; equipment, approximately for 20%. The only difference is in the cost of roofs which accounts for 10 to 25% of total costs and increases with stadium capacity. Estimates of average capital expenditures on the construction of a new stadium are usually based on the cost of construction per one spectator seat. These figures are different in different countries and depend on the stadium type, size and capacity, materials, etc. Construction cost can also vary a great deal depending on retail and catering infrastructure which increases the construction cost but also reduces investment payback period. Averaged ranges of per-seat construction costs of new stadiums with different capacities are given in Table 1.

Construction cost per spectator seat is usually higher for large stadiums, mostly due to higher cost of bearing structures, roofs and auxiliary infrastructure servicing larger numbers of people (elevators, stairs, parking space, etc.). Moreover, large stadiums also have greater number of VIP seats offering greater comfort. An analysis of average figures showed a price increase rate of 5 to 10% per annum which can be explained by inflation, increasing complexity of design solutions and greater stadium comfort.

Table 1. Cost of Stadium Construction per Spectator Seat

Stadium capacity, thousand seats	Cost per seat, US dollars
60-80	4500 - 9000
40-60	3000 - 6000
20-40	2000 - 4000

ENVIRONMENTAL ISSUES

These play an increasingly important role. FIFA proposed the Green Goal Program aiming at environmental optimization of stadium construction. There are various methods and certification systems for task setting and performance assessment. The most common ones are LEED (Leadership in Energy and Environmental Design), BREEAM (Building Research Establishment Environmental Assessment Method) and a system of green building criteria. Green technologies reduce stadium construction and operation expenses, make for more efficient use of resources, prevent climate change while creating a healthier and more productive environment for human life and work. Green building principles include efficient use of energy and resources as well as responsible attitude to the environment:

Water use efficiency: reduced consumption and use of alternative water resources. The program proposes rainwater collection and storage to support the water cycle, which includes use for pitch watering. Even greater water savings are achieved through the installation of water-saving technology in sanitary fittings. Energy saving: maximum use of daylighting and natural ventilation, use of energy-saving technologies in air-conditioning, lighting and

other systems. It will increase project costs but reduce operating expenses. It is important to implement energy-saving measures at the stadium design and construction stages through the use of alternative energy sources, including photovoltaic technologies. Choice of materials: environmentally clean, nontoxic (preferably local) construction materials selected so as to minimize greenhouse gas emissions. Measures should be taken to reduce quantities of materials required for the project, cut down waste, avoid the need for garbage disposal at landfills, recycle and reuse materials. Waste reduction: use of reusable containers for drinks, waste sorting and sale of unpackaged food and souvenirs. Positive environmental impact: reduction of carbon dioxide emissions causing the greenhouse effect. Environmental compatibility of stadium site: site selection with due consideration of natural and social environments and transport systems so as to mitigate impact on the surroundings.

REFERENCES

1. Allen, D.E. "Limit state design – A probabilistic study", Canadian Journal Civ. Eng. 1975.
2. European Stadium Insight 2011. Prospects for Football Stadium Development and Commercialisation Across Europe. KPMG. 2012.
3. Krishnamurthy N. Forensic Engineering in Structural Design and Construction. Proceedings of the Third International Congress. India. Bangalore - 2007.
4. Majowiecki.M. Conceptual design of long span structures: a knowledge based synthetical approach. Proceedings of the IASS Symposium. Stuttgart/Germany, vol.I. 1996,
5. www.pamag.ru (Science and Safety Portal).
6. Yeremeyev P.G. "Modern football stadia of the world". Kucherenko Central Research Institute for Building Structures, 2012. (in russian).
7. Yeremeyev P.G. "Roofs of modern football stadium stands". Industrial and Civil Engineering, No. 10, 2013. (in russian).
8. Yeremeyev P.G. "Stadia. Safety. Accidents". Mechanics of Structures and Structural Analysis, No. 6, 2013. (in russian).

EVOLUTIONARY OPTIMIZATION OF WELDED FRAME CONSTRUCTION IN INDUSTRIAL BUILDINGS

Anatoly Alekseytsev
(aalexw@mail.ru)

Natalia Kurchenko
(ms.kurchenko@mail.ru)

**Bryansk State Academy of Engineering and Technology
Department of building production, Bryansk, Russia**

ABSTRACT

This paper describes modifications of the evolutionary optimization algorithm to support rational structural/shape/size design of metal plane frames for industrial buildings. Under consideration is the variation of the cross-section of composite welded profiles. Structural synthesis is performed by means of introducing redundant topologies frames. The composite section in welded thin-walled profiles with varying degrees of accuracy can be described by a system of rectangles and flat figures given by the integral geometric characteristics. The iterative optimization scheme is based on using a modified genetic algorithm. This modification includes the equations between the parameters of composite welded sections. To ensure the convergence of the computational process well-known genetic operators are used: selection, crossover and mutation. To maintain the best solutions we used the database of survivable and rational objects, functioning in accordance with the principle of "elitism". The example demonstrates the optimization of a planar metal frame of industrial buildings.

INTRODUCTION

The task of designing bearing systems of industrial buildings is currently associated with the creation of firm structures of minimum weight. At the same time designers solve problems of structural synthesis and choosing rational parameters of cross-sections of frame members. This problem can be solved to a large extent using genetic iterative optimization schemes of rod systems [1, 3, 5] etc.

SETTING THE TASK

We will consider a linearly deformable planar rod system. The objective of the optimum design (criterion of survival) is minimizing the volume V of frame material:

$$V(\{C, P_1, P_2\}) \Rightarrow \min, \quad (1)$$

where C is the finite set of coordinates of extreme points of section of the rod, in which changes are allowed; P_1 - sets of variable cross-sections of rod shapes predetermined by integral geometric characteristics of the rolled shapes; P_2 – sets of profiles with a constant composite welded section along the rod, defined by the parameters of its constituent plane figures. The evaluation of the stress-strain state of the structure is performed by means of the finite element method using a flat bar elements with the hard consoles [7].

CONSTRAINTS

In the course of optimal synthesis the following constraints are taken into account: the geometric changeability of the rod system, the equilibrium condition for the nodes of the finite element model, the conditions for the rigidity according to normative documents, the condition of strength and stability of the rods, the total resistance, the unification of the parameters and the symmetry of the bearing system, and also technological and design requirements.

OPTIMIZATION ALGORITHM

For the general case of synthesis of rod designs the main stages of the optimization algorithm are given in the work [4]. The presented algorithm is different in the thing that it takes into account the specific nature of the task and does not require any a priori culling procedures of design options, the use of simulation models [5], etc.

For the rod system as a redundant structure we will consider the topology scheme that is generated based on the standard of design solutions. For each element of this topology scheme there is a possibility of introducing small bending stiffness (MSBS) (5–6 times less than the minimum stiffness of the cross sections in the sets P_1). In this case a rod with this low bending stiffness can be regarded as absent. Discrete sets of admissible parameter values are defined based on the availability at the manufacturer's standard profiles and sheet metal used for the construction of industrial buildings.

We use the following active constraints for the optimization process: a geometric object invariability, equilibrium model nodes, the strength and stability of bars, as well as requirements for the span of frame stiffness. Checking the overall sustainability is performed after the iterative optimization procedure. The registration of geometrically changeable systems will be made according to the estimation of the determinants of their stiffness matrices of finite element models. The criterion for survival [4] is the volume of the construction material. The smaller the volume, the higher is the survival rate.

We believe that the composite section of thin-walled profiles with varying degrees of accuracy can be described using the system of rectangles and flat figures given by the integral geometric characteristics. Vector $\{\Psi\}$ of parameters defining this section can be written as

$$\{\Psi\} = \begin{Bmatrix} \Psi_1 \\ \Psi_2 \end{Bmatrix}, \tag{2}$$

where vectors $\{\Psi_1\}$, $\{\Psi_2\}$ can be expressed as follows:

$$\{\Psi_1\} = \{z_{\phi 1} \ y_{\phi 1} \ \delta_1 \ z_{\zeta \phi 1} \ y_{\zeta \phi 1} \ z_{\phi 2} \ y_{\phi 2} \ \delta_2 \ z_{\zeta \phi 2} \ y_{\zeta \phi 2} \ \dots \ z_{\phi n} \ y_{\phi n} \ \delta_n \ z_{\zeta \phi n} \ y_{\zeta \phi n} \ z_{\eta 1} \ y_{\eta 1} \ z_{\eta 2} \ y_{\eta 2} \ \dots \ z_{\eta m} \ y_{\eta m}\}^T; \ \{\Psi_2\} = \{N_1 \ N_2 \ \dots \ N_s\}^T. \tag{3}$$

Here $z_{\phi i}$, $y_{\phi i}$ are coordinate axes Oz and Oy base corner point ϕ_i for i -th rectangle (Figure 1); δ_i - the thickness of the wall or shelves associated with this rectangle; $z_{\zeta \phi i}$, $y_{\zeta \phi i}$ - coordinates of the second corner point ζ_i relative to the point ϕ_i (both points are located on one of the long sides of the rectangle); n - the number of rectangles in the considered section; $z_{\eta j}$, $y_{\eta j}$ - base point of the j -th figure given by the integral geometric characteristics; N_j - option number j -th figure on set of feasible realizations; s - number of such cross-sectional shapes.

We define the relationship between the parameters of the cross section from the following formula:

$$\{\Psi_{1\alpha}\} = \{\Psi_{1O}\} + [S]\{\Psi_{1\beta}\}, \tag{4}$$

where $\{\Psi_{1\alpha}\}$ is the value of the vector $\{\Psi_1\}$, finally obtained after the modification of the object; $\{\Psi_{1O}\}$, $[S]$ – the vector and the matrix of constants; $\{\Psi_{1\beta}\}$ – the value of the vector $\{\Psi_1\}$, taking into account only the changes compared to the base design independently of varying magnitudes. We will illustrate the use of the formula (4) on the section shown in Figure 1. We believe that in this case we have the independent change of values $z_{\phi 1}$, $y_{\phi 1}$, δ_1 , $z_{\zeta \phi 1}$, $y_{\zeta \phi 1}$, δ_2 , $z_{\zeta \phi 2}$, $y_{\zeta \phi 2}$ and N_1 . In and N_I . In this case the vector $\{\Psi_{1O}\} = 0$, and the matrix

	1								
		1							
			1						
				1					
1			0,5			0,5			
	1	1							
						1			
							1		
1			0,5					1	
	1	1							1

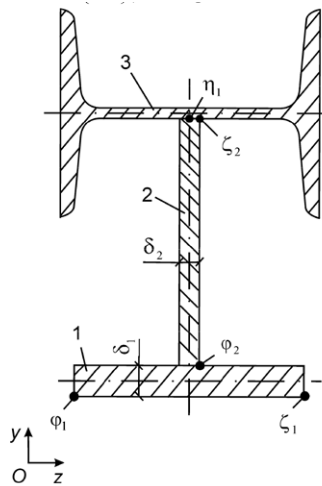


Figure 1. The definition of the relations between the parameters of the composite welded cross section

The main stages of the iterative optimization procedure of flat frames of industrial buildings are given below.

1. *Preparation of general data.* The following information is to be given:
 - topology, material, and other parameters of a FEA model of the redundant structure design;
 - considered loading options in accordance with the standards for the values of the construction area;
 - sets of admissible values for the variable parameters;
 - the equation of connection between the variable parameters of composite sections;
 - constraints of strength, stiffness and stability for construction elements.
2. *Selection of the initial variants of the constructions.* The even number N of constructions is formed. For each of these constructions are randomly selected values of variable parameters from discrete sets of acceptable values .
3. *Analysis of geometric variability of the construction and testing the strength, stiffness and stability of the rods.* A global stiffness matrix is formed and its determinant is evaluated. If the stiffness matrix is positively definite and well-conditioned, the calculation is performed by the FEA method, and conclusions are made about the implementation of constraints of strength and stiffness [2]. If the variant of the construction meets these requirements, it can be registered in the database of survivable and rational projects.
4. *Editing the database of survivable and rational projects.* For registering in the database each variant of the construction should conform to the following conditions:
 - the variant should not be present in the database;
 - the survival criterion of the construction should be less than the worst value of any project already registered in the database.

If the variant design satisfies these conditions, it is recorded in the database of survivable and rational projects. If the number of survivable and rational projects in the database exceeds a certain maximum, the construction with the worst survival criterion is removed.

5. *Checking the conditions for cancelling iterations.* Calculations show that in cases of the optimal design of frame rod systems there are no changes in the database of survivable and rational projects during 500 generations, which indicates the necessity of optimization cancellation.
6. *Single-point mutation.* For each variant of the synthesized construction one parameter can be changed at random. The realization of the operator of mutations is considered in the articles [4,6].
7. *Selection.* The roulette-wheel selection method is used to select successively $N/2$ pairs of construction variants.
8. *Parameter exchange.* For each selected pair the one-point crossover procedure is performed [4, 6]. The iterative process comprising stages 3–8 is executed until the iteration cancellation condition is satisfied.

EXAMPLE OF SOLVING THE OPTIMIZATION TASK

To illustrate the high enough effectiveness of the proposed algorithm, we will consider some results of its use on the example of the optimal design of the metal frame of the general-purpose industrial building (figure 2,a).

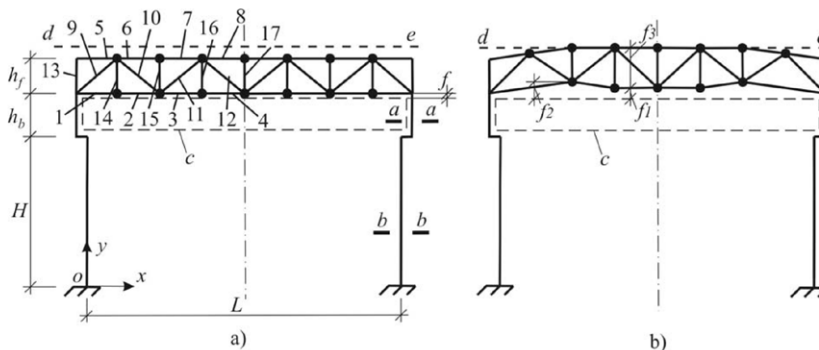


Figure 2. Conditions and results of the synthesis of the frame:
 1-17 – the elements of the covering truss;
 c – the boundary of the dimensions of the crane bridge;
 f – the distance from the top face of the crane bridge to the lower truss belt;
 f_1 - f_3 – the geometrical parameters of the frame obtained from the optimum synthesis

For this frame the following parameters were set: $L = 24$ m, $H = 10$ m, $h_b = 4$ m, $h_f = 3,15$ m, $f = 0,1$ m. The base location of the rods corresponds to the standard solutions 1.460.2 - 10/88 (RU). This topological structure is seen as excessive. We use various sizes of rods cross-sections as varying system parameters. These sizes were chosen from the sets P_I of paired angles: «MSBS», 2L 50x5, 2L 75x5, 2L 90x7, 2L 100x8, 2L 125x10, 2L 140x10, 2L 180x12, 2L 200x12, 2L

220x14 }. Also the sizes of composite welded cross-sections of columns were varying, their structures, in accordance with the marks *a-a*, *b-b* (see Figure 1, a) are shown in Figure 2.

The *y*-coordinates of the nodes could be varying, they are presented as shaded circles in Figure 1. These coordinates are selected from the set $C = \{C1\}, \{C2\}$. The nodes of the upper belt truss coordinates were chosen from the set $C1 = \{16,90; 16,95; 17,0; 17,05; 17,10; 17,15; 17,20; 17,25; 17,30; 17,35; 17,40\}$, and the nodes of the lower belt - from the set $C2 = \{14,00; 14,10; 14,20; 14,30; 14,40; 14,60; 14,80; 15,00; 15,15; 15,30; 15,45\}$. According to the technological requirements it was not allowed to move the nodes of the upper belt higher than level *de*.

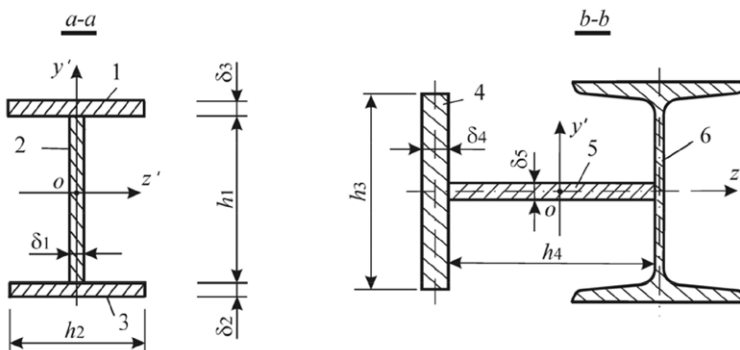


Figure 2. The base structures of the cross-sections of the upper and lower parts of the columns: 1-5 - rectangles; 6 - I-beam

There was allowed independent variation of each of the construction rods with the consequent modification of its other rods as defined by symmetry. The subsets $\{\delta1\}-\{\delta5\}, \{h1\}-\{h4\}$ of P_2 parameter sets of welded cross-sections were formed taking into consideration the size of the universal metal sheet. The calculation was performed of the effect of linear combinations of permanent and temporary loads (crane, snow, wind). The object is considered to be designed in the town of Bryansk, the load capacity of the bridge crane is 50 tons and the pitch of frames is 6m.

The result of the optimization is the frame with the topology shown in Figure 1,b. The results obtained are the following: $f_1=0,3m, f_2=1,25m, f_3=3,4m$. The characteristics of the cross-sections of the frame rods before and after the optimization are shown in Table 1. The parameters of the column cross-section are shown in Figure 2: $h1= 0,45 m, h2 = 0,24 m, \delta1 = 0,008 m, \delta2 = \delta3 = 0,01 m$, for the crane runway part of the column $h3 = 0,28 m, \delta4 = 0,012 m, h4 = 0,98 m, \delta5 = 0,008 m$. The profile, mark 6 is obtained, in form of I-beam S 250x52.

Table 1. Profiles in the cross-sections of the truss rods

Position number in Figure 1,a	Name of the frame element	The sizes of the paired angles	
		Original 1.460.2 – 10/88	Rational
1	rod of the lower belt of the truss	75x75x5	90x90x7
2	The same	90x90x7	75x75x5
3	"	125x125x10	90x90x7
4	"	125x125x10	90x90x7
5	The rod of the upper belt of the truss	75x75x5	50x50x5
6	The same	140x140x10	90x90x7
7	"	180x180x12	90x90x7
8	"	180x180x12	125x125x10
9	The diagonal brace	140x140x10	90x90x7
10	The same	125x125x10	90x90x7
11	"	90x90x7	75x75x5
12	"	75x75x5	50x50x5
13	The rack	75x75x5	100x100x8
14	The same	75x75x5	-
15	"	75x75x5	75x75x5
16	"	75x75x5	90x90x7
17	"	75x75x5	75x75x5

CONCLUSION

1. There was developed an optimization algorithm for metal plane frames, allowing the performance of structural/shape/size synthesis of rational structures using discrete sets of design parameters.
2. When performing the optimization of frames of general-purpose industrial buildings the reduction of the materials consumption is 10% if compared to standard solutions projects.
3. The given optimization example shows that the given version of the genetic iterative scheme allows us to find new rational design decisions.

NOTES

This article was supported by the grant of the Russian Fund for Fundamental Research № 13-08-00457 (2013-2014).

REFERENCES

- [1] Balling, R.J., Briggs, R.R., Gillman K. 2006. Multiple optimum size/shape/topology designs for skeletal structures using a genetic algorithm. J. Struct. Eng., ASCE. 132(7), pp. 1158–1165.
- [2] EN 1993-1-3: 2006 Eurocode 3: Design of steel structures. Part 1–3: Supplementary rules for cold-formed members and sheeting.

- [3] Hasançebi, O. Çarbaş, S. Doğan, E. Erdal, F. Saka, M.P. 2010. Comparison of non-deterministic search techniques in the optimum design of real size steel frames. *Comput. Struct.* 88, 1033–1048.
- [4] Serpik I.N., Alekseytsev A.V., Lewkowicz F.N. etc. 2005. Structural and parametric optimization of rod metal structures based on evolutionary modeling. *Proceedings of the higher educational institutions. Building.* 8, 16–24.
- [5] Togan, V., Daloglu, A.T. 2008. An improved genetic algorithm with initial population strategy and self-adaptive member grouping. *Comput. Struct.* 11, 1204–1218.
- [6] Leite, J.P.B., Topping, B.H.V. 1998. Improved genetic operators for structural engineering optimization. *Adv. Eng. Softw.* 29(7-9), 529–562.
- [7] Zienkiewicz, O.C., Taylor, R.L. 2000. *The finite element method.* (Fifth edition). Oxford. 689 pp.

SAFETY MEASURES FOR STORING OF LIQUEFIED GASES IN LARGE WELDED LOW PRESSURE TANKS

Khanukhov K.M.

**Doctor of technical Sciences.
Member-correspondent of RF Academy for Engineering.
General Director of Consortium "Isotermic"**

Under consideration are the ways of safe storing of LPG, LNG, oxygen, nitrogen, helium, hydrogen, regarded as basis for chemical, petrochemical industries and as well as future source of energy for cosmic and rail road transport.

Transportation and storage of liquefied gases is regarded as the most economic and effective way to handle them (volume of liquid is 250–1500 time less than volume of gas, metal savings prove to be 3–4 times less per 1 ton of handled product, in comparison with storage under pressure, the storage area decreases by 30 %). Large welded low-pressure storage tanks (LWLPST) stand high in Russian civil engineering code of hazard classification.

Nowadays, the lack of domestic coding on design, fabrication, construction and maintenance of lwlpst is being overwhelmed by developing of Special Individual Standards (SIS) for every particular project. Experience of "SIK Isotermik" on developing of such "SIS" for LWLPST design demonstrates possibilities of harmonization between (API) and local codes respecting safe maintenance of LWLPST, as well as specific conditions of domestic tank construction such as severe climate, local steels and other materials, demands of industrial codes and human factors. Nevertheless, new codes, reflecting common safety questions of LWLPST are needed. SIK Isotermik, if financed, is ready to initiate and lead developing of such codes.

To secure safe operation of LWLPST in terms of construction and design methods SIK Isotermic offers as follows:

- Using of two equally-strained walls in two wall lwlpst with suspended internal roof and vacant inter-wall space. Insulation to be used under common bottom and all over the outer surface of the tank – is foam glass. Presence of the outer wall equal to the internal will prevent product spills in case of failure of the internal tank shell, allowing to increase safety and minimize risks. When circumstances dictate, the content from adjacent tank can be promptly pumped into inter-wall space;
- using of foam glass for insulation of single and double wall tank external surface gives the following advantages: it is totally non-combustible, is good moisture and vapour sealant. Life service of the foam glass is compatible with that of the tank.

Safe operation of LWLPST is (being) provided by automatic and continuous control over liquid level, vapour pressure, tightness and spills into workspace between shells. It makes possible to detect and stop stratification of LNG, creation of “warm lenses” which result in dramatic increase of gaseous phase. Equipping of tanks with monitoring systems, as offered by local engineers, will permit to obtain all operating data of LWLPST and assess their performance and residual service life in real time. The monitoring system consists of an acoustic emission sensor over the tank’s hull, to control growing flaws in zones of concentrated stresses, vibration detectors of nozzles, temperature gauges of concrete foundation.

Basing on monitoring of process data (level of liquid, vapour pressure, temperature, density) and data of current conditions of the tank (defects of the geometric form, flaws of welded joints, change of properties of materials, seismic loads) the combined maintenance system will allow to assess risks in real time and run them.



This book covers the papers presented and submitted for the annual Metnet Seminar in October 2014 held at Moscow State University of Civil Engineering MGSU. The seminar continued the METNET tradition of presenting scientific and development papers of high caliber.

METNET seminars deal with technical aspects of metal construction as well as issues of concern to industry on management, planning and sustainability of projects.

Metnet cooperation promotes regional innovation environments and strengthens knowledge structures, especially in the European regions represented by its members. At the annual seminars, the participating partner organization represents its regional innovation environment but simultaneously is a partner of a larger and stronger international innovation world created by active cooperation between the institutes and enterprises.

PRINTED

ISBN 978-951-784-693-6
ISSN 1795-4231
HAMKin julkaisuja 15/2014

ELECTRONIC

ISBN 978-951-784-694-3 (PDF)
ISSN 1795-424X
HAMKin e-julkaisuja 35/2014

HAMK
UNIVERSITY OF APPLIED SCIENCES